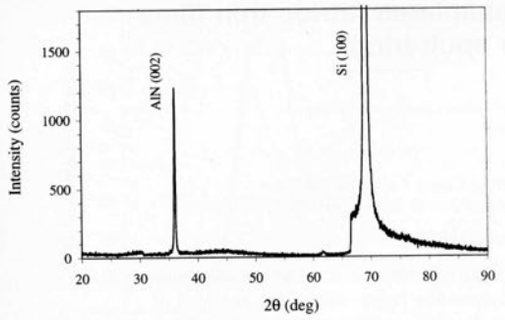

FIG. 1. X-ray diffractions patterns of aluminum nitride thin films deposited on silicon substrate.

technique[9] to be in the order of 7.3 dB cm^{-1}. Higher losses have been obtained for higher-order modes excited in the film. The wave guide losses are known to be strongly dependent on the surface roughness of the film. The surface morphology of AlN samples has been examined by atomic force microscopies (AFM) showing a good surface quality for our films (r_{ms} about of 40 Å). In order to minimize the optical losses, the epitaxial growth of AlN thin films is required.

From the angular position of the guided modes, we computed the corresponding effective indices and hence the refractive indices and the film thickness. For our samples, the ordinary (n_0) and the extraordinary (n_e) refractive indices are 2.0058 ± 0.0004 and 2.0374 ± 0.0006 ($\lambda = 632.8$ nm) respectively. These values are similar to those reported in the literature.[6,10] However, slight deviations of refractive indices are obtained in comparison with the corresponding AlN single crystal ordinary refractive index n_0 which is around 2.16.[11] This is mainly attributed to the nitrogen vacancy or oxygen impurities. The thickness was determined to be $1.28 \pm 0.04\,\mu$m which is in agreement with the scanning electron microscope (SEM) investigation.

Note that in this study, we focused our attention to the simple case of light propagation in anisotropic uniaxial thin film deposited onto an isotropic substrate. In this configuration, TE and TM modes can exist separately. Therefore, the problem was treated using the well-known guided-modes dispersion equation. However, the deposition technique may

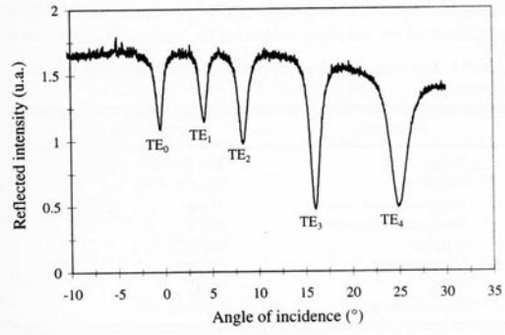

FIG. 2. TE guided mode spectra obtained by measuring the reflected intensity vs the angle of incidence (n_0 excitation).

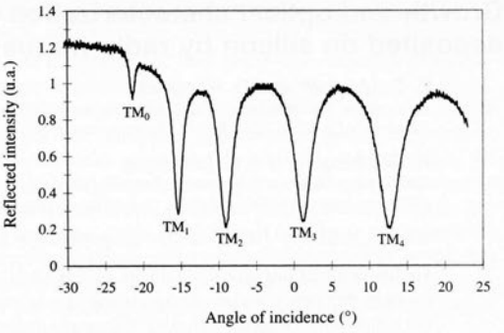

FIG. 3. TM guided mode spectra obtained by measuring the reflected intensity vs the angle of incidence (n_e excitations).

yield thin films with the optical axis tilted from normal to the substrate surface. In this situation, TM modes are affected by the tilt angle (φ) of the optical axis which determines the refractive index seen by the optical wave propagating within the guiding structure. The calculation procedure[12] provides a weak tilt angle (φ) of nearly 6° with respect to the normal to the substrate surface, confirming the uniaxial nature of our AlN thin films deposited by rf sputtering, with the optical axis very likely oriented perpendicular to the substrate surface.

To complete this analysis, we have reconstructed the refractive index profiles directly from the measured effective indices by using an improved version of the inverse Wentzel–Kramer–Brillouin (*i*WKB) method. This method only depends on the refractive index distributions within the guiding layer. More details of calculation are given by Chiang.[13] Using a polynomial interpolation of the measured effective indices, we computed the refractive index profiles as a smooth function of the thickness. As shown in Fig. 4, the refractive index profiles indicate a step-index variation which is synonymous of a good optical homogeneity along the film thickness. Indeed, the refractive index remains constant within the guiding region and decreases rapidly near the film–substrate interface. Therefore, this result did not show any clear influence of the substrate on the growth process.

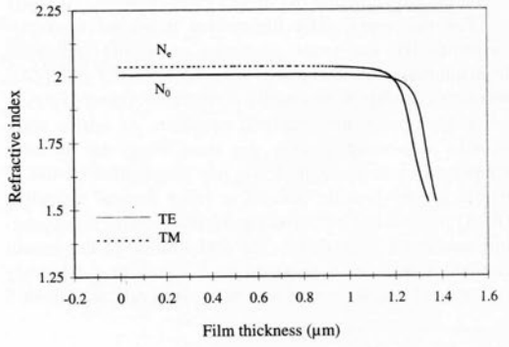

FIG. 4. Ordinary (n_0) and extraordinary (n_e) refractive index profiles obtained by an improved inverse WKB method for AlN thin films deposited on silicon substrates.

Using TE guided modes, we have investigated the electrooptic (EO) coefficient using the angular shift technique as described by Boudrioua *et al.*[14] The top electrode consists of a semitransparent gold film with a thickness of 10 nm. By applying a transverse electric field through the AlN layer, a change of the resonant coupling angle ($\Delta\theta$) in the guided-modes spectrum has been observed. This effect is directly correlated to the variation of the refractive index (Δn) due to the EO effect. Finally, the linear EO coefficient r_{13} obtained is evaluated to be 0.98 pm/V.

In summary, AlN thin films have been grown on Si/SiO_2 substrates by radio-frequency magnetron sputtering from an aluminum nitride target. The deposition parameters and annealing process were optimized for the elaboration of highly textured AlN thin films. We have investigated the optical performances of the films using the prism-coupling technique. Refractive indices were therefore determined to be $n_0 = 2.0058$ and $n_e = 2.0374$ at 632.8 nm. From the effective guided-mode indices, the analysis of the optical anisotropy confirmed the uniaxial nature of the AlN thin film with the optical axis likely oriented normal to the surface of the substrate. The optical losses were evaluated to be around 7 dB cm^{-1}. The EO measurements using the angular shift method showed a linear electro-optic coefficient r_{13} of about 0.98 pm/V. These results demonstrate the interest of AlN thin films to be used in integrated optics applications.

[1] H. Okano, N. Tanaka, Y. Takahashi, T. Tanaka, K. Shibata, and S. Nakano, Appl. Phys. Lett. **64**, 166 (1994).
[2] M. A. Khan, J. N. Kuznia, D. T. Olson, J. M. Van Hove, and M. Blasingame, Appl. Phys. Lett. **60**, 2917 (1992).
[3] S. Nakamura, M. Senoh, S. Nagahama, N. Iwasa, T. Yamada, T. Matasushita, H. Kiyoku, and Y. Sugimoto, Jpn. J. Appl. Phys., Part 2 **35**, L74 (1996).
[4] E. Calleja, M. A. Sanchez-Garcia, E. Monroy, F. J. Sanchez, and E. Munoz, J. Appl. Phys. **82**, 4681 (1997).
[5] K. Dovidenko, S. Oktyabrsky, J. Narayan, and M. Razeghi, Appl. Phys. Lett. **79**, 2439 (1996).
[6] X. Tang, Y. Yuan, K. Wongchotigul, and M. Spencer, Appl. Phys. Lett. **70**, 3206 (1997).
[7] P. K. Tien, R. Ulrich, and J. R. Martin, Appl. Phys. Lett. **14**, 291 (1969).
[8] F. Flory, G. Albrand, D. Endelma, N. Maythaveekulchai, E. Pelletier, and H. Rigneault, Opt. Eng. (Bellingham) **33**, 1669 (1994).
[9] E. Dogheche, B. Jaber, and D. Rémiens, Appl. Opt. **37**, 4245 (1998).
[10] S. Strike and H. Morkoç, J. Vac. Sci. Technol. B **10**, 1237 (1992).
[11] L. Roskovcova, J. Pastrnak, and R. Babuskova, Phys. Solid State **20**, k29 (1967).
[12] F. Horowitz and S. B. Mendes, Appl. Opt. **33**, 2659 (1994).
[13] K. S. Chiang, J. Lightwave Technol. **LT3**, 85 (1985).
[14] A. Boudrioua, E. Dogheche, D. Rèmiens, and J. C. Loulergue, J. Appl. Phys. **85**, 1 (1999).

Appendix 1029-B

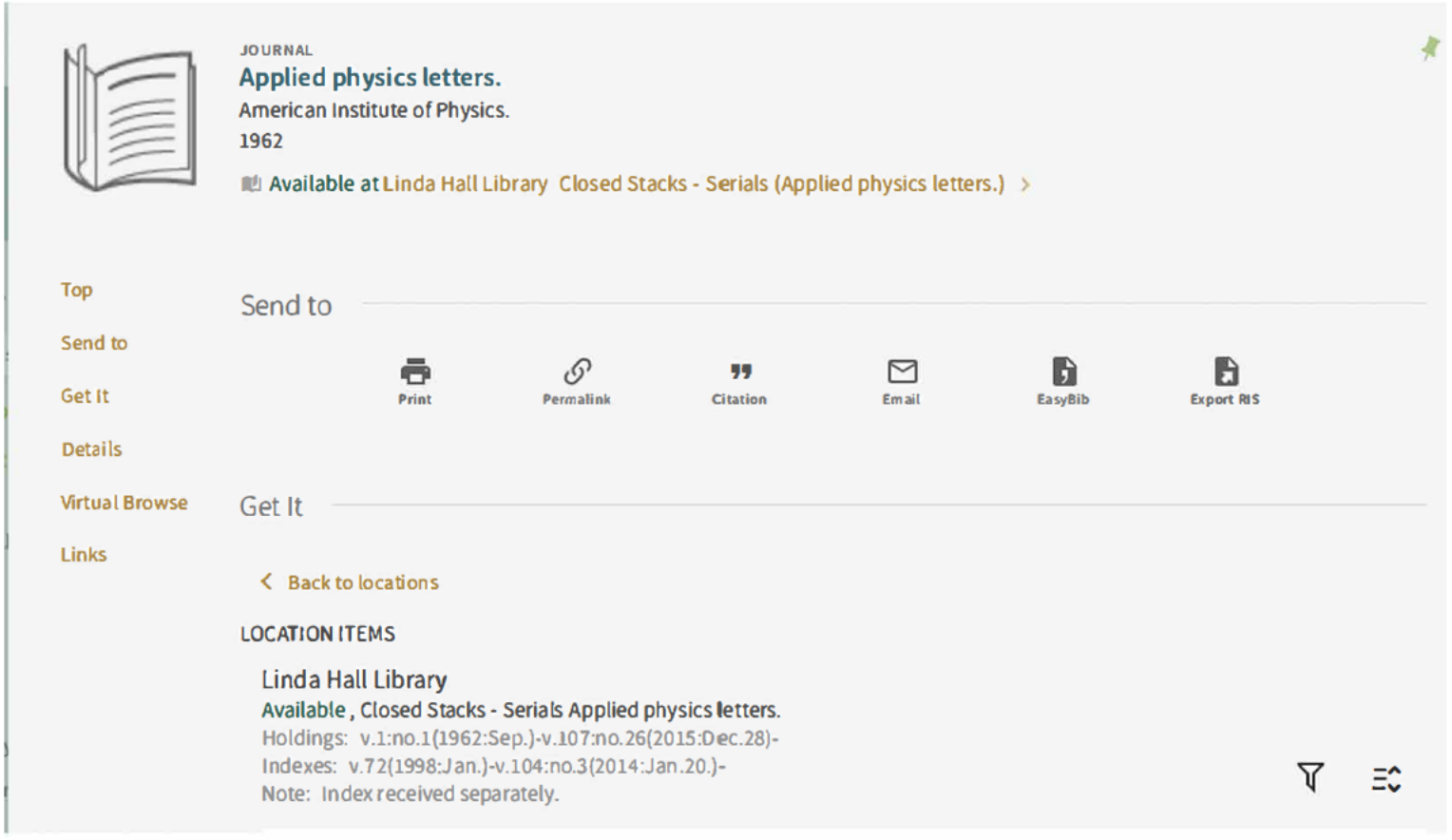
JOURNAL
Applied physics letters.
American Institute of Physics.
1962
Available at Linda Hall Library Closed Stacks - Serials (Applied physics letters.)
Top
Send to
Get It
Details
Virtual Browse
Links
Send to
Print
Permalink
Citation
Email
EasyBib
Export RIS
Get It
Back to locations
LOCATION ITEMS
Linda Hall Library
Available , Closed Stacks - Serials Applied physics letters.
Holdings: v.1:no.1(1962:Sep.)-v.107:no.26(2015:Dec.28)-
Indexes: v.72(1998:Jan.)-v.104:no.3(2014:Jan.20.)-
Note: Index received separately.

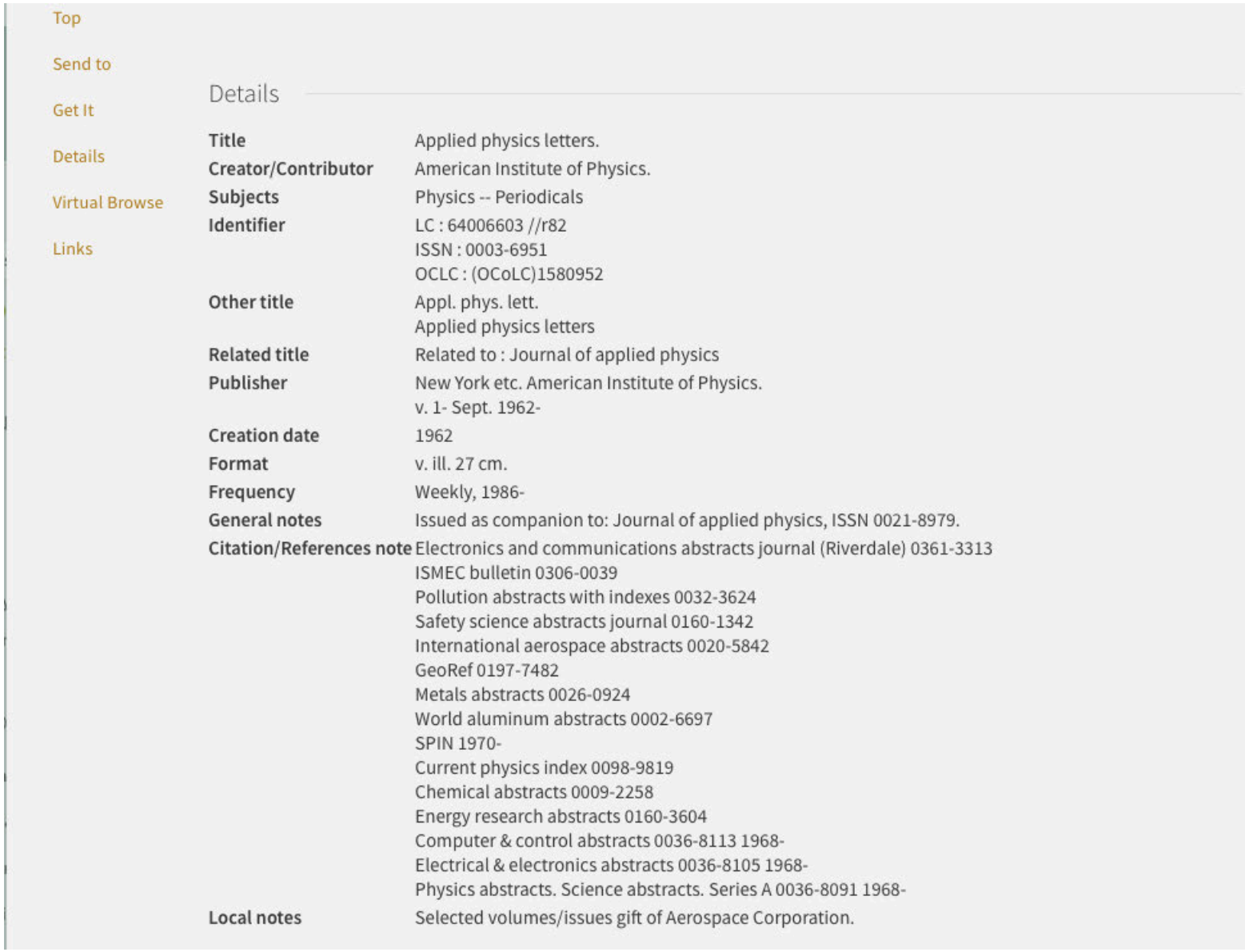
Top
Send to
Get It
Details
Virtual Browse
Links
Details
Title
Applied physics letters.
Creator/Contributor
American Institute of Physics.
Subjects
Physics -- Periodicals
Identifier
LC : 64006603 //r82
ISSN : 0003-6951
OCLC : (OCoLC)1580952
Other title
Appl. phys. lett.
Applied physics letters
Related title
Related to : Journal of applied physics
Publisher
New York etc. American Institute of Physics.
v. 1- Sept. 1962-
Creation date
1962
Format
v. ill. 27 cm.
Frequency
Weekly, 1986-
General notes
Issued as companion to: Journal of applied physics, ISSN 0021-8979.
Citation/References note
Electronics and communications abstracts journal (Riverdale) 0361-3313
ISMEC bulletin 0306-0039
Pollution abstracts with indexes 0032-3624
Safety science abstracts journal 0160-1342
International aerospace abstracts 0020-5842
GeoRef 0197-7482
Metals abstracts 0026-0924
World aluminum abstracts 0002-6697
SPIN 1970-
Current physics index 0098-9819
Chemical abstracts 0009-2258
Energy research abstracts 0160-3604
Computer & control abstracts 0036-8113 1968-
Electrical & electronics abstracts 0036-8105 1968-
Physics abstracts. Science abstracts. Series A 0036-8091 1968-
Local notes
Selected volumes/issues gift of Aerospace Corporation.

```
02287cas a22006011  4500
992785733405961
20191029185840.0
750829c19629999nyuwr1p       0   a0eng
##$a 64006603 //r82
##$a3 $b3 $en $i8811 $k1 $m1
##$a1481730
0#$a0003-6951
##$aAPPLAB
##$a028520 $bUSPS
##$a(OCoLC)1580952
##$9386026
##$a(MoKL)278573-lhalldb
##$a(lhalldb)278573-lhalldb
##$z(OCoLC)1481730
##$aDLC $cUDI $dCOO $dHUL $dCOO $dDLC $dNSD $dOCL $dYUS $dDLC $dSER $dAIP $dOCL $dNYG $dNST $dOCL $dNST
##$ansdp $alc
##$aLHLA
00$aQC1 $b.A74
0#$aAppl. phys. lett.
#0$aApplied physics letters
00$aApplied physics letters.
##$aNew York [etc.] $bAmerican Institute of Physics.
##$av. $bill. $c27 cm.
##$aWeekly, $b1986-
##$aSemimonthly, $b1963-1985
##$aMonthly, $b1962
0#$av. 1- Sept. 1962-
2#$aElectronics and communications abstracts journal (Riverdale) $x0361-3313
2#$aISMEC bulletin $x0306-0039
2#$aPollution abstracts with indexes $x0032-3624
2#$aSafety science abstracts journal $x0160-1342
2#$aInternational aerospace abstracts $x0020-5842
2#$aGeoRef $x0197-7482
2#$aMetals abstracts $x0026-0924
```

```
2#$aMetals abstracts $x0026-0924
2#$aWorld aluminum abstracts $x0002-6697
1#$aSPIN $b1970-
2#$aCurrent physics index $x0098-9819
2#$aChemical abstracts $x0009-2258
2#$aEnergy research abstracts $x0160-3604
1#$aComputer & control abstracts $x0036-8113 $b1968-
1#$aElectrical & electronics abstracts $x0036-8105 $b1968-
1#$aPhysics abstracts. Science abstracts. Series A $x0036-8091 $b1968-
0#$av1-23(1962-73) SEE Jrl. of applied physics; 30-39(1977-81) bd w/39; 40-49(1982-86) bd w/49 and index to every 10 vols. thereafter bound with la
##$aIssued as companion to: Journal of applied physics, ISSN 0021-8979.
##$aSelected volumes/issues gift of Aerospace Corporation.
#0$aPhysics $vPeriodicals.
2#$aAmerican Institute of Physics.
1#$tJournal of applied physics $x0021-8979 $w(DLC) 33023425
##$aCaMWUC $aDLC $aNN $aNcRS $aPU
##$aApr. 1978
##$aLTI 04/26/2017
```

Appendix 1029-C

Item Details

FMT	SE
LDR	nas a22002417a 4500
001	014532647
003	Uk
005	20200701010345.0
007	ta
008	840320c19629999xxuer p 0 a0eng
0220	|a 0003-6951
040	|a Uk |c Uk |d Uk
08204	|a 621 |2 21
084	|a PQ 00 |2 blsrissc
24500	|a Applied physics letters.
260	|a New York : |b American Institute of Physics, |c 1962-
300	|a v. ; |c 27 cm.
310	|a Fortnightly
336	|a text |2 rdacontent
337	|a unmediated |2 rdamedia
338	|a volume |2 rdacarrier
595	|a SEE ALSO SERIAL RECORDS KCS SE.
555	|a Cumulative index.
7102	|a American Institute of Physics.
945	|a APPLIED PHYSICS LETTERS
85271	|a British Library |b STI |k (P) |h PQ 00 |m -E(12) |2 blsrissc
866 0	|a Volume 1(1962)- ; Deficient: v. 62, no.27, 1993
85249	|a British Library |b DSC |j 1576.400000
866 0	|a Volume 1 (1962)- |z UKRR Retained Title
SYS	014532647

Appendix 1029-D

Early Citations to Dogheche

Deposition of AlN Thin Films with Cubic Crystal Structures on Silicon Substrates at Room Temperature

Zhong-Min REN, Yong-Feng LU, Yeow-Whatt GOH, Tow-Chong CHONG, Mei-Ling NG[1], Jian-Ping WANG[1], Boon-Aik CHEONG[1] and Yun-Fook LIEW[1]

Laser Microprocessing Laboratory, Department of Electrical Engineering and Data Storage Institute, National University of Singapore, 10 Kent Ridge Crescent, Singapore 119260
[1]*Data Storage Institute, 5 Engineering Drive 1, Singapore 117608*

(Received September 20, 1999 accepted for publication March 6, 2000)

Cubic AlN thin films were deposited at room temperature by nitrogen-ion-assisted pulsed laser ablation of a hexagonal AlN target. The full-width at half maximum (FWHM) of the X-ray diffraction peak in the $\theta \sim 2\theta$ scan can reach a value of 0.27 degrees. In the Raman spectroscopy measurement, a new peak at 2333 cm^{-1} originating from cubic AlN polycrystalline was observed. Nitrogen ions not only effectively promote the formation of stable Al–N bonds but also improve the crystal properties of the deposited thin films. A nitrogen ion energy of 400 eV is proposed for the thin-film deposition.

KEYWORDS: AlN pulsed laser deposition thin films cubic crystalline Raman spectroscopy XRD XPS

Recently there has been tremendous interest in the synthesis of AlN thin film due to its wide band gap and other desirable properties of thermal conductivity, electrical resistivity (dielectric constant) and acoustic properties.[1–3] Many experimental methods have been used to deposit AlN thin films, including metalorganic chemical vapor deposition (MOCVD),[4] plasma-assisted molecular beam epitaxy (PAMBE),[5–7] RF reactive magnetron sputtering,[8–11] ion-assisted chemical vapor deposition[12] and pulsed laser deposition (PLD).[13–19] A number of new theoretical works have also been published recently.[20 21] Almost all the deposition methods require high substrate temperatures (normally above 600°C) although the defects both inside the thin films and at the interface between the substrate and the thin film cannot be avoided.[6] To date, all the deposited AlN thin films have hexagonal structures with a highly textured orientation of (0001) on sapphire, silicon and glass substrates.[3 6 7 9 10 18 19]

In our study, we attempted to use pulsed laser ablation to deposit AlN thin films on silicon substrates at room temperature. PLD has been proven to be suitable to fabricate AlN thin films on silicon and sapphire substrates. Compared with other methods, PLD has two main aspects of advantages. First, it can faithfully transfer the target material to the substrate surface without an obvious change in the compositional ratios of compound materials. Second, the energetic radicals in the ablated plume are beneficial to the formation of ideal crystalline structures in the deposited thin films. In our experiments, the ion-assisted PLD combines the advantages of ion bombardment and laser ablation. With this approach, we can independently control the energies of the AlN radicals in the ablated plasma and the nitrogen ions in the ion beam to improve the quality of the deposited thin films. Moreover, the nitrogen ions can also compensate for the loss of nitrogen species in the ablation process.

In the experiment, we used a KrF excimer laser at a wavelength of 248 nm to ablate an AlN target. The deposition was carried out in a PLD system with a background vacuum of 1×10^{-6} Torr. An AlN target with a standard hexagonal crystal structure and a purity of 99.995% was mounted on a target holder that was rotated by an external motor. The target was placed 2 cm away from the substrate surface. The laser pulse duration was 30 ns. The laser fluence was set at 2 $J cm^{-2}$ with produced by a 1-cm Kaufman-type ion source irradiated the substrate surface to assist the deposition. The ion flux was set at 1 mA/cm^2. The deposition rate was 0.1 nm/s as measured by a microbalance mounted on the substrate. Si(100) wafers were used as substrates. The deposited thin films have thicknesses of around 200 $\sim$ 300 nm. After deposition, X-ray diffraction (XRD), Raman spectroscopy and X-ray photoelectron spectroscopy (XPS) measurements were carried out to characterize the crystal, chemical binding and compositional properties of the deposited thin films.

Figure 1 shows the XRD $\theta \sim 2\theta$ spectrum of an AlN thin film deposited by 400 eV nitrogen ion bombardment. The measurements were performed on a Philips X'Pert-MRD system. Cu Kα irradiation with an average wavelength of 1.5418 Å was used as an X-ray source in the diffraction measurements. In the spectrum, besides the Si(200) and Si(400) diffraction peaks, there are four distinct peaks at $2\theta = 38.5$, 44.7, 65.3 and 78.3, corresponding respectively to orientations of (111), (200), (220) and (311) of the cubic AlN crystal[22] although the crystal structure of the target is hexagonal. Hexagonal structures are not detected from Fig. 1 when the resolution of the MRD system is taken into account. The FWHM of the AlN(200) peak is about 0.27 degrees, lower than that of films deposited by plasma source molecular beam epitaxy.[6] The formation of AlN cubic structures on Si(100)

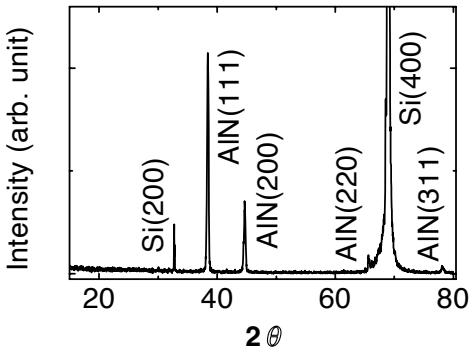

Fig. 1. XRD $\theta \sim 2\theta$ spectrum of a AlN thin film deposited by KrF laser

substrates is different from most other research results in which hexagonal AlN structures are formed.[15 18 19] In the detailed studies[6 7] of the microstructures and initial stages of thin-film deposition, AlN films have an initial amorphous region at the interface between the substrate and the thin film, followed by *c*-axis-oriented columnar grains. Substrate temperatures higher than 600°C can significantly reduce the amorphous regions at the interface and promote to grow AlN with hexagonal (0001) orientation. However, in our deposition, since substrate temperature is low, the *c*-axis-orientated growth of hexagonal AlN is not preferred. Instead, another metastable state of the crystal AlN with a cubic structure was obtained from our deposition, although the hexagonal AlN is possibly in a much stable state. The PLD at room temperature with the assistance of ion-beam coprocessing leads to mainly (111)-oriented c-AlN thin films.

We also deposited AlN thin films without nitrogen ion bombardment. These deposited thin films exhibit no XRD peaks, indicating only amorphous structures. The result reveals the important role of nitrogen ions in the synthesis of AlN thin films with cubic crystal structures. Moreover, nitrogen ion energy lower than 400 eV leads to weaker and broader XRD peaks. Therefore, nitrogen ions with an energy of 400 eV can effectively assist in the formation of cubic crystalline structures in the deposited thin films. When the nitrogen ion energy exceeds 400 eV, the deposition will be impeded due to the resputtering effect caused by the ion bombardment.

Figure 2 shows the Raman spectra of the AlN thin films deposited under the different nitrogen ion energies of 100, 200, and 400 eV. Similar to most other research findings,[19 23 24] the Raman peaks of the AlN thin films are weak. The peaks at 618, 670 and 826 cm^{-1} reflect the phonon modes of E_1(TO), A_1(LO) and E_1(LO), respectively,[23 24] indicating the crystal structures of the deposited thin films. The intensities of these Raman peaks increase with increasing nitrogen ion energy from 100 to 400 eV, implying that the nitrogen ion energy of 400 eV is optimal for the deposition of crystal AlN thin films, in agreement with the XRD analysis result. Besides these peaks, there is a sharp and strong peak at 2333 cm^{-1} which is observed for the first time. The intensity of this peak also increases with the nitrogen ion energy and reaches a maximum when the ion energy increases to 400 eV. Therefore, this peak must originate from the cubic structure of AlN.

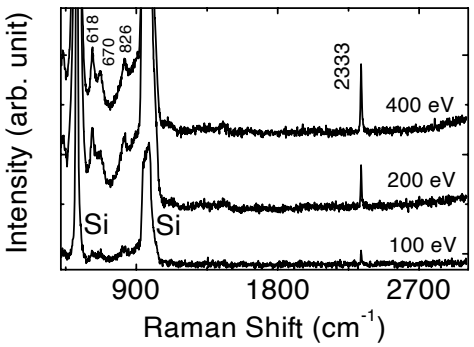

Fig. 2. Raman spectra of AlN thin films deposited under different nitrogen

For the thin films deposited without nitrogen ions, no obvious Raman peak can be observed, implying that the nitrogen ions can effectively improve the crystal property of the thin film. Although it induces defects, ion implantation can possibly benefit the growth of the crystal grains. The energetic nitrogen ions can enhance the chemical combinations between Al and N atoms and thus lead to more and larger AlN crystal grains.

The chemical binding and compositional properties of the AlN thin films were analyzed by XPS measurements. Figure 3 shows the XPS Al 2p spectra for three AlN thin films deposited with different ion energies. The binding energy of the Al 2p electron increases slightly with increasing nitrogen ion energy from 100 to 400 eV, due to the fact that the energetic nitrogen ions can effectively react with Al atoms to form AlN compounds. The binding energy of the Al 2p electron in the AlN compound is higher than that in atomic Al due to the weak shielding effect. Higher ion energy can lead to the for-

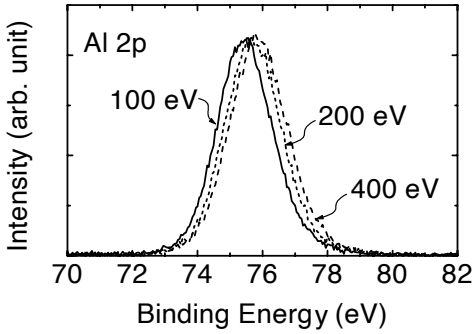

Fig. 3. XPS Al 2p spectra for AlN thin films deposited under different nitrogen ion energies of 100, 200, and 400 eV. The laser fluence is 2 J/cm^2. The ion flux is 1 mA/cm^2.

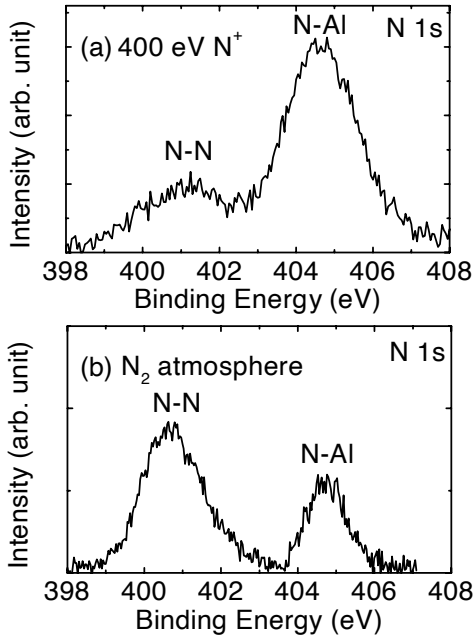

mation of more Al–N bonds and therefore an increase in the Al 2p binding energy.

Figure 4 shows two XPS N 1s spectra for AlN thin films deposited with and without the assistance of nitrogen ions, respectively. It is evident that, in the thin films, there are two nitrogen statuses related to N–N and N–Al bonds. The difference between these two spectra in Fig. 4 is quite obvious. The thin film deposited in the N_2 atmosphere has a very strong N–N peak whereas that deposited with 400 eV N^+ implantation has a strong N–Al peak. The nitrogen ions in the deposition promote the formation of Al–N bonds and reduce the density of N–N bonds. Therefore, nitrogen ions with an energy of about 400 eV are beneficial to the synthesis of AlN thin films, in agreement with the above XRD and Raman results.

The N/Al atomic ratio of the deposited thin films is in the range of 0.90 to 1.12. The N/Al atomic ratio is evaluated using $N : Al = A_N/S_N : A_{Al}/S_{Al}$, where A_N and A_{Al} are the areas under the N1s and Al2p peaks, and the constants S_N and S_{Al} are the sensitivity factors of nitrogen and aluminum, respectively. The ratio is slightly lower than 1.0 when the ion energy is 400 eV, due to the resputtering effect. Deposition with ion-beam bombardment is a nonequilibrium process. The low substrate temperature does not provide any energy for the equilibrium growth of an AlN crystal. The deposition is accomplished by energetic ions with energies of about 400 eV. Therefore, the crystalline growth mechanism is quite different from other deposition methods where high substrate temperatures and low ion energies are employed. Hexagonal AlN thin films were deposited by PLD at substrate temperatures above 675°C[15,18] and by RF magnetic sputtering and molecular beam epitaxy with substrate temperatures higher than 400°C,[6,9,10,19] even on silicon[6,9,18] and glass[10] substrates. However, in our deposition, the *c*-axis-oriented growth which leads to the hexagonal structure is not possible due to the low substrate temperature. In contrast, the energetic ions promote the formation of another metastable state of crystal AlN with a cubic structure. Therefore, the use of nitrogen ions with the energy of about 400 eV plays an important role in the formation of a cubic AlN crystal.

In summary, AlN thin films were deposited at room temperature on Si(100) substrates by nitrogen-ion-assisted pulsed laser ablation of a hexagonal AlN target. The thin films have cubic crystal structures with orientations of (111), (200), (220) and (311), different from most other research results in which hexagonal AlN was obtained. Energetic nitrogen ion implantation plays an important role in the formation of a cubic AlN crystal. An ion energy of 400 eV was determined to be appropriate for the deposition process.

Acknowledgements

The authors would like to thank Miss. H. L. Koh for her technical assistance in this research.

1) W. R. L. Lambrecht: Mater. Res. Symp. Proc. **339** (1994) 565.
2) F. A. Ponce, S. P. DenBaars, B. K. Meyer, S. Nakamura and S. Strite: *Nitride Semiconductors* (Materials Research Society, Boston, 1998).
3) K. A. Jones, K. Xie, D. W. Eckart, M. C. Wood, V. Talyansky, R. D. Vispute, T. Venkatesan, K. Wongchotigul and M. Spencer: J. Appl. Phys. **83** (1998) 8010.
4) P. Kung, A. Saxler, X. Zhang, D. Walker, T. C. Wang, I. Furguson and M. Razeghi: Appl. Phys. Lett. **66** (1995) 2958.
5) K. S. Stevens, A. Ohtani, M. Kinniburgh and R. Beresford: Appl. Phys. Lett. **65** (1994) 321.
6) G. W. Auner, F. Jin, V. M. Naik and R. Naik: J. Appl. Phys. **85** (1999) 7879.
7) J. R. Heffelfinger, D. L. Medlin and K. F. Mccarty: J. Appl. Phys. **85** (1999) 466.
8) W. J. Meng, J. Heremans and Y. T. Chang: Appl. Phys. Lett. **59** (1991) 2097.
9) E. Dogheche, D. Remiens, A. Boudrioua and J. C. Loulergue: Appl. Phys. Lett. **74** (1999) 1209.
10) A. Rodriguez-Navarro, W. Otano-Rivera, L. J. Pilione, R. Messier and J. M. Garcia-Ruiz: J. Vac. Sci. & Technol. A **16** (1998) 1244.
11) H. Y. Joo, H. J. Kim, S. J. Kim and S. Y. Kim: J. Vac. Sci. & Technol. A **17** (1999) 862.
12) J. C. Sanchez-Lopez, L. Contreas, A. Fernandez, A. R. Gonzalez-Elipe, J. M. Martin and B. Vacher: Thin Solid Films **317** (1998) 100.
13) T. F. Huang and J. S. Harris, Jr.: Appl. Phys. Lett. **72** (1998) 1158.
14) V. Talyansky, R. D. Vispute, R. Ramesh, R. P. Sharma, T. Venkatesan, Y. X. Li, L. G. Salamanca-Riba, M. C. Wood, R. T. Lareau, K. A. Jones and A. A. Iliadis: Thin Solid Films **323** (1998) 37.
15) G. S. Sudhir, H. Fujii, W. S. Wong, C. Kisielowski, N. Newman, C. Dieker, Z. Liliental-Weber, M. D. Rubin and E. R. Weber: Appl. Surf. Sci. **127** (1998) 471.
16) R. D. Vispute, J. Narayan and J. D. Budai: Thin Solid Films **299** (1997) 94.
17) M. He, N. Cheng, P. Zhou, H. Okabe and J. B. Halpern: J. Vac. Sci. & Technol. A **16** (1998) 2372.
18) A. Kumar, H. L. Chan, J. J. Weimer and L. Sanderson: Thin Solid Films **308/309** (1997) 406.
19) K. Jagannadham, A. K. Sharma, Q. Wei, R. Kalyanraman and J. Narayan: J. Vac. Sci. & Technol. A **16** (1998) 2804.
20) R. Di Felice and J. E. Northrup: Appl. Phys. Lett. **73** (1998) 936.
21) R. Di Felice, C. M. Bertoni and A. Catellani: Appl. Phys. Lett. **74** (1999) 2137.
22) H. Vollstadt: Proc. Jpn. Acad. B **66** (1990) 7.
23) C. Carlone, K. M. Lakin and H. R. Shanks: J. Appl. Phys. **55** (1984) 4010.
24) L. E. McNeil, M. Grimsditch and R. H. French: J. Am. Ceram. Soc. **76** (1993) 1132.

Room temperature synthesis of c–AlN thin films by nitrogen-ion-assisted pulsed laser deposition

Cite as: Journal of App ied Physics **88**, 7346 (2000); https://doi.org/10.1063/1.1320010
Submitted: 10 April 2000 . Accepted: 28 August 2000 . Published Online: 28 November 2000

Z. M. Ren, Y. F. Lu, H. Q. Ni, T. Y. F. Liew, B. A. Cheong, S. K. Chow, M. L. Ng, and J. P. Wang

Room temperature synthesis of *c*-AlN thin films by nitrogen-ion-assisted pulsed laser deposition

Z. M. Ren, Y. F. Lu,[a] and H. Q. Ni
Laser Microprocessing Laboratory, Department of Electrical Engineering and Data Storage Institute, National University of Singapore, 10 Kent Ridge Crescent, 119260 Singapore

T. Y. F. Liew, B. A. Cheong, S. K. Chow, M. L. Ng, and J. P. Wang
Data Storage Institute, 5 Engineering Drive 1, 117608 Singapore

(Received 10 April 2000; accepted for publication 28 August 2000)

Cubic aluminum nitride (*c*-AlN) thin films have been deposited at room temperature on silicon substrates by nitrogen-ion-assisted pulsed laser ablation of a hexagonal AlN target. The deposited thin films exhibit good crystal properties with sharp x-ray diffraction peaks. The influences of the nitrogen ion energy on the morphological, compositional, and electronic properties of the AlN thin films have been studied. The nitrogen ions can effectively promote the formation of Al–N bonds and improve the crystal properties of the deposited thin films. A nitrogen ion energy of 400 eV is proposed to deposit high quality *c*-AlN thin films. © *2000 American Institute of Physics*. [S0021-8979(00)03623-9]

I. INTRODUCTION

Aluminum nitride is increasingly receiving high interest from the material research community due to its wide band gap, high thermal conductivity, high electrical resistivity (dielectric constant), and good acoustic properties.[1–3] Many research groups are exploring the synthesis of high quality AlN. Some experimental methods have been used to deposit AlN thin films, including metalorganic chemical vapor deposition,[4] plasma-assisted molecular beam epitaxy,[5–7] rf reactive magnetron sputtering,[8–11] ion-assisted chemical vapor deposition[12] and pulsed laser deposition (PLD).[13–19] Most of the deposition methods require high substrate temperatures (normally above 800 C) although the defects, both in the thin films and at the interface between the substrate and the thin film, cannot be avoided.[6] Such a high substrate temperature is undesirable for semiconductor industries and, therefore, impedes the practical applications of the AlN material. To date, most of the deposited AlN thin films have hexagonal structures with a highly textured orientation of (0001) on sapphire, silicon, and glass substrates.

In this study, PLD was used to deposit AlN thin films on silicon substrates at room temperature. PLD has been proven to be suitable to fabricate AlN thin films on silicon and sapphire substrates.[13–19] In the experiments, nitrogen-ion-assisted PLD combines the advantages of both PLD and ion bombardment. With this technology, we can independently control the energy of the AlN radicals in the ablated plasma as well as the nitrogen ions in the ion beam to determine the optimal conditions to obtain high quality thin films. Moreover, the nitrogen ion implantation can also compensate for the loss of nitrogen species in the ablation process.

[a]Electronic mail: eleluyf@nus edu sg

II. EXPERIMENT

In the experimental set up, as shown in Fig. 1, a KrF excimer laser at a wavelength of 248 nm was used as a light source to ablate an AlN target. The deposition was carried out on a PLD system with a background vacuum of 1×10^{-6} Torr. The AlN target with a hexagonal crystal structure and a purity of 99.995% was mounted on a target holder that was rotated by an external motor. The target was placed 2 cm away from the substrate surface. The laser pulse duration was 30 ns. The laser fluence at the target was around 2 Jcm^{-2} with a repetition rate of 10 Hz. The laser spot size on the target surface was about 5 mm^2. A nitrogen ion beam which was produced by a 1 cm Kaufman-type ion source irradiated the substrate surface spontaneously to assist the deposition. The ion flux was adjusted in a range of 1–2 $\mathrm{mA/cm}^2$. The energetic nitrogen ions traveled 10 cm distance before arriving on the substrate. The incident angle of the ion beam was 45 . By monitoring the microbalance mounted on the substrate, the deposition rate was set at $\leqslant 1$ Å/s by adjusting the ion beam flux. Si(100) wafers were used as substrates. Before deposition, the polished Si (100) substrates were cleaned by acetone in an ultrasonic bath.

X-ray diffraction (XRD), x-ray photoelectron spectroscopy (XPS), Raman spectroscopy, and Fourier transfer infrared (FTIR) spectroscopy measurements were carried out to characterize the crystal, compositional, and electronic properties of the deposited thin films. XRD measurements were performed on a Philips X'Pert-MRD system. Cu $K\alpha$ irradiation with an average wavelength of 1.5418 Å was used as the x-ray source in the diffraction measurements. XPS measurements were carried out using a Mg $K\alpha$ 1253.6 eV x-ray source with power of 300 W. Raman spectroscopy measurements were done on a Renishaw Raman Scope. FTIR measurements were carried out by a micro-FTIR spectrometer (model FTS 6000 by BIO-RAD).

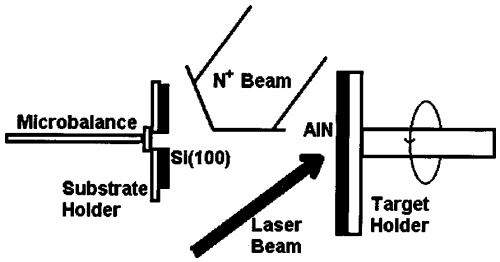

FIG 1 Experimental setup In a vacuum chamber, a KrF excimer laser beam is focused to ablate a ceramic AlN target which is rotated by an external motor A N^+ beam is bombarding on the substrate surface simultaneously to assist the AlN deposition A microbalance where Si substrates are attached is use to monitor the deposition rate the AlN thin films

III. RESULTS AND DISCUSSIONS

Figure 2 shows the XRD θ–2θ spectrum of an AlN thin film deposited with 400 eV N^+ bombardment. In the spectrum, besides the Si(200) and Si(400) diffraction peaks, there are four obvious peaks at 2θ=38.37 , 44.74 , 65.58 , and 78.09 , corresponding to orientations of (111), (200), (220), and (311), respectively, of the *c*-AlN crystalline with rocksalt structure[20] though the crystal structure of the target is hexagonal. The formation of cubic crystal structures of AlN on Si(100) substrates is unique compared with most of other works where hexagonal crystal structures were formed.[15 18 19] In other studies[6 7] of the microstrucrures and initial stages of thin film deposition, AlN films formed an initial amorphous region at the interface between the substrate and the thin film, followed by *c*-axis oriented columnar grains. Substrate temperature above 600 C can significantly reduce the amorphous region at the interface and promote the hexagonal (0001) orientation of AlN. However, in this study, since high substrate temperature was not used, the *c*-axis orientated growth of hexagonal AlN was not promoted. Instead, another metastable state of cubic crystalline AlN was obtained, although the hexagonal AlN crystal is possibly more stable due to its close packed stacking.

In the experiments, AlN thin films were also deposited without N^+ bombardment. The deposited thin films exhibit no XRD peaks, indicating amorphous structures. This result

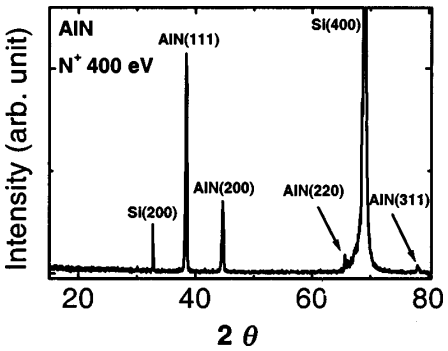

FIG 2 XRD θ–2θ spectrum of an AlN thin film deposited by KrF laser ablation with 400 eV N^+ bombardment at room temperature The laser fluence is 2 J/cm^2

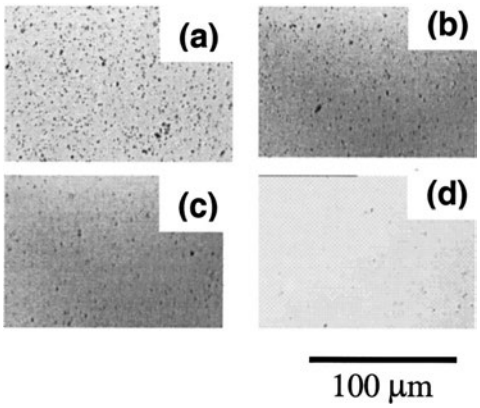

FIG 3 Optical microscopic images of AlN thin films deposited with different N^+ energies: (a) 0 (in N_2 atmosphere with a pressure of 100 mTorr), (b) 100, (c) 200, and (d) 400 eV

demonstrates the important role of the nitrogen ions in the synthesis of AlN thin films with cubic crystal structures. Moreover, N^+ energies lower than 400 eV lead to weaker and broader XRD peaks. Therefore, the nitrogen ions with the energy of 400 eV can effectively assist the formation of cubic crystalline in the deposited thin films. When nitrogen ion energy exceeds 400 eV, the deposition will be impeded due to the resputtering effect caused by the ion bombardment.

The deposition with the assistance of ion-beam bombardment is a nonequilibrium process. The low substrate temperature does not provide any energy for the equilibrium growth of crystalline AlN. The deposition is accomplished with energetic ions of hundreds eV. Therefore, the crystalline growth mechanism is quite different from other deposition methods where high substrate temperatures and low ion energies were employed. Hexagonal AlN thin films were deposited by PLD at substrate temperature higher than 675 C[15 18] and by rf magnetic sputtering and molecular beam epitaxy with substrate temperature higher than 400 C[6 9 10 19] on silicon[6 9 18] and glass substrates.[10] However, in this study, the *c*-axis oriented growth which leads to hexagonal structures is not possible due to the lack of high substrate temperatures. On the contrary, the energetic nitrogen ions of 400 eV promote the formation of cubic AlN crystals.

Figures 3(a)–3(d) present the surface morphologies of the AlN thin films deposited with different N^+ energies of (a) 0 (in N_2 atmosphere with a pressure of 100 mTorr), (b) 100, (c) 200, and (d) 400 eV, respectively. The effect of N^+ bombardment is quite obvious. In Fig. 3(a), there is a high area density of large particles on the surface of the thin film deposited in N_2 atmosphere without N^+ assistance. However, in the case of deposition with N^+ assistance, especially with N^+ energy of 400 eV, the formation of large particles in the deposited thin films can be effectively eliminated, as shown from Fig. 3(b)–3(d). The surface morphology in Fig. 3(d) is smooth and nearly free of large particles.

The large particles in the deposited thin films can be formed in two possible ways. First, laser ablation of a solid

target can produce large particles in the ablated plasma. The ablated large particles propagate towards the substrate and deposit on the substrate surface. The other way is the aggregation of atoms and small radicals in the plasma into large particles during the rapid cooling process after the ablation. The ablated atoms and radicals have very high cooling rate that can be estimated by[21]

$$\dot{T}=\left(\frac{6}{D\rho C_p}\right)\epsilon\sigma(T^4-T_0^4), \tag{1}$$

where D is the radical diameter, ρ is the material density, C_p is the heat capacity of the material, ϵ is the radiant emissivity, σ is the Boltzmann constant, T is the temperature of the radical, and T_0 is the ambient temperature. For a molten droplet of AlN, it can be assumed that the physical properties of the droplet are similar to those of the bulk material. According to the calculations[21] and experimental measurements of inorganic compounds such as BN and YBCO,[22] the cooling rate of the inorganic compounds is of the order of 10^6 K/s. In this experiment, assuming that the velocity of the ablated radical is around 100 ms^1,[21] the temperature reduction of the ablated radical before it reaches the substrate is in the order of 10^2-10^3 K. Such a rapid cooling process is accompanied by the aggregation of small radicals into large ones in the plasma. According to Eq. (1), the cooling rate for the small size radical should be higher than that of the large one. The aggregation and cooling processes can be accomplished by collisions among the small radicals during the expansion of the plasma. In this experiment, the N_2 atmosphere with pressure of 100 mTorr accelerates the cooling process through the collisions between the N_2 molecules and the ablated AlN radicals. Therefore, a high density of large particles is resulted in the thin films deposited in 100 mTorr N_2 atmosphere. In the case of N^+-assisted deposition as in Figs. 3(b)–3(d), the energetic N^+ can provide ablated AlN radicals with kinetic energy through collisions with them and, hence, raise the equivalent temperature of the ablated radicals. Considering an AlN radical composed of 10,000 atoms, its inelastic collision with a 400 eV nitrogen ion can lead to an average temperature rise of 300 K for each atom with the assumption that all the kinetic energy is transferred to temperature rise. Such a temperature rise is comparable to the temperature reduction of the ablated radical propagating from the target surface to the substrate. Therefore, collisions with N^+ can reduce the cooling rate of the ablated radicals and, therefore, reduce the opportunity to form large particles in the plasma expansion. Moreover, the energetic N^+ can also bombard the deposited large particles on the substrate surface and reduce their size. Therefore, in our experiment, a higher N^+ energy is preferred in the attempt to eliminate large-size particles in the deposited thin films.

The compositional and electronic properties of the AlN thin films were analyzed by XPS measurements. The atomic [N]:[Al] ratio of the deposited thin films is in the range of 0.68–1.12, as shown in Fig. 4. The ratio is much lower than 1.0 when the deposition was carried out in N_2 atmosphere with a pressure of 100 mTorr. On the contrary, in the case of N^+-assisted deposition, the [N]:[Al] value is always higher than 1.0 due to the continuous supply of nitrogen atoms into the thin films. The [N]:[Al] value saturates at 1.12 when N^+ energy increases to 400 eV with a deposition rate about 1 Å/s.

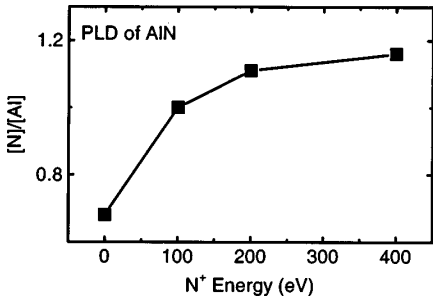

FIG 4 Atomic ratio of [N]:[Al] as a function of N^+ energy, determined by XPS measurement results

Although most researchers reported that the films deposited by PLD have compositions similar to those of the targets, the deposited thin films are usually deficient in the element with lower melting temperature.[21] In this experiment, thin film deposition without N^+ assistance result in a [N]:[Al] value lower than 1.0. On the contrary, N^+ beam can compensate the loss of nitrogen element and, therefore, retain the physical and chemical properties of the AlN target.

Figure 5(a) shows the XPS Al $2p$ spectra of three AlN thin films deposited with different ion energies of 100, 200, and 400 eV. The dependence of the Al $2p$ peak position and their full width at half maximum (FWHM) on N^+ energy are illustrated in Fig. 5(b). It can be seen that the binding energy of Al $2p$ increases slightly with the increasing ion energy

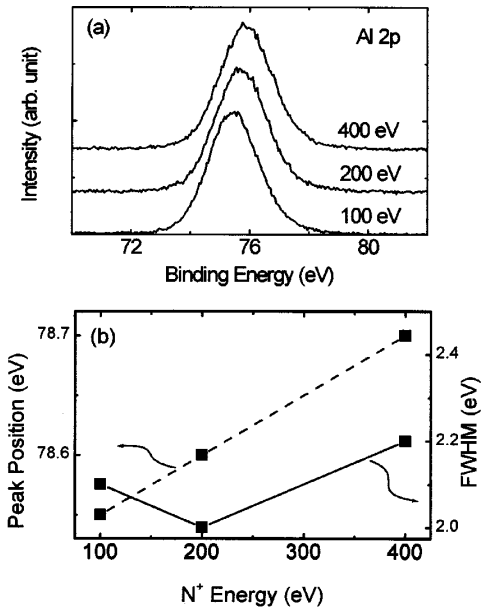

FIG 5 (a) XPS Al $2p$ spectra of AlN thin films deposited with 100, 200, and 400 eV N^+ bombardment (b) FWHM and peak position of the XPS Al $2p$ peaks as a function of N^+ energy

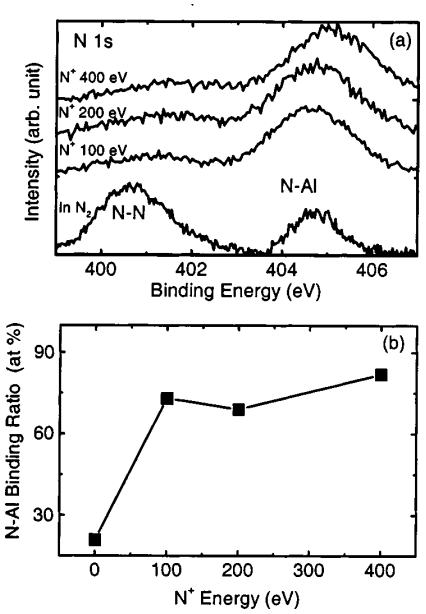

FIG 6 (a) XPS N 1*s* spectra of AlN thin films deposited in N_2 atmosphere with a pressure of 100 mTorr and with the assistance of N^+ with energies of 100, 200 and 400 eV (b) The influence of the N^+ energy on the N–Al binding ratio (defined by [N–Al]/{[N–Al]+[N–N]}) in the AlN thin films

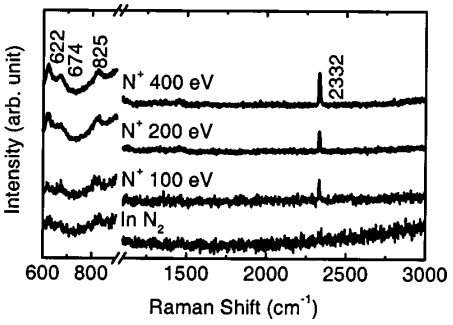

FIG 7 Raman spectra of AlN thin films deposited in N_2 atmosphere with a pressure of 100 mTorr and with the assistance of N^+ with different ion energies

from 100 to 400 eV. This is due to the formation of more AlN compounds owning to the high energies supplied by the nitrogen ions. Generally, the binding energy of the Al 2*p* electron in the AlN compound is higher than that in atomic aluminum due to less shielding effect. The increase in N^+ energy causes formation of more Al–N bonds and thus increases the average binding energy of the Al 2*p* electrons. The FWHM of the Al 2*p* peak increases slightly when N^+ energy increases to 400 eV, possibly due to the bombardment-induced disorders in the deposited thin films.

Figure 6(a) shows XPS N 1*s* spectra of AlN thin films deposited in N_2 atmosphere with a pressure of 100 mTorr and with the assistance of N^+ with different energies of 100, 200 and 400 eV. It can be seen that there are two nitrogen states, related to N–N and N–Al bonds. The difference between the thin films deposited with and without N^+ assistance is quite obvious. The thin film deposited in N_2 atmosphere has a very strong N–N peak while that deposited with N^+ assistance has a strong N–Al peak. The N^+ bombardment during the deposition promotes the formation of N–Al bonds and eliminates the formation of N–N bonds. The dependence of the ratio of [N–Al]/{[N–Al]+[N–N]} that reflects the percentage of the nitrogen elements contributing to the formation of N–Al bonds is illustrated in Fig. 6(b). It can be seen that less than 30% of the nitrogen atoms in the thin film deposited in N_2 atmosphere form bonds with Al atoms. This percentage increases to around 75% when N^+ is used to assist the deposition. It reaches the maximum of about 80% when N^+ energy is 400 eV. Therefore, the nitrogen ion energy about 400 eV is beneficial to the synthesis of AlN thin films with a high content of stable Al–N bonds.

Figure 7 shows the Raman spectra of AlN thin films deposited in N_2 atmosphere with a pressure of 100 mTorr and with assistance of N^+ bombardment with energies of 100, 200, and 400 eV. The peaks at 622, 674, and 825 cm^{-1} reflect the phonon modes of E_1 transverse optical (TO), A_1 longitudinal optical (LO), and E_1 longitudinal optical (LO), respectively.[23,24] The intensities of these Raman peaks increase with the increasing nitrogen ion energy from 100 to 400 eV, implying that the nitrogen ion energy of 400 eV is optimal to the PLD deposition of crystal AlN thin films, in coincidence with the results of XRD, XPS, and microscopic measurements. Besides these Raman peaks, there is a sharp and intense peak at 2332 cm^{-1} which is observed for the first time in the case of AlN fabrication. The intensity of this peak also increases with the nitrogen ion energy and reaches the maximum when ion energy increases to 400 eV. This new peak should originate from the structures of the *c*-AlN thin films deposited in this experiment.

Figure 8(a) illustrates the FTIR spectra of AlN thin films deposited under different ion energies of 100, 200, 300, and 400 eV respectively. The spectra were obtained by subtracting the background of the Si(100) substrate cut from the same wafer. A strong absorption peak at 725 cm^{-1} is quite obvious. This strong and broad asymmetric peak is believed to be composed of several phonon modes with Lorentzian distributions: A_1(TO) at 514 cm^{-1}, A_1(LO) at 650–746 cm^{-1}, E_1(TO) at 514 cm^{-1}, and E_1(LO) at 765–790 cm^{-1}.[19,23] The FTIR peak position at 725 cm^{-1} does not shift with the N^+ energy change from 100 to 400 eV. Inside the deposited thin films, there is hydrostatic stress that induces shift of FTIR peaks from their characteristic positions. According to a recent publication,[19] the presence of hydrostatic stress in the AlN thin films can result in FTIR peaks shifting toward higher wave number. The FTIR results in this experiment suggest that the N^+ beam with energies higher than 100 eV can saturate the hydrostatic stress in the deposited thin films. However, N^+ energy still has significant influences on the structural and electrical properties of the deposited thin films. The FTIR peak width is increased when N^+ energy increases from 100 to 400 eV, as shown in Fig. 8(b). The increase of ion energy leads to a high level of disorder and thus an increase of peak width in the FTIR spectra. The peak at 2360 cm^{-1} is caused by the fluctuation of the atmo-

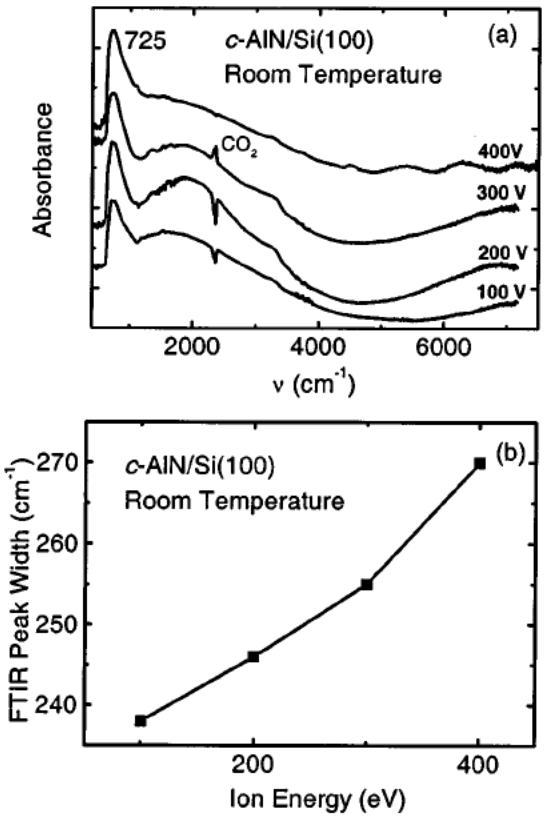

FIG. 8. (a) FTIR spectra of AlN thin films deposited under N^+ bombardment with different energies of 100, 200, 300, and 400 eV. The ion beam flux was kept at 2 mA/cm^2. In the deposition, the substrate was left at room temperature. (b) The dependence of FTIR peak width on N^+ energy.

spheric CO_2 density during the measurements of the silicon substrate and the samples.

IV. CONCLUSIONS

c-AlN thin films have been deposited at room temperature on Si(100) substrates by pulsed laser ablation of an AlN target with N^+ implantation. The deposited thin films exhibit cubic crystal structures though the target is hexagonal. The N^+ beam can improve the surface smoothness and eliminate the formation of large particles in the deposited thin films. The N^+ beam can also compensate the loss of nitrogen in the thin films and promote the formation of Al–N bonds. The crystal property can be improved by the N^+ beam. A N^+ energy of 400 eV is optimal to produce *c*-AlN thin films with good crystal and electronic properties.

ACKNOWLEDGMENTS

The authors would like to thank H. L. Koh and Y. W. Goh for their technical assistance in this research work.

[1] R. L. Lambrecht, Mater. Res. Soc. Symp. Proc. **339**, 565 (1994).
[2] F. A. Ponce *et al.*, Nitride Semiconductors Symposium, Boston, MA, 1–5 December 1997 (Materials Research Society, Pittsburgh, 1998).
[3] K. A. Jones *et al.*, J. Appl. Phys. **83**, 8010 (1998).
[4] P. Kung, A. Saxler, X. Zhang, D. Walker, T. C. Wang, I. Furguson, and M. Razeghi, Appl. Phys. Lett. **66**, 2958 (1995).
[5] K. S. Stevens, A. Ohtani, M. Kinniburgh, and R. Beresford, Appl. Phys. Lett. **65**, 321 (1994).
[6] G. W. Auner, F. Jin, V. M. Naik, and R. Naik, J. Appl. Phys. **85**, 7879 (1999).
[7] J. R. Heffelfinger, D. L. Medlin, and K. F. Mccarty, J. Appl. Phys. **85**, 466 (1999).
[8] W. J. Meng, J. Heremans, and Y. T. Chang, Appl. Phys. Lett. **59**, 2097 (1991).
[9] E. Dogheche, D. Remiens, A. Boudrioua, and J. C. Loulergue, Appl. Phys. Lett. **74**, 1209 (1999).
[10] A. Rodriguez-Navarro, W. Otano-Rivera, L. J. Pilione, R. Messier, and J. M. Garcia-Ruiz, J. Vac. Sci. Technol. A **16**, 1244 (1998).
[11] H. Y. Joo, H. J. Kim, S. J. Kim, and S. Y. Kim, J. Vac. Sci. Technol. A **17**, 862 (1999).
[12] J. C. Sanchez-Lopez, L. Contreas, A. Fernandez, A. R. Gonzalez-Elipe, J. M. Martin, and B. Vacher, Thin Solid Films **317**, 100 (1998).
[13] T. F. Huang and J. S. Harris, Jr., Appl. Phys. Lett. **72**, 1158 (1998).
[14] V. Talyansky *et al.*, Thin Solid Films **323**, 37 (1998).
[15] G. S. Sudhir *et al.*, Appl. Surf. Sci. **127**, 471 (1998).
[16] R. D. Vispute, J. Narayan, and J. D. Budai, Thin Solid Films **299**, 94 (1997).
[17] M. He, N. Cheng, P. Zhou, H. Okabe, and J. B. Halpern, J. Vac. Sci. Technol. A **16**, 2372 (1998).
[18] A. Kumar, H. L. Chan, J. J. Weimer, and L. Sanderson, Thin Solid Films **308–309**, 406 (1997).
[19] K. Jagannadham, A. K. Sharma, Q. Wei, R. Kalyanraman, and J. Narayan, J. Vac. Sci. Technol. A **16**, 2804 (1998).
[20] H. Vollstadt, Proc. Jpn. Acad., Ser. B: Phys. Biol. Sci. **66**, 7 (1990).
[21] D. B. Chrisey and G. K. Hubler, *Pulsed Laser Deposition of Thin Films* (Wiley, Toronto, 1994), Chap. 6.
[22] D. B. Geohegan, Mater. Res. Soc. Symp. Proc. **285**, 27 (1993).
[23] C. Carlone, K. M. Lakin, and H. R. Shanks, J. Appl. Phys. **55**, 4010 (1984).
[24] L. E. McNeil, M. Grimsditch, and R. H. French, J. Am. Ceram. Soc. **76**, 1132 (1993).

ELSEVIER

Thin Solid Films 382 (2001) 56–60

thin solid films

www.elsevier.com/locate/tsf

Structural properties of AlN films grown on Si, Ru/Si and ZnO/Si substrates

Won Taeg Lim*, Byoung Keun Son, Dong Hae Kang, Chang Hyo Lee

Department of Physics, Hanyang University, Seoul 133-791, South Korea

Received 3 February 2000; received in revised form 3 August 2000; accepted 27 September 2000

Abstract

The structural properties of r.f.-sputtered AlN films grown on Si, Ru/Si, and ZnO/Si substrates were investigated. From the X-ray diffraction analysis, the crystallite size, biaxial stress and standard deviation (S.D.) of the rocking curve for the AlN films are calculated. For AlN films prepared on Si substrates, a crystallite size of 205.7 Å, a biaxial stress of -3.27×10^9 Pa and a S.D. of 5.96° were obtained. For the AlN films prepared on the Ru/Si substrates, a crystallite size of 213.4 Å, a biaxial stress of -9.80×10^9 Pa and a S.D. of 4.05° were obtained. Likewise, a crystallite size of 293.4 Å, a biaxial stress of $+1.62\times10^9$ Pa and a S.D. of 1.19° were obtained for the AlN films prepared on the ZnO/Si substrates. It is concluded that the ZnO/Si substrates are the most suitable for growing AlN films, compared with the other substrates. In addition, the strong *c*-axis orientation of the AlN films on the ZnO/Si substrates is found to have a direct relationship with the density of the films. It is shown that the growth behavior and quality of the AlN films can be successfully controlled by lattice matching with their substrates.

Keywords: Structural properties; Sputtering; Aluminum nitride; X-Ray diffraction; Scanning electron microscopy

1. Introduction

Aluminum nitride (AlN) thin films are useful materials for surface acoustic wave (SAW) devices because of their low acoustic loss and high ultrasonic velocity [1–3]. To obtain good SAW characteristics, it is necessary that the piezoelectric axis (*c*-axis) is uniformly oriented in the same direction within the AlN films. AlN thin films have been prepared on a variety of substrates using several techniques [4–11]. The selection of a substrate is a very important factor for the epitaxial growth of the AlN film, because the matching between the film and the substrate in the lattice parameter and the crystal structure significantly affects the growth habit of the films.

In our previous paper, we reported the correlation between the *c*-axis orientation of ZnO films and substrates [12]. The Ru/Si and the Al/Si substrates were used for the growth of the ZnO films. It was found that the Ru/Si substrates are more suitable substrate for growing the ZnO films than the Al/Si substrates, because the Ru metal has the hexagonal-closed-packed (HCP) structure which is the same structure as the ZnO films.

In this study, we have prepared three kinds of substrates; Si wafer, Ru/Si and ZnO/Si for the growth of AlN films. AlN thin films were deposited on the substrates by reactive sputtering of an Al metal target. The structural properties of the films were investigated.

2. Experimental

AlN thin films were grown on the Si(100), the Ru (~230 nm)/Si and the ZnO (~400 nm)/Si substrates

* Corresponding author. Tel.: +82-2-2290-0917; fax: +82-2-2295-6868.

E-mail address: wtlim@orgio.net (W.T. Lim).

0040-6090/01/$ - see front matter
PII: S0040-6090(00)01780-6

Table 1
Sputtering conditions of the AlN, Ru and ZnO thin films

	AlN	Ru	ZnO
Target	Al metal	Ru metal	ZnO ceramic
r.f. power density (W/cm^2)	5.92	2.47	5.92
Substrate temperature (°C)	150	400	400
Working gases	N_2/Ar = 1/2	Ar	O_2/Ar = 1/5
Working pressure (Pa)	0.07	0.66	0.47
Growth rate (nm/min)	8.4	30	70
Thickness (nm)	500–600	230	400
Target-to-substrate distance (mm)	50	60	50

by an r.f. magnetron sputtering system. The sputtering target for AlN was a 2-inch disk of Al (purity 99.999%, PureTech Co.) metal. The sputtering conditions are listed in Table 1. The base pressure was less than 10^{-4} Pa before deposition.

Reactive sputtering was carried out in a mixture of argon and nitrogen in order to deposit the AlN films. The Ar and N_2 flow rates were separately controlled by mass-flow-controllers (MFC). The substrate temperature, N_2/Ar flow ratio, working pressure, and input r.f. power were fixed at 150°C, 1/2, 0.07 Pa and 120 W, respectively. These were the optimal conditions for growing the AlN films with high *c*-axis orientation in our experiments.

The crystallographic characteristics of the AlN thin films were analyzed by X-ray diffraction (XRD) methods using CuKα radiation (Rigaku Co., Model D/MAXI-A). The cross-sectional view of the films was observed by a field-emission scanning electron microscope (FE-SEM). The film thickness was measured with a surface profilometer (Dektak III).

3. Results and discussion

Fig. 1 shows the XRD patterns of the AlN films grown on the various substrates. Fig. 1a–c represents the AlN films deposited on the Si, the Ru/Si and the ZnO/Si substrates, respectively. The AlN films deposited on the ZnO/Si substrates (AlN/ZnO/Si) have the highest intensity of the (002)-oriented peak, compared with the films deposited on the other substrates. The (002)-peak intensity of the AlN films on the ZnO/Si substrates is approximately 10 times stronger than that of the film on the Ru/Si substrates, and also, surprisingly, 30 times stronger than that of the films on the Si wafers. It is observed that the AlN/ZnO/Si films have only the (002) peak, while both the AlN/Ru/Si and AlN/Si films have a small intensity of (101) as well as the (002) peak. These results mean that the structural properties of the AlN films are closely related to their substrates. We believe that the AlN/ZnO/Si and AlN/Ru/Si films have a better *c*-axis-oriented structure than AlN/Si, because the ZnO and Ru layers have the same structure of HCP as the AlN films. A similar result was obtained in our previous paper [12]. In particular, the AlN/ZnO/Si films are much more *c*-axis-oriented than AlN/Ru/Si, even though both ZnO and Ru have the HCP structure. This is, we think, due to a smaller lattice mismatch between the AlN films and the ZnO substrates. The lattice constants are given as follows: $a = 3.111$ Å and $c = 4.979$ Å for AlN (JCPDS no. 25-1133); $a = 3.245$ Å and $c = 5.206$ Å for ZnO (JCPDS no. 36-1451); and $a = 2.706$ Å and $c = 4.282$ Å for Ru (JCPDS no. 6-0663). The lattice mismatch between AlN and ZnO, which is defined as $[(a_{AlN} - a_{ZnO})/a_{ZnO}]$, in the direction of the

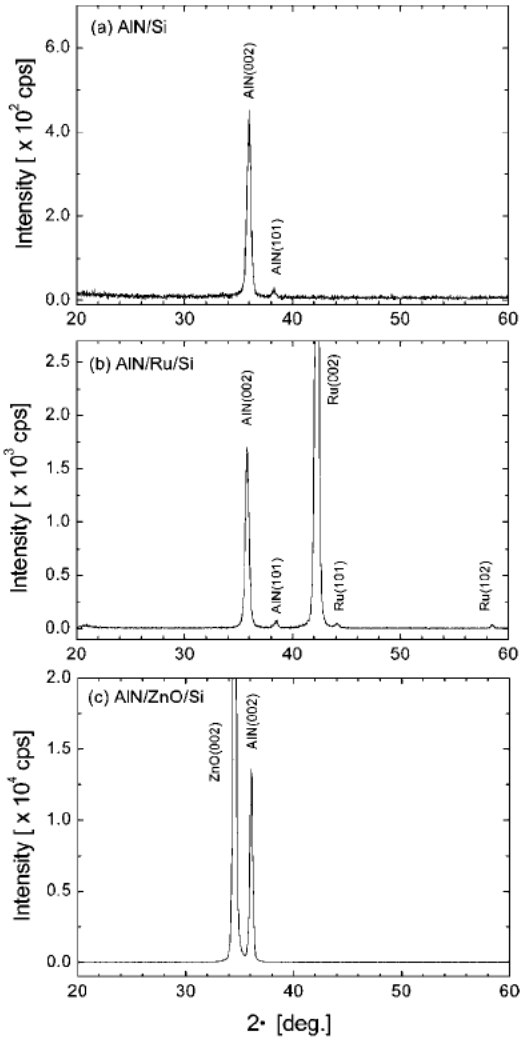

Fig. 1. The XRD patterns of AlN films grown on (a) Si wafers, (b) Ru/Si substrates, (c) ZnO/Si substrates.

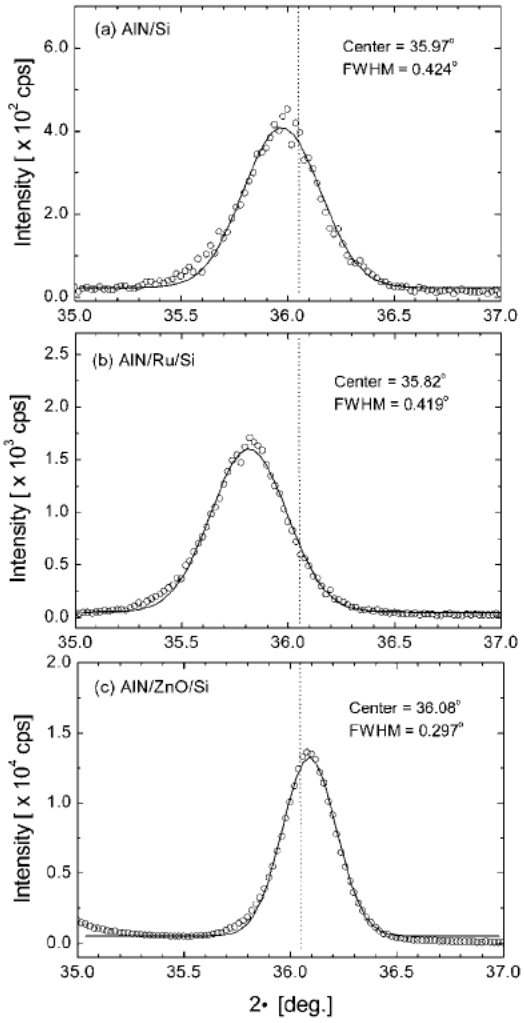

Fig. 2. The (002)-oriented peak of AlN films grown on (a) Si wafers, (b) Ru/Si substrates, (c) ZnO/Si substrates. The dotted line indicates the (002) peak position of 36.04° for an AlN powder sample.

a-axis is −4.1%, and that between AlN and Ru is approximately +15%.

To accurately observe the (002) peak of the AlN films, the above XRD patterns were replotted in Fig. 2.

Table 2
Characteristics of the AlN thin films grown on various substrates

	AlN/Si	AlN/Ru/Si	AlN/ZnO/Si
FWHM (radians)	7.40×10^{-3}	7.13×10^{-3}	5.18×10^{-3}
Crystallite size (Å)	205.7	213.4	293.4
c-Lattice constant (Å)	4.989	5.009	4.974
Strain ε_z	$+2.01\times10^{-3}$	$+6.03\times10^{-3}$	-1.00×10^{-3}
Stress (Pa)	-3.27×10^{9}	-9.80×10^{9}	$+1.62\times10^{9}$

The dotted line in the figure indicates the (002) peak position of 36.04° for an AlN powder sample. The crystallite size of the films was calculated from the full width at half maximum (FWHM) of the (002) diffraction peak by the Sherrer equation [13,14]: $D = 0.94\lambda/(B\cos\theta)$, where λ is the X-ray wavelength (λ = 1.5405 Å) and B is the FWHM in radians. The calculated crystallite sizes of the AlN films are as follows: 205.7 Å for AlN/Si, 213.4 Å for AlN/Ru/Si and 293.4 Å for AlN/ZnO/Si, respectively.

The biaxial stress of the AlN films was calculated from measuring the *c*-lattice constant. The biaxial stress σ is related to the *c*-axis strain by the modulus of elasticity [15]:

$$\sigma = [(2C_{13} - (C_{11} + C_{12})(C_{33}/C_{13}))]\varepsilon_z$$

where C_{ij} are the elastic constants for AlN, given as $C_{11} = 396$ GPa, $C_{12} = 137$ GPa, $C_{13} = 108$ GPa and $C_{33} = 373$ GPa [16]. By using these values, it is found that the tensile *c*-axis strain is proportional to the compressive biaxial stress, and is given by $\sigma = -1.6248 \times 10^{12}\ \varepsilon_z$ (Pa). The film strain ε_z along the *c*-axis is given by $\varepsilon_z = (c - c_0)/c_0$, where c_0 is the strain-free lattice parameter ($c_0 = 4.979$ Å) measured from an AlN powder sample, and the lattice constant c is equal to twice the interplanar spacing d, measured from the position of the (002) peak using the Bragg equation. The stresses of the films are calculated: -3.27×10^9 Pa for AlN/Si, -9.80×10^9 Pa for AlN/Ru/Si, and $+1.62\times10^9$ Pa for AlN/ZnO/Si. The lowest value of stress is obtained in the AlN/ZnO/Si film. In addition, it is observed that the biaxial stress is tensile for AlN/ZnO/Si, and compressive for AlN/Ru/Si and AlN/Si. Such results indicate that the amount of stress and the type of stress in the AlN films are correlated with the mismatch of the *a*-lattice constant between the AlN films and substrates. All results are given in Table 2.

Fig. 3 shows the S.D. of the rocking curve, s, of the (002) peak for the AlN films. The rocking curves, which are the solid lines in the figure, are found to fit well with the Gaussian distribution. The S.D. values of the AlN films are as follows: $s = 5.96°$ for AlN/Si, $s = 4.05°$ for AlN/Ru/Si, and $s = 1.19°$ for AlN/ZnO/Si. The AlN/ZnO/Si films have the smallest S.D., which means that they have the highest quality of *c*-axis orientation. The S.D. of 1.19° is a lower value than that reported by some researchers [4,5,17].

From the XRD analysis, it is found that the AlN films deposited on the ZnO/Si substrate have the highest intensity of the (002) peak and the lowest S.D. of the *c*-axis. This indicates that the ZnO/Si substrates are quite suitable for the growth of AlN films with high *c*-axis orientation.

Fig. 4 shows the SEM images of the AlN/Si, AlN/Ru/Si and the AlN/ZnO/Si films. It is observed that the AlN/ZnO/Si and the AlN/Ru/Si films are much denser than the AlN/Si. The AlN/Si films show a columnar structure with voids between the columns, while the AlN/ZnO/Si and the AlN/Ru/Si films show a dense structure without any columns. It is thought that the higher *c*-axis orientation of the AlN/ZnO/Si and the AlN/Ru/Si films compared with the AlN/Si film, is closely related to their density.

4. Conclusions

The AlN films deposited on the ZnO/Si substrates have the highest *c*-axis orientation, compared with the films deposited on both the Ru/Si and Si wafers. The crystallite sizes calculated from XRD analysis are 205.7 Å for AlN/Si, 213.4 Å for AlN/Ru/Si, and 293.4 Å for AlN/ZnO/Si films. The biaxial stresses of the AlN films are calculated as -3.27×10^{9} Pa for AlN/Si, -9.80×10^{9} Pa for AlN/Ru/Si, and $+1.62\times10^{9}$ Pa for AlN/ZnO/Si. In addition, the S.D. values of the AlN films are found to be 5.96° for AlN/Si, 4.05° for AlN/Ru/Si, and 1.19° for AlN/ZnO/Si.

It is observed that the strong *c*-axis orientation of the AlN/ZnO/Si is closely related to the density of the films. The ZnO/Si is found to be a promising substrate for growing the AlN films. From this study, it is suggested that the growth behavior of the AlN films can be controlled by lattice matching with the substrates.

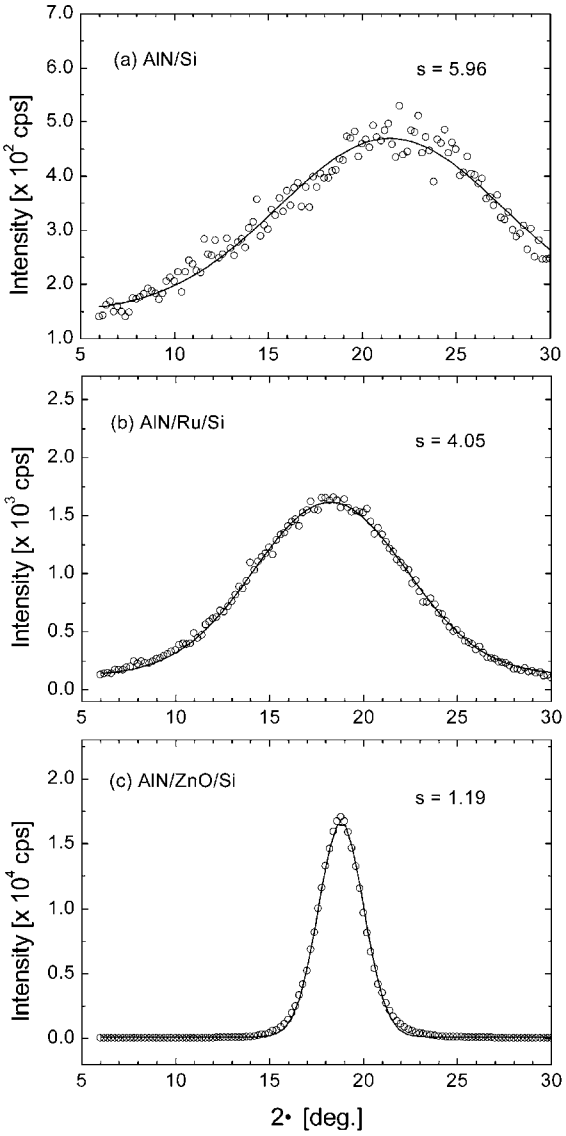

Fig. 3. The rocking curve of the (002) peak for AlN films grown on (a) Si wafers, (b) Ru/Si substrates, (c) ZnO/Si substrates.

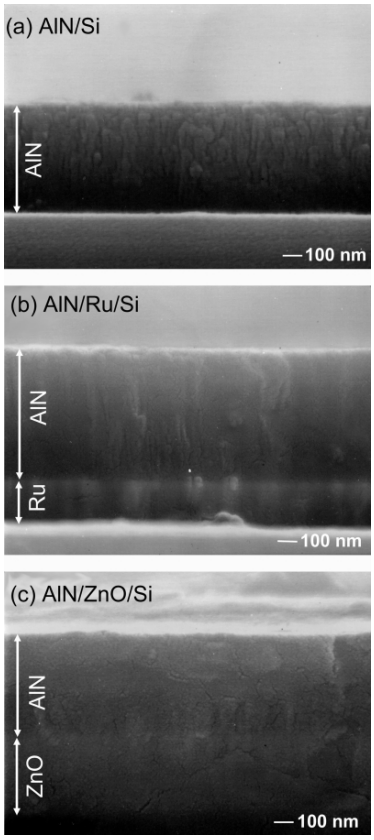

Fig. 4. The SEM images of AlN films grown on (a) Si wafers, (b) Ru/Si substrates, (c) ZnO/Si substrates.

Acknowledgements

The authors wish to acknowledge the financial support of Hanyang University, Korea, made in the program year of 1999.

References

[1] J.A. Ruffner, P.G. Clem, B.A. Tuttle, D. Dimos, D.M. Gonzales, Thin Solid films 354 (2000) 256.

[2] H. Okano, T. Tanaka, K. Shibata, Jpn. J. Appl. Phys. 31 (1992) 3017.
[3] M. Penza, M.F. De Riccardis, L. Mirenghi, M.A. Tagliente, E. Verona, Thin Solid Films 259 (1995) 154.
[4] K. Tominaga, T. Ao, I. Mori, K. Kusaka, T. Hanabusa, Jpn. J. Appl. Phys. 35 (1996) 4972.
[5] J.W. Soh, J.H. Kim, W.J. Lee, Jpn. J. Appl. Phys. 35 (1996) L1518.
[6] E. Dogheche, D. Remiens, A. Boudrioua, J.C. Loulergue, Appl. Phys. Lett. 74 (1999) 1209.
[7] K. Jagannadham, A.K. Sharma, Q. Wei, R. Kalyanraman, J. Narayan, J. Vac. Sci. Technol. A 16 (1998) 2804.
[8] S. Tungasmita, J. Brirch, P.O.A. Persson, K. Jarrendahl, L. Hultman, Appl. Phys. Lett. 76 (2000) 170.
[9] J. Meinschien, F. Falk, R. Hergt, H. Stafast, Appl. Phys. A 70 (2000) 215.
[10] G. Ferro, H. Okumura, T. Ide, S. Yoshida, J. Crystal Growth 210 (2000) 429.
[11] A.E. Gorodetsky, R.Kh. Zalavutdinov, A.P. Zakharov, W.L. Hsu, B.V. Spitsyn, L.L. Bouilov, V.P. Stoyan, Diamond Relat. Mater. 8 (1999) 1267.
[12] W.T. Lim, C.H. Lee, Thin Solid Films 353 (1999) 12.
[13] L.V. Azavoff, Elements of X-ray Crystallography, McGraw-Hill, New York, 1968.
[14] B.D. Culity, Elements of X-ray Diffraction, Addison-Wesley, Reading, MA, 1978.
[15] M.K. Puchert, P.Y. Timbrell, R.N. Lamb, J. Vac. Sci. Technol. A 14 (1996) 2220.
[16] A.F. Wright, J. Appl. Phys. 82 (1997) 2833.
[17] M Akiyama, C. Xu, K. Nonaka, K. Shoubu, T. Watanabe, Thin Solid Films 315 (1998) 62.

Thin Solid Films
Volume 382, Issues 1–2, 1 February 2001, Pages 56-60

Structural properties of AlN films grown on Si, Ru/Si and ZnO/Si substrates

Won Taeg Lim, Byoung Keun Son, Dong Hae Kang, Chang Hyo Lee

Show more

https://doi.org/10.1016/S0040-6090(00)01780-6

Abstract

The structural properties of r.f.-sputtered AlN films grown on Si, Ru/Si, and ZnO/Si substrates were investigated. From the X-ray diffraction analysis, the crystallite size, biaxial stress and standard deviation (S.D.) of the rocking curve for the AlN films are calculated. For AlN films prepared on Si substrates, a crystallite size of 205.7 Å, a biaxial stress of -3.27×10^9 Pa and a S.D. of 5.96° were obtained. For the AlN films prepared on the Ru/Si substrates, a crystallite size of 213.4 Å, a biaxial stress of -9.80×10^9 Pa and a S.D. of 4.05° were obtained. Likewise, a crystallite size of 293.4 Å, a biaxial stress of $+1.62\times10^9$ Pa and a S.D. of 1.19° were obtained for the AlN films prepared on the ZnO/Si substrates. It is concluded that the ZnO/Si substrates are the most suitable for growing AlN films, compared with the other substrates. In addition, the strong *c*-axis orientation of the AlN films on the ZnO/Si substrates is found to have a direct relationship with the density of the films. It is shown that the growth behavior and quality of

the AlN films can be successfully controlled by lattice matching with their substrates.

Previous Next

Keywords

Structural properties; Sputtering; Aluminum nitride; X-Ray diffraction; Scanning electron microscopy

Recommended articles Citing articles (37)

View full text

Table of contents

Volume 39

Part 2, Number 5A, May 2000

‹ Previous issue Next issue ›

Open all abstracts

Semiconductors

General Physics

Magnetic Promotion and Quenching of Surface Oxidation with Pt Catalyst

L436

Nobuko I. Wakayama

+ Open abstract View article PDF

JOURNAL LINKS

Submit an article

About the journal

Editorial board

Author guidelines

Publication charges

News and editorial

Awards

Journal collections

Pricing and ordering

Contact us

Applied Physics Express

Appendix 1036

Pergamon

Vacuum/volume 51/number 4/pages 641 to 646/1998

0042 207X/98 $ see front matter

PII: S0042-207X(98)00265-6

High-rate reactive DC magnetron sputtering of oxide and nitride superlattice coatings

W D Sproul,*, *Sputtered Films, Inc., 320 Nopal Street, Santa Barbara, California 93103, U.S.A.*

Over the past 10 years, there have been three major advancements in reactive sputtering technology that now make it possible to deposit both conductive and non-conductive fully-dense films at high rates. These three advances are unbalanced magnetron sputtering, partial pressure control of the reactive gas, and pulsed dc power. Multicathode unbalanced magnetron sputtering systems provide a dense secondary plasma that is used for producing a well-adhered, fully dense film that is difficult to achieve with conventional magnetron sputtering. Online automatic partial pressure control of the reactive gas prevents the poisoning of the target surface during deposition, which leads to compound film deposition rates that approach or are equal to those for the pure metal rate. Pulsed dc power, where the polarity of the voltage on the sputtering target is alternately switched briefly between negative and positive, prevents arcing on the target surface during the deposition of nonconducting films. With both pulsed dc power and partial pressure control of the reactive gas, films such as aluminum oxide can now be deposited reactively at rates up to 78% of the pure metal rate. The reactive unbalanced magnetron sputtering process is used to deposit polycrystalline nitride superlattice films such as TiN/NbN or TiN/VN with hardnesses exceeding 50 GPa, which is more than double the hardness of either component in the multilayered film. The nitride superlattice work is being extended to oxide films, and initial results are encouraging. Nanometer scale, multilayer Al_2O_3/ZrO_2 and Y_2O_3/ZrO_2 films have been deposited at high rates. The Al_2O_3/ZrO_2 films are amorphous and optically clear, whereas the Y_2O_3/ZrO_2 films are crystalline as well as being optically clear. © *1998 Published by Elsevier Science Ltd. All rights reserved*

Introduction

Since the middle 1980s, there have been three major advance ments in sputtering technology that have greatly affected the ability to reactively sputter fully dense, well adhered films at high deposition rates. In 1986, Window and Savvides[1–3] intro duced the concept of unbalanced magnetron sputtering, and in the years since, it has been widely embraced by the sputtering community. Combined with partial pressure control of the reactive gas during the reactive sputter deposition of coatings, unbalanced magnetron sputtering today is one of the primary techniques for the deposition of hard coatings.

Most recently, the introduction of pulsed direct current (dc) power is already having an important effect on the reactive sputtering of non conducting films such as aluminum oxide (Al_2O_3). The combination of partial pressure control of the reactive gas, unbalanced magnetron sputtering, and pulsed dc power is a powerful tool for the high rate reactive deposition of compound films. Each of these three techniques will be reviewed, and then they will be looked at together to show the full potential for the synergistic effects for the deposition of non conducting films.

*To whom all correspondence should be addressed

Unbalanced magnetron sputtering

A conventional magnetron sputtering cathode has magnets located along the outer edge and the centerline or at the center if the cathode is round. If the strength of the inner and outer magnets is roughly equal, the magnetron is said to be balanced, and most of the magnetic field lines will loop between the inner and outer magnets as is shown in Figure 1. If one of the sets of magnets is made stronger than the other, then the magnetron becomes unbalanced. Typically the outer set of magnets in the magnetron cathode is made stronger than the inner ones. Although there is still linkage between magnetic fields of the inner and outer magnets, not all of the field line will make the link. The excess field lines from the stronger magnets will radiate away from the magnet surfaces as is shown in Figure 2.

During magnetron sputtering, energetic electrons escape from the primary magnetic trap between the inner and outer magnets, and in a balanced magnetron, these electrons go to the anode. It is the primary electron trap that is responsible for the formation of the dense plasma directly in front of the sputtering target and for the high deposition rate of the mag netron cathode compared to a diode cathode.

In an unbalanced magnetron, the escaping energetic elec trons are trapped by the excess magnetic field lines, and the

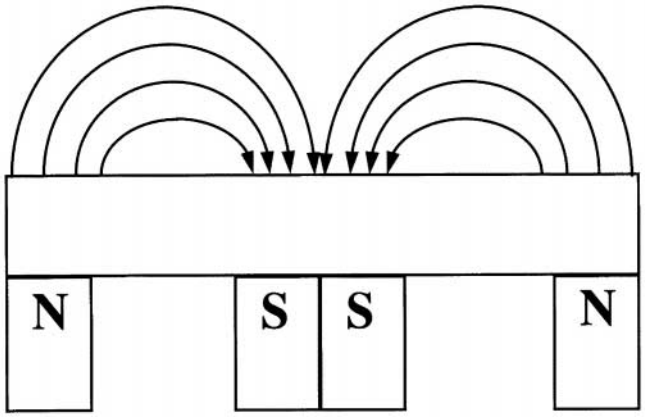

Figure 1. Schematic drawing of a balanced magnetron sputtering cath ode.

electrons spiral along the field lines and undergo ionizing col lisions with gas atoms. A secondary plasma is formed away from the target surface from these ionizing collisions, and this secondary plasma can be used for ion assisted deposition of the growing film. The current density collected on the sub strate during unbalanced magnetron sputtering is usually an order of magnitude higher than it is in conventional balanced magnetron sputtering, and substrate current densities are typi cally 5 10 mA cm^{-2} with unbalanced magnetron sputtering. These current densities match or exceed the substrate current densities found in other ion assisted deposition techniques.

When multiple unbalanced magnetron cathodes are used in the same chamber, it is important to link their magnetic fields in order to maximize the trapping of electrons. In an opposed, two cathode system, the polarity of the outer and inner mag nets on one cathode should be opposite to that polarity of the magnets in the cathode that it is facing; i.e., north pole should face south pole and vice versa. The magnetic trap cannot be complete if an odd number of cathodes are used. It is necess

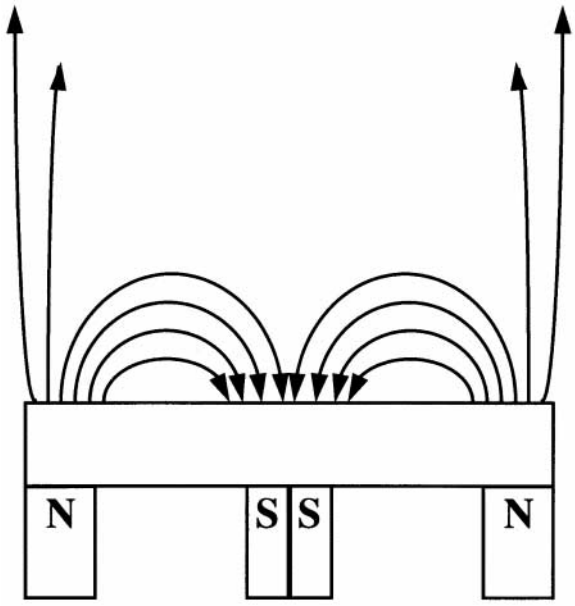

Figure 2. Schematic drawing of an unbalanced magnetron sputtering cathode.

ary to have an even number of cathodes to prevent a hole in the magnetic trap.

Four cathode rectangular unbalanced magnetron systems link magnetic fields with the cathode next to it and not to the one opposite it in the chamber. This linking provides good magnetic trapping of the electrons in one plane, but not in another. At the top and bottom of the cathodes, the magnetic field lines are in opposite directions, and there are holes in the magnetic trap. To overcome this problem, steel plates are placed at the top and bottom of the cathodes, and an electro static charge on these plates prevents the electrons from escap ing from the trap. The electrostatic charge can come simply by letting the plates electrically float in the plasma.

Ion assisted deposition is very important for forming fully dense, well adhered hard coatings. Both the ion current den sity and the ion energy (bias voltage) play significant roles in ion assisted deposition. In balanced magnetron sputtering, the ion current density is limited, and what is lacking in ion cur rent density has to be made up with the energy of the arriving ions. Typical ion current densities in balanced magnetron sput tering are less than 1 mA cm^{-2}, which produces low ion to arriving neutral species ratios. High bias voltages can be used to overcome partially the low ion to neutral ratio, but high bias voltages produce more damage than can be annealed out by the ion energy input.

Unbalanced magnetron sputtering, by producing a dense secondary plasma around the substrate, provides a high ion current density, on the order of 1 5 mA cm^{-2}, and the ion energy does not have to be as high as it is in balanced magne tron sputtering. Ion to neutral ratios greater than one are often reported for the unbalanced magnetron sputtering of hard coatings such as titanium nitride. Fully dense coatings are usually produced when the negative substrate bias voltage is in the 100 150 V range.

Reactive sputtering

Reactive sputtering is the sputtering of a metallic target in the presence of a gas that will react with the metal atom ejected from the target surface. Historically mass flow control has been used to control the amount of reactive gas flowing into the chamber, but flow control of the reactive gas can lead to problems. If the target is set at a fixed power and the flow of the reactive gas is increased, initially all of the reactive gas will be consumed by the reaction with the metal.

However, a point is reached as is shown in Figure 3 (point A) for the reactive sputtering of titanium in an argon/oxygen atmosphere where the amount of reactive gas in the chamber is sufficient to react with the surface of the target. When this happens and the oxide compound covers the surface of the target (the target is said to be poisoned), the sputtering rate drops rapidly because the sputtering rate of the compound is much less than that for the metal. Since the rate has decreased, not as much reactive gas is consumed, and its partial pressure jumps rapidly from point A to point B as is shown in Figure 3. With flow control, it is very difficult to operate between points A and B, and there is a range of compositions that is forbid den between these two points.

Partial pressure control of the reactive gas overcomes the problems of the flow control.[4–6] Using a sensor such as a quadrupole mass spectrometer that can provide a quick feed

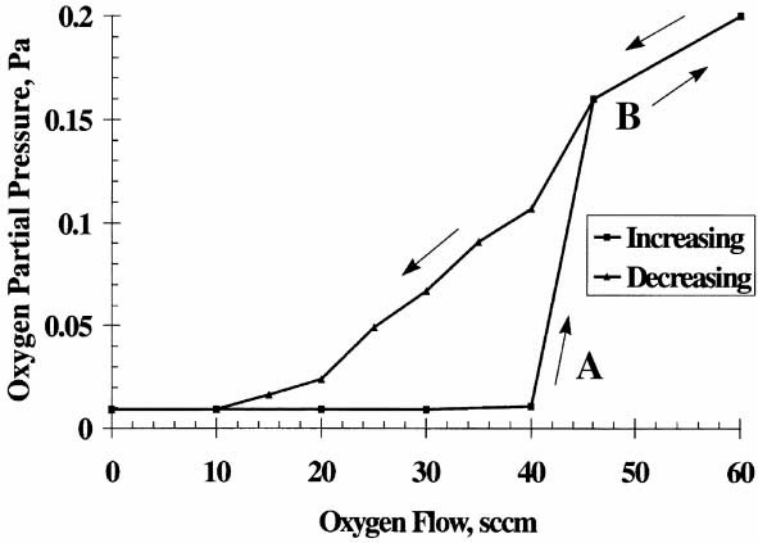

Figure 3. Hysteresis plot for the reactive sputtering of titanium in an argon/oxygen atmosphere with flow control of the reactive gas. The target power was 8 kW, and the total pressure during deposition was 1.1 Pa.

back signal for the partial pressure of the reactive gas, it is possible to control the partial pressure of the reactive gas at any desired set point as is shown in Figure 4 for the reactive sputtering of titanium in an argon/oxygen atmosphere. There are no forbidden compositions with partial pressure control, and it is possible to operate at any point between A and B in Figure 4. At point B, the target is fully poisoned, and the sput tering rate is very low. As the partial pressure is lowered toward point A, the deposition rate increases, and the chal lenge is to operate at as low a partial pressure that will pro duce the desired composition.

There are two main benefits of partial pressure control of the reactive gas. The first is that it is possible to reactively sputter hard compounds such as TiN at the same deposition rate as is found for the pure metal.[4] No higher rate can be achieved. Secondly, partial pressure control provides precise control of the composition of the compound, and it is possible to produce the same compound material in every run.

Reactive sputtering of oxides until just recently had been a difficult task. Oxygen reacts much more quickly with the target surface than does nitrogen, and it often forms an insulating compound on the target surface, which leads to difficulty in sputtering the desired material. When an insulating material forms on the surface of the sputtering target during depo sition, those insulating surfaces build up a charge and then dis charge during dc reactive sputtering, which results in arcing. This arcing is particularly violent for reactive dc sputtering of Al_2O_3, and it can result in damage to the power supply and liquid droplet ejection from the target surface.

Radio frequency (rf) power can be used for the reactive sputtering of oxides, but it has its own set of problems. Essentially half of the power is not used for sputtering, and

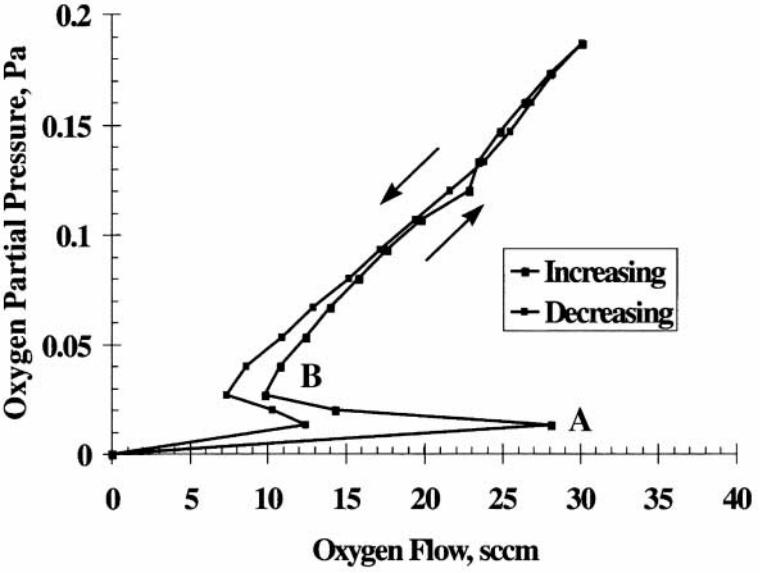

Figure 4. Hysteresis plot for the reactive sputtering of titanium in an argon/oxygen atmosphere with partial pressure control of the reactive gas. The target power was 5 kW, and the total pressure during deposition was 1.1 Pa.

the deposition rates for reactive rf power are much lower than that for the pure metal. For example, aluminum oxide reactive sputters with rf power at only 2 3% of the metal deposition rate.

One method used to overcome the problems of using dc power for reactive sputtering of nonconducting coatings is to shield the sputtering target from the reactive gas. Typically, the target is enclosed in a box, with a mesh screen over the target to let the sputtered atoms out. The argon sputtering gas is injected into the system next to the target, and the reactive gas is injected next to the substrate. Although this method does allow dc power to be used for the sputtering of noncon ducting coatings, the screen does reduce the sputtering rate since it intercepts part of the sputtered flux. Keeping the screen open is a problem with this method, and constant main tenance of the screen is required.

Pulsed dc power

Within the past few years, it has been shown[7–11] that bipolar pulsed dc power can be used for the reactive sputter deposition of oxides. With bipolar pulsed power, the polarity of the target power is switched from negative to positive, and during the positive pulse any charging of the oxide layer is discharged when electrons are attracted to the positive surface. During the negative pulse, ions are attracted to the target surface, and sputtering takes place initially from all surfaces on the target even those that have formed a compound since the charge on that surface has been neutralized during the positive pulse.

Bipolar pulsed power is classified as either symmetric or asymmetric, which refers to the pulse height in the positive and negative directions.[12] Symmetric bipolar pulsed dc power has equal pulse heights in both the positive and negative direc tions, as is shown in Figure 5, and the width of both the posi tive and negative pulses can be varied independently as can the time off between pulses. Symmetric bipolar pulsed dc power is often used for the reactive deposition of an oxide coating from two magnetron cathodes. These two cathodes, which are located side by side, are both connected to the same symmetric bipolar pulsed dc power supplied. One power lead goes to one cathode, and the other power lead is connected to the second cathode. With this electrical hookup, one sputtering target is the anode for the system, while the other is the cath

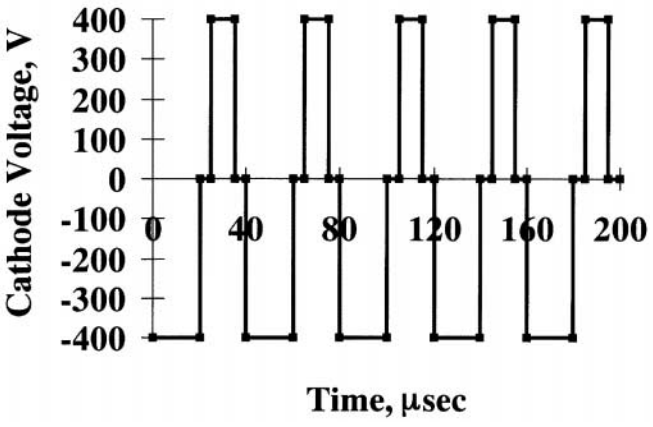

Figure 5. Schematic representation of symmetric bipolar pulsed dc power.

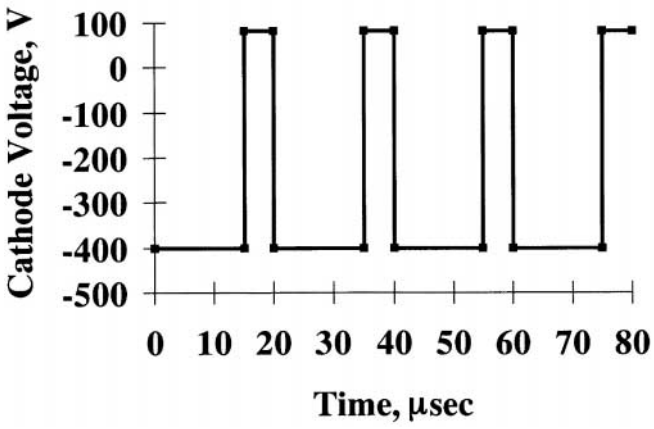

Figure 6. Schematic representation of asymmetric bipolar pulsed dc power.

ode. When the polarity of the voltage on the targets changes, the anode and cathode switch as well. Sputtering from the cathode surface during the negative pulse keeps the target sur face clean, and when it switches to act as an anode, it is not covered by an oxide. This procedure avoids the disappearing anode problem, which can occur in pulsed dc sputtering of ox ides when all surfaces in the chamber become covered with an insulating oxide.

Asymmetric bipolar pulsed dc power, on the other hand, has unequal pulse heights. The negative pulse height is greater than the positive one, and there is no off time between pulses as is shown in Figure 6. The width of the positive pulse is a fraction of the negative pulse width, and its width is usually 10 20% of the width of the negative one. A significant portion of the power cycle is spent in the sputtering mode, and the de position rate from asymmetric power can be close to that of pure dc power. The frequency of pulsed dc power covers a wide range from 0 (normal dc) up to 250 kHz, and typical operating frequencies for the pulsed dc power during reactive sputtering of oxides are in the 20 100 kHz range.

The frequency selected is a function of the material being reactively sputtered. Whereas no arcing can be achieved for the reactive sputtering of titanium dioxide at a pulsing fre quency of 30 kHz, it takes a frequency between 50 and 70 kHz for all arcing to disappear for aluminum oxide.[11] With both partial pressure control of the reactive gas and asymmetric pulsed dc power, we have been able to reactively sputter aluminum oxide with no arcing at a frequency of 70 kHz.

Although in theory pulsed dc power has a rectangular wave form, in fact it does not. There can be overshoot in the nega tive pulse and ringing on the positive pulse as is shown in Figure 7. This overshoot can be significant, and the target vol tage shown on the power supply can be quite misleading.[13,14] For the example shown in Figure 7, the average target voltage is about 450 volts, which was displayed on the front panel of the power supply, but in fact the peak to peak voltage was about 1500 volts. Such high voltages will produce much more energetic particles during part of the pulse cycle, and the effect of these energetic particles on the structure and properties of the coating is still being evaluated. Initially there has been no noticeable effect of these high energetic neutrals on the proper ties of the coatings, but there may be applications where this high energy could be detrimental. In many ways, the voltages

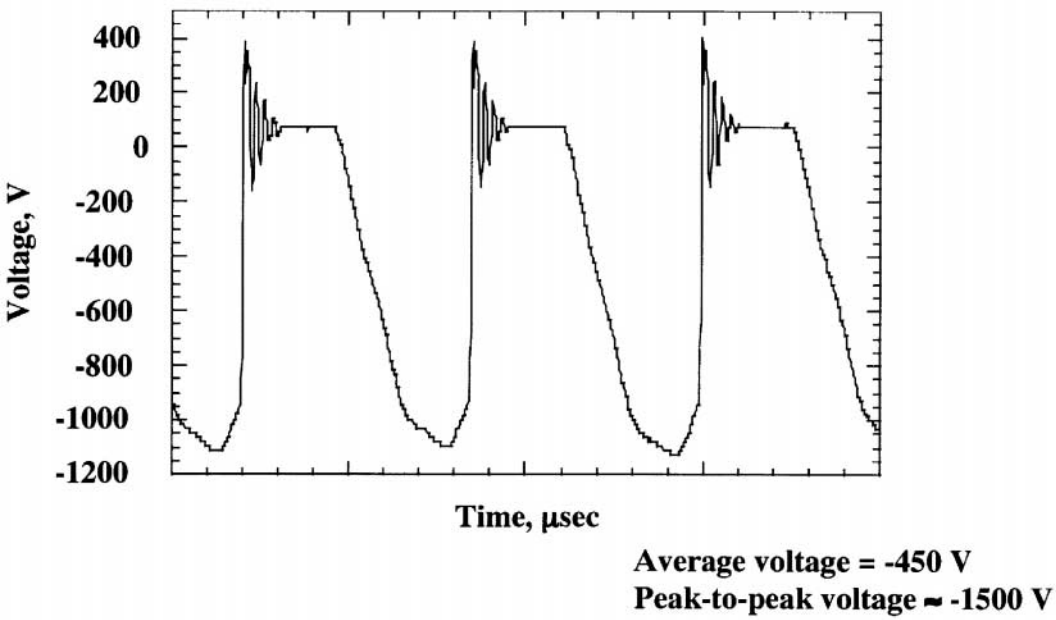

Figure 7. Trace of pulsed dc power during the reactive sputter of aluminum in an argon/oxygen atmosphere.

produced during asymmetric pulsed dc sputtering are similar to the voltages found in dc diode systems.

Reactive unbalanced magnetron sputtering of multilayered coatings

Reactive unbalanced magnetron sputtering in an opposed cathode system has been used very successfully to deposit nanometer scale multilayer nitride and oxide films that have enhanced physical properties.[15–19] The first work in this area was with titanium nitride/niobium nitride (TiN/NbN) and titanium nitride/vanadium nitride (TiN/VN) coatings. Partial pressure control of the reactive gas was crucial to achieve the cubic form of NbN, and the high degree of ion bombardment from the unbalanced magnetron sources led to fully dense well adhered films. The hardness of the TiN/NbN and TiN/VN films was greater than 50 GPa, which is more than twice the hardness of either component in these two multilayered films, when the superlattice period, which is the bilayer thickness of the TiN and NbN or TiN and VN, was in the range of 50 to 80 Å. The individual layer thicknesses were approximately equal.

The importance of the combination of pulsed dc power and partial pressure control of the reactive gas really came into the spotlight with the reactive unbalanced magnetron sputtering of non conducting oxides such as aluminum oxide (Al_2O_3). Without this combination of pulsed dc power and partial pressure control, it really was not possible to reactively sputter Al_2O_3 at high deposition rates in a practical way. A portion of the hysteresis loop for the reactive sputtering of aluminum in

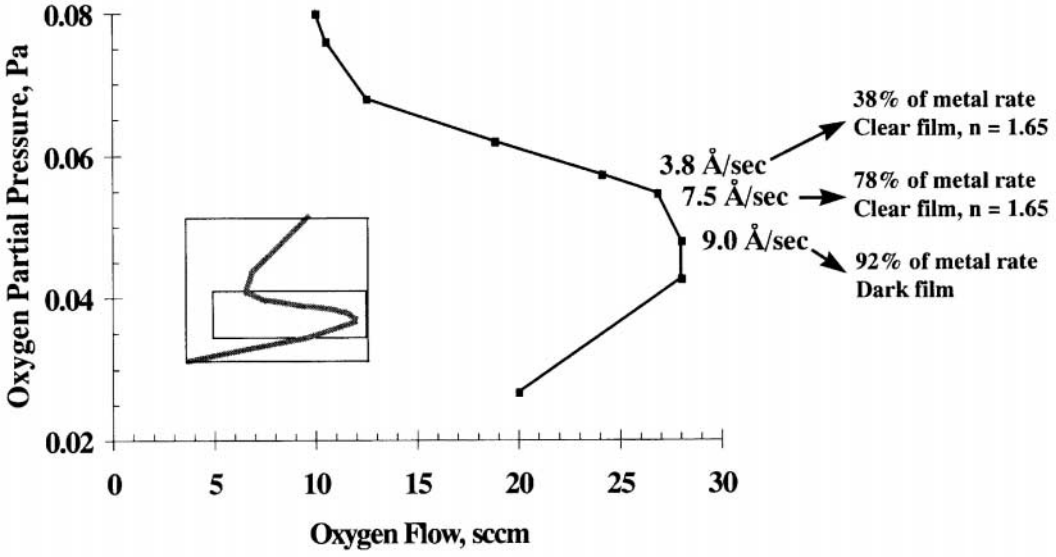

Figure 8. Nose region of the hysteresis curve for the reactive sputtering of aluminum in an argon/oxygen atmosphere. Full curve is shown in the inset in the lower left corner of the diagram.

an oxygen/argon atmosphere[20,21] is shown in Figure 8. As is shown in this figure, small changes in the partial pressure of oxygen lead to large changes in the deposition rate, and rates as high as 78% of the metal deposition rate can be achieved for an optically clear amorphous film of Al_2O_3. To achieve this sensitive control of the reactive sputtering of Al_2O_3, both pulsed dc power and partial pressure control of the reactive gas must be used.

Other oxide films have also been deposited using the com bined pulsed dc power and partial pressure control of the reac tive gas in the unbalanced magnetron sputtering system. Oxides of titanium, zirconium, hafnium, chromium, mag nesium, silicon, yttrium, tantalum, and an alloy of zirconium and yttrium have all been successfully deposited using this technology.

Multilayered oxide films have been deposited very success fully via reactive unbalanced magnetron sputtering using pulsed dc power and partial pressure control of the reactive gas. Aluminum oxide/zirconium oxide ($Al_2O_3/Zr0_2$) films were deposited simultaneously in an opposed cathode unbalanced magnetron sputtering system,[19] and the substrate was rotated between the two cathodes. The deposition rate was approxi mately 75% of each metal rate, and both individual layer thicknesses of the Al_2O_3 and ZrO_2 were about 45 Å each, which gave a bilayer thickness of 90 Å. The films were opti cally clear, and the structure of the multilayer film was amor phous as determined by X ray diffraction.

Most recently, multilayer oxide films of yttrium oxide and zirconium oxide (Y_2O_3/ZrO_2) have been deposited in the opposed cathode unbalanced magnetron sputtering system again using pulsed dc power and partial pressure control of the reactive gas.[14] The Y_2O_3/ZrO_2 films were similar to the Al_2O_3/ZrO_2 in that they were optically clear, but they were different because the Y_2O_3/ZrO_2 were crystalline with a cubic structure. The cubic structure of the Y_2O_3 forced the ZrO_2, which normally has a monoclinic structure, into a cubic struc ture. The overall film had a dense columnar structure, and within a column there was a true superlattice structure for the Y_2O_3/ZrO_2 film. Satellite peaks were clearly visible in the X ray diffraction patterns from these films. Work is currently underway to determine other properties of these multilayer oxide films.

Summary

Advances in reactive sputtering have made it much easier to deposit fully dense well adhered coatings. Non conducting coatings such as aluminum oxide, which could not be done with conventional dc power, can now be reactively sputter deposited in a very controlled, stable way at very high depo sition rates if pulsed dc power is used in conjunction with par tial pressure control of the reactive gas. The high ion flux that is available with unbalanced magnetron systems assures a high ion to neutral ratio, which in turn leads to dense films. Other oxide coatings including oxides of silicon, titanium, zirconium, hafnium, chromium, and tantalum have also been deposited at very high rates compared to convention deposition techniques when pulsed dc power and partial pressure control are used. This advancement in reactive sputtering technology is opening up many new opportunities for the oxide films.

References

1. Window, B. and Savvides, N., *J. Vac. Sci. Technol. A,* 1986, **4**(2), 196.
2. Window, B. and Savvides, N., *J. Vac. Sci. Technol. A,* 1986, **4**(3), 453.
3. Window, B. and Savvides, N., *J. Vac. Sci. Technol. A,* 1986, **4**(3), 504.
4. Sproul, W. D., *Thin Solid Films,* 1983, **107**, 141.
5. Sproul, W. D., *Surf. Coat. Technol.,* 1987, **33**, 73.
6. Sproul, W. D., Rudnik, P. J., Graham, M. E., Gogol, C. A. and Mueller, R. M., *Surf. Coat. Technol.,* 1989, **39/40**, 499.
7. Schiller, S., Goedicke, K., Reschke, J., Kirchhoff, V., Schneider, S. and Milde, F., *Surf. Coat. Technol.,* 1993, **61**, 331.
8. Frach, P., Heisig, U., Gottfried, Chr. and Walde, H., *Surf. Coat. Technol.,* 1993, **59**, 177.
9. Graham, M.E. and Sproul, W.D., 37th Annual Technical Conference Proceedings, Society of Vacuum Coaters, Albuquerque, New Mexico, 1994, p. 275.
10. Sproul, W. D., Graham, M. E., Wong, M. S., Lopez, S., Li, D. and Scholl, R. A., *J. Vac. Sci. Technol. A.,* 1995, **13**(3), 1188.
11. Schiller, S., Goedicke, K., Kirhhoff, V. and Kopte, T., 38th Annual Technical Proceedings, Society of Vacuum Coaters, Albuquerque, NM, 1995, p. 293.
12. Sellers, J., Asymmetric Bipolar Pulsed DC, ENI Tech Note, ENI, Division of Astec America, Inc., 100 Highpower Road, Rochester, NY 14623.
13. Schneider, J.M., Sproul, W.D. and Matthews, A., Phase Formation and Mechanical Properties of Alumina Coatings Prepared at Substrate Temperatures $< 500°C$ by Ionized and Conventional Sputtering, paper presented at the International Conference on Metallurgical Coatings and Thin Films, Town and Country Hotel, San Diego, California, April 23, 1997 and accepted for publication in Surface and Coatings Technology.
14. Sproul, W.D., Wong, M.S., Yashar, P., Wang, Y.Y., Barnett, S.A. and Chung, Y.W., Stabilization of Metastable Phases in Polycrystalline Nanometer Scale Multilayered Coatings, paper presented at the International Conference on Metallurgical Coatings and Thin Films, Town and Country Hotel, San Diego, California, April 23, 1997.
15. Chu, X., Wong, M. S., Sproul, W. D., Rohde, S. L. and Barnett, S. A., *J. Vac. Sci. Technol. A.,* 1992, **10**(4), 1604.
16. Chu, X., Wong, M. S., Sproul, W. D. and Barnett, S. A., *Surf. Coat. Technol.,* 1993, **57**, 13.
17. Chu, X., Wong, M. S., Sproul, W. D. and Barnett, S. A., *Mat. Res. Soc. Symp. Proc.,* 1993, **286**, 379.
18. Sproul, W. D., *Science,* 1996, **273**, 889.
19. Sproul, W. D., *Surf. Coat. Technol.,* 1996, **86-87**, 170.
20. Schneider, J.M., Sproul, W.D., Wong, M. S. and Matthews, A., Very High Rate Pulsed DC Sputter Deposition of AlO_x Coatings, accepted for publication in Surface and Coatings Technology.
21. Schneider, J.M., Sproul, W.D., Lefkow, A.R.T., Rechner, J. and Matthews, A., *39th Annual Technical Proceedings*, Society of Vacuum Coaters, Albuquerque, NM, 1996, p. 168.

Appendix 1036-A

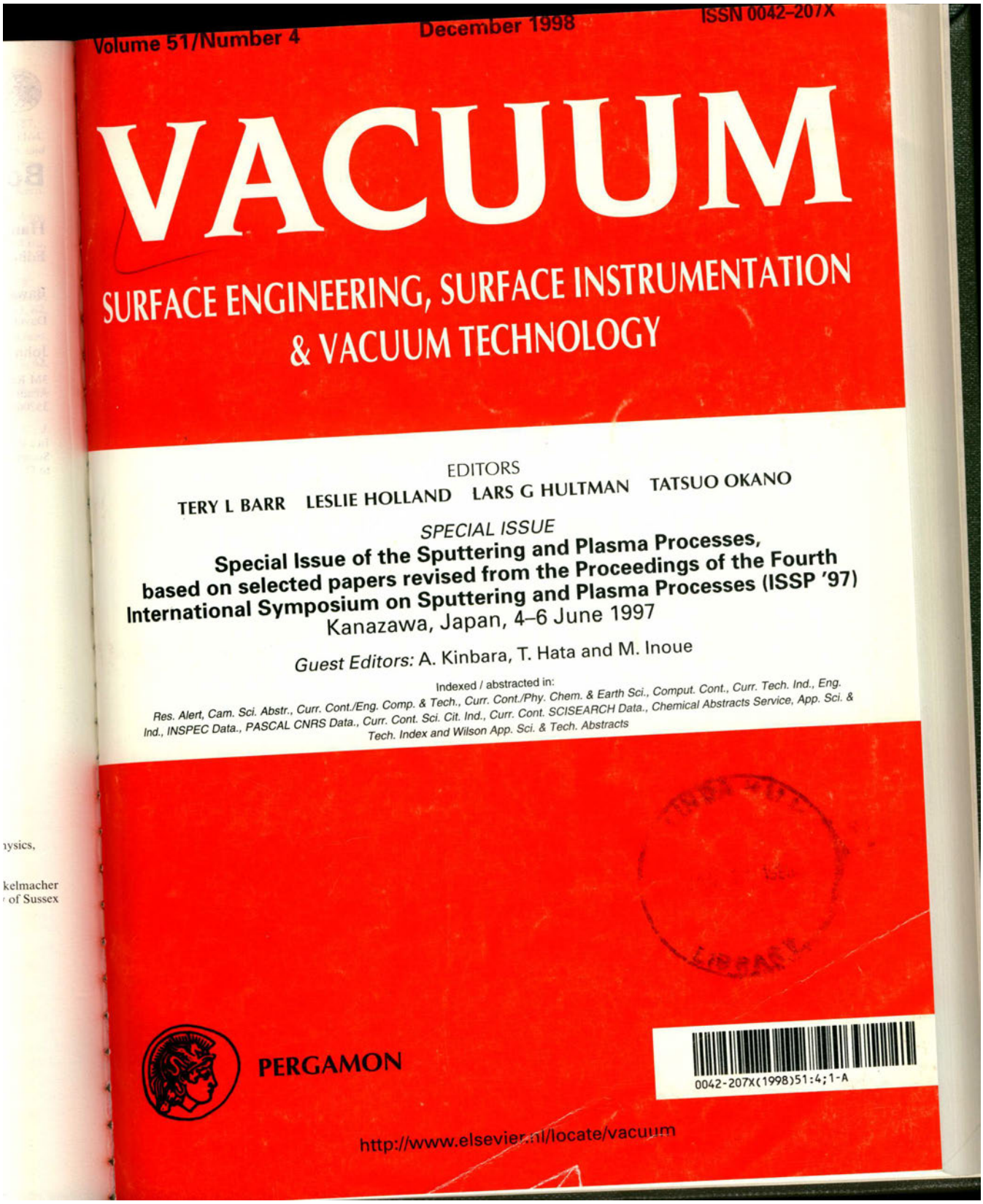
Volume 51/Number 4
December 1998
ISSN 0042-207X
VACUUM
SURFACE ENGINEERING, SURFACE INSTRUMENTATION & VACUUM TECHNOLOGY
EDITORS
TERY L BARR LESLIE HOLLAND LARS G HULTMAN TATSUO OKANO
SPECIAL ISSUE
Special Issue of the Sputtering and Plasma Processes, based on selected papers revised from the Proceedings of the Fourth International Symposium on Sputtering and Plasma Processes (ISSP '97)
Kanazawa, Japan, 4–6 June 1997
Guest Editors: A. Kinbara, T. Hata and M. Inoue
Indexed / abstracted in:
Res. Alert, Cam. Sci. Abstr., Curr. Cont./Eng. Comp. & Tech., Curr. Cont./Phy. Chem. & Earth Sci., Comput. Cont., Curr. Tech. Ind., Eng. Ind., INSPEC Data., PASCAL CNRS Data., Curr. Cont. Sci. Cit. Ind., Curr. Cont. SCISEARCH Data., Chemical Abstracts Service, App. Sci. & Tech. Index and Wilson App. Sci. & Tech. Abstracts
PERGAMON
0042-207X(1998)51:4;1-A
http://www.elsevier.nl/locate/vacuum

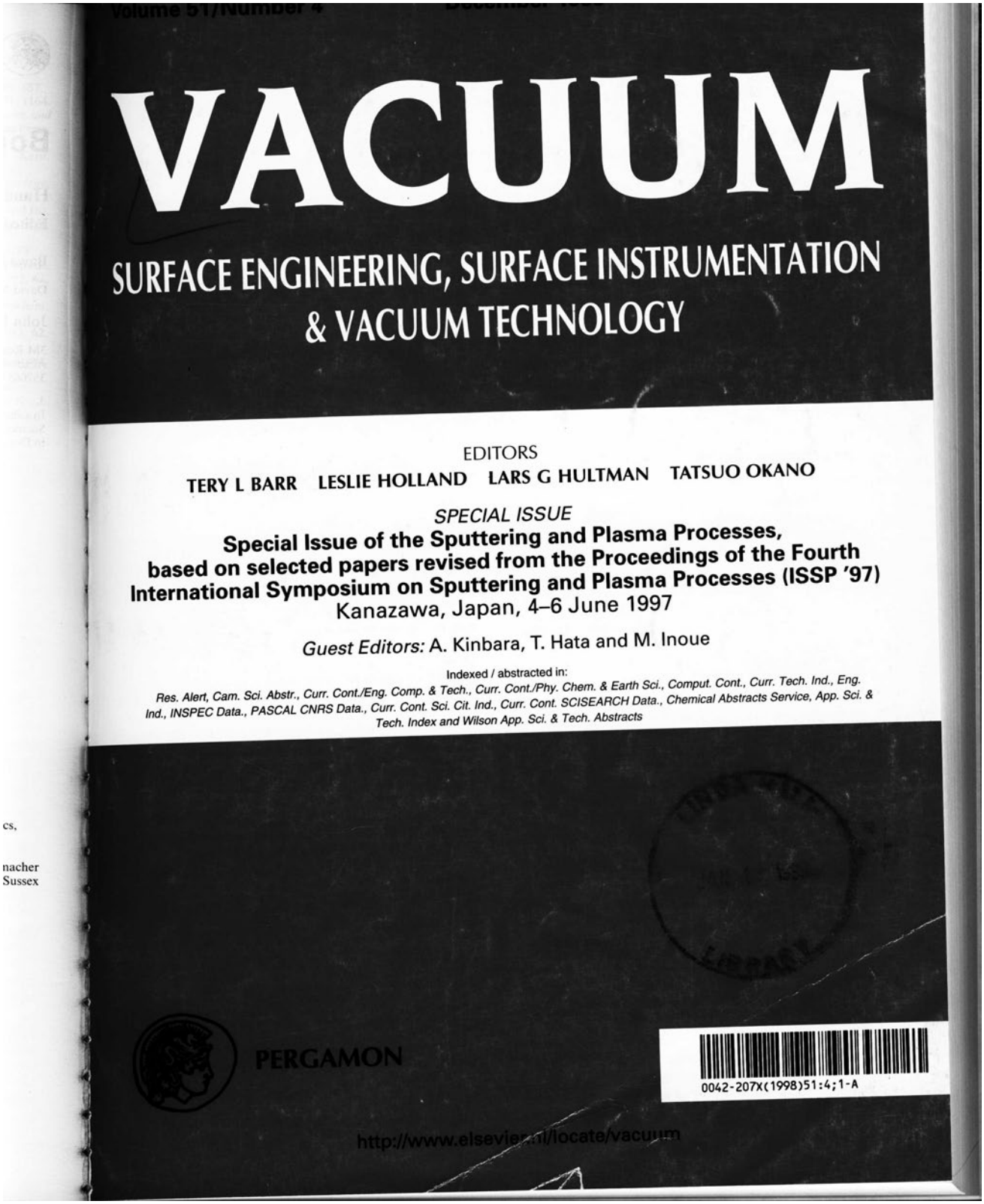

cs,

nacher
Sussex

ume 51/Number 4 December 1998 ISSN 0042-207X

VACUUM

SURFACE ENGINEERING, SURFACE INSTRUMENTATION & VACUUM TECHNOLOGY

EDITORS
TERY L BARR LESLIE HOLLAND LARS G HULTMAN TATSUO OKANO

SPECIAL ISSUE

Special Issue of the Sputtering and Plasma Processes, based on selected papers revised from the Proceedings of the Fourth International Symposium on Sputtering and Plasma Processes (ISSP '97)

Kanazawa, Japan, 4–6 June 1997

Guest Editors: A. Kinbara, T. Hata and M. Inoue

Indexed / abstracted in:
Res. Alert, Cam. Sci. Abstr., Curr. Cont./Eng. Comp. & Tech., Curr. Cont./Phy. Chem. & Earth Sci., Comput. Cont., Curr. Tech. Ind., Eng. Ind., INSPEC Data., PASCAL CNRS Data., Curr. Cont. Sci. Cit. Ind., Curr. Cont. SCISEARCH Data., Chemical Abstracts Service, App. Sci. & Tech. Index and Wilson App. Sci. & Tech. Abstracts

PERGAMON

http://www.elsevier.nl/locate/vacuum

VACUUM

SURFACE ENGINEERING, SURFACE INSTRUMENTATION & VACUUM TECHNOLOGY

Contributors
Manuscripts should be submitted in duplicate to one of the journal Editors at the addresses given below. Details of style are given on the inside back cover

The Item-Fee Code for this publication is: 0042-207X/98 $19.00+.00

Subscription Rates
Published monthly (3 volumes, 4 issues per volume)
Annual Institutional Subscription Rates 1999: Europe, The CIS and Japan 4108.00 Dutch Guilders. All other countries US$2085.00. Associated Personal Subscription Rates are available on request for those whose institutions are library subscribers. Dutch Guilder prices exclude VAT. Non-VAT registered customers in the European Community will be charged the appropriate VAT in addition to the price listed. Prices include postage and insurance and are subject to change without notice.
Author Service Department: For queries relating to the general submission of articles (including electronic text and artwork) and the status of accepted manuscripts, pleaase contact the Author Service Department: *e-mail*: authors@elsevier.co.uk; *Fax*: +44 (0) 1865 843905; Tel.: +44 (0)1865 843900.
Any enquiry relating to subscriptions should be sent to:
The Americas: Elsevier Science Customer Support Department, P.O. Box 945, New York, NY 10010, USA [Tel: (+1) 212-633-3730 / 1-888 4ES-INFO. Fax: (+1) 212-633-3680. E-mail: usinfo-f @elsevier.com]. **Japan:** Elsevier Science Customer Support Department, 9–15 Higashi-Azabu 1-chome, Minato-ku, Tokyo 106, Japan [Tel: (+3) 5561-5033. Fax: (+3) 5561-5047. E-mail: info@elsevier.co.jp]. **Asia Pacific (*excluding Japan*):** Elsevier Science (Singapore) Pte Ltd, No. 1 Temasek Avenue, 17-01 Millenia Tower, Singapore 039192 [Tel: (+65) 434-3727. Fax: (+65) 337-2230. E-mail: asiainfo@elsevier.com.sg]. **Rest of the World:** Elsevier Science Customer Service Department, P.O. Box 211, 1001 AE Amsterdam, The Netherlands [Tel: (+31) 20-485-3757. Fax: (+31) 20-485-3432. E-mail: nlinfo-f@elsevier.nl].

Periodicals postage paid at Newark, NJ and additional entry points. *Vacuum* (ISSN 0042-207X) is published monthly, January to December in 3 volumes, by Elsevier Science Ltd., The Boulevard, Langford Lane, Kidlington, Oxford OX5 1GB, UK. The annual subscription in the USA is $2085.00. *Vacuum* is distributed by Mercury Airfreight International Ltd., 365 Blair Road, Avenel, NJ 07001, U.S.A. Postmaster: please send address changes to *Vacuum*, c/o Elsevier Science Regional Sales Office, Customer Support Department, 655 Avenue of the Americas, New York, NY 10010, USA.

Typeset in Great Britain by BPC Digital Data Ltd. Printed by BPC-AUP Aberdeen Ltd.

Publishing Office: *Elsevier Science Ltd, Bampfylde St, Exeter EX1 2AH, UK. Tel: (+1392) 251558 Fax: (+1392) 425370*
Advertising Offices: *The Boulevard, Langford Lane, Kidlington, Oxford OX5 1GB, UK. Tel: (+1865) 843000 Fax: (+1865) 843010*
Elsevier Science Inc., 655 Avenue of the Americas, New York, NY 10010, USA.

Perga

Funda
proces

A. Kinbara,*
Kariya 448, Ja

Fundamental
veyed and dis
strate and tran
during plasma
was discussed

Introduction

Sputtering is a
induced by c
computer simu
in by many w
Averback at I
have remaine
are many way
and their beha
discharge in
most widely
glow discharg
ions, electron
Some of then
tively in low
and the energ
The preser
out in our la
tering proce
closely conn
hence, we f
charge plasn
thin films du

Target proce

Self bias vo
one targets
cesses at th
isolated fro

*Correspo

Volume 51 number 4

Selected papers revised from the Proceedings of the Fourth International Symposium on Sputtering and Plasma Processes (ISSP '97)

(W)

er. Interelectrode distan-
1 Pa, (b) $F(N_2)/F(Ar)$/

decreases and, conse-
(111) decreases.
using the helium–ni-
titanium production
ecreases. Ternary gas
n, or neon–argon–ni-
ess due to the highly
argon ions and nitro-
g process.
) or $(N_2 + Ar + He)$,
itly enhances the TiN
Penning effect and to
to the nitrogen mol-

R. V., Mauscher, P.,
Vac. Sci. Technol. A.,

C. G., *Thin Solid Films*,

erson, D. R., Lampert,
s, 1990, **191**, 55.
te, D., Kiss, A., Musa,
n Reactive Plasmas and
ra, Japan, 1997, p. 275.
Plasma Discharges and
4, p.353.
ans. on Plasma Science,

Pergamon

Vacuum/volume 51/number 4/pages 641 to 646/1998

0042-207X/98 $ - see front matter

PII: S0042-207X(98)00265-6

High-rate reactive DC magnetron sputtering of oxide and nitride superlattice coatings

W D Sproul,*, *Sputtered Films, Inc., 320 Nopal Street, Santa Barbara, California 93103, U.S.A.*

Over the past 10 years, there have been three major advancements in reactive sputtering technology that now make it possible to deposit both conductive and non-conductive fully-dense films at high rates. These three advances are unbalanced magnetron sputtering, partial pressure control of the reactive gas, and pulsed dc power. Multicathode unbalanced magnetron sputtering systems provide a dense secondary plasma that is used for producing a well-adhered, fully dense film that is difficult to achieve with conventional magnetron sputtering. Online automatic partial pressure control of the reactive gas prevents the poisoning of the target surface during deposition, which leads to compound film deposition rates that approach or are equal to those for the pure metal rate. Pulsed dc power, where the polarity of the voltage on the sputtering target is alternately switched briefly between negative and positive, prevents arcing on the target surface during the deposition of nonconducting films. With both pulsed dc power and partial pressure control of the reactive gas, films such as aluminum oxide can now be deposited reactively at rates up to 78% of the pure metal rate. The reactive unbalanced magnetron sputtering process is used to deposit polycrystalline nitride superlattice films such as TiN/NbN or TiN/VN with hardnesses exceeding 50 GPa, which is more than double the hardness of either component in the multilayered film. The nitride superlattice work is being extended to oxide films, and initial results are encouraging. Nanometer scale, multilayer Al_2O_3/ZrO_2 and Y_2O_3/ZrO_2 films have been deposited at high rates. The Al_2O_3/ZrO_2 films are amorphous and optically clear, whereas the Y_2O_3/ZrO_2 films are crystalline as well as being optically clear.

Introduction

Since the middle 1980s, there have been three major advancements in sputtering technology that have greatly affected the ability to reactively sputter fully dense, well-adhered films at high deposition rates. In 1986, Window and Savvides[1–3] introduced the concept of unbalanced magnetron sputtering, and in the years since, it has been widely embraced by the sputtering community. Combined with partial pressure control of the reactive gas during the reactive sputter deposition of coatings, unbalanced magnetron sputtering today is one of the primary techniques for the deposition of hard coatings.

Most recently, the introduction of pulsed direct current (dc) power is already having an important effect on the reactive sputtering of non-conducting films such as aluminum oxide (Al_2O_3). The combination of partial pressure control of the reactive gas, unbalanced magnetron sputtering, and pulsed dc power is a powerful tool for the high-rate reactive deposition of compound films. Each of these three techniques will be reviewed, and then they will be looked at together to show the full potential for the synergistic effects for the deposition of non-conducting films.

*To whom all correspondence should be addressed

Unbalanced magnetron sputtering

A conventional magnetron sputtering cathode has magnets located along the outer edge and the centerline or at the center if the cathode is round. If the strength of the inner and outer magnets is roughly equal, the magnetron is said to be balanced, and most of the magnetic field lines will loop between the inner and outer magnets as is shown in Figure 1. If one of the sets of magnets is made stronger than the other, then the magnetron becomes unbalanced. Typically the outer set of magnets in the magnetron cathode is made stronger than the inner ones. Although there is still linkage between magnetic fields of the inner and outer magnets, not all of the field line will make the link. The excess field lines from the stronger magnets will radiate away from the magnet surfaces as is shown in Figure 2.

During magnetron sputtering, energetic electrons escape from the primary magnetic trap between the inner and outer magnets, and in a balanced magnetron, these electrons go to the anode. It is the primary electron trap that is responsible for the formation of the dense plasma directly in front of the sputtering target and for the high deposition rate of the magnetron cathode compared to a diode cathode.

In an unbalanced magnetron, the escaping energetic electrons are trapped by the excess magnetic field lines, and the

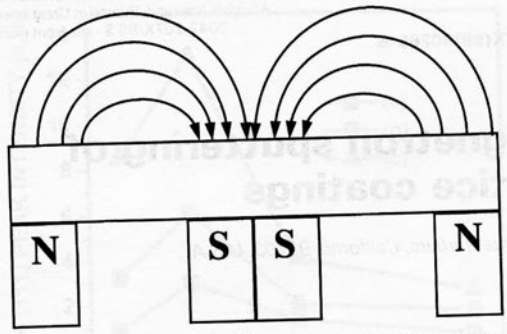

Figure 1. Schematic drawing of a balanced magnetron sputtering cathode.

electrons spiral along the field lines and undergo ionizing collisions with gas atoms. A secondary plasma is formed away from the target surface from these ionizing collisions, and this secondary plasma can be used for ion-assisted deposition of the growing film. The current density collected on the substrate during unbalanced magnetron sputtering is usually an order of magnitude higher than it is in conventional balanced magnetron sputtering, and substrate current densities are typically 5–10 mA cm^{-2} with unbalanced magnetron sputtering. These current densities match or exceed the substrate current densities found in other ion-assisted deposition techniques.

When multiple unbalanced magnetron cathodes are used in the same chamber, it is important to link their magnetic fields in order to maximize the trapping of electrons. In an opposed, two cathode system, the polarity of the outer and inner magnets on one cathode should be opposite to that polarity of the magnets in the cathode that it is facing; i.e., north pole should face south pole and vice-versa. The magnetic trap cannot be complete if an odd number of cathodes are used. It is necessary to have an even number of cathodes to prevent a hole in the magnetic trap.

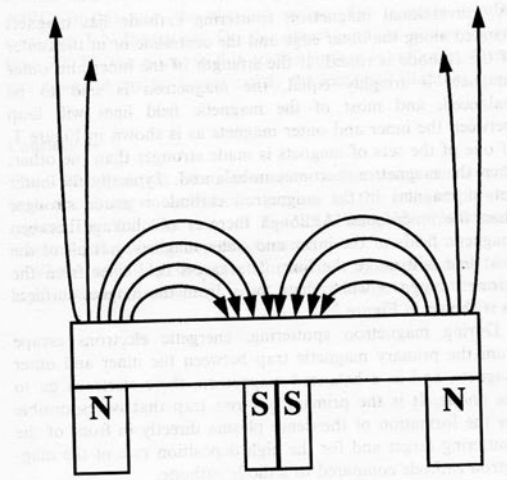

Figure 2. Schematic drawing of an unbalanced magnetron sputtering cathode.

Four cathode rectangular unbalanced magnetron systems link magnetic fields with the cathode next to it and not to the one opposite it in the chamber. This linking provides good magnetic trapping of the electrons in one plane, but not in another. At the top and bottom of the cathodes, the magnetic field lines are in opposite directions, and there are holes in the magnetic trap. To overcome this problem, steel plates are placed at the top and bottom of the cathodes, and an electrostatic charge on these plates prevents the electrons from escaping from the trap. The electrostatic charge can come simply by letting the plates electrically float in the plasma.

Ion-assisted deposition is very important for forming fully dense, well-adhered hard coatings. Both the ion-current density and the ion energy (bias voltage) play significant roles in ion-assisted deposition. In balanced magnetron sputtering, the ion current density is limited, and what is lacking in ion current density has to be made up with the energy of the arriving ions. Typical ion current densities in balanced magnetron sputtering are less than 1 mA cm^{-2}, which produces low ion to arriving neutral species ratios. High bias voltages can be used to overcome partially the low ion to neutral ratio, but high bias voltages produce more damage than can be annealed out by the ion energy input.

Unbalanced magnetron sputtering, by producing a dense secondary plasma around the substrate, provides a high ion current density, on the order of 1–5 mA cm^{-2}, and the ion energy does not have to be as high as it is in balanced magnetron sputtering. Ion to neutral ratios greater than one are often reported for the unbalanced magnetron sputtering of hard coatings such as titanium nitride. Fully dense coatings are usually produced when the negative substrate bias voltage is in the 100–150 V range.

Reactive sputtering

Reactive sputtering is the sputtering of a metallic target in the presence of a gas that will react with the metal atom ejected from the target surface. Historically mass flow control has been used to control the amount of reactive gas flowing into the chamber, but flow control of the reactive gas can lead to problems. If the target is set at a fixed power and the flow of the reactive gas is increased, initially all of the reactive gas will be consumed by the reaction with the metal.

However, a point is reached as is shown in Figure 3 (point A) for the reactive sputtering of titanium in an argon/oxygen atmosphere where the amount of reactive gas in the chamber is sufficient to react with the surface of the target. When this happens and the oxide compound covers the surface of the target (the target is said to be poisoned), the sputtering rate drops rapidly because the sputtering rate of the compound is much less than that for the metal. Since the rate has decreased, not as much reactive gas is consumed, and its partial pressure jumps rapidly from point A to point B as is shown in Figure 3. With flow control, it is very difficult to operate between points A and B, and there is a range of compositions that is forbidden between these two points.

Partial pressure control of the reactive gas overcomes the problems of the flow control.[4–6] Using a sensor such as a quadrupole mass spectrometer that can provide a quick feed-

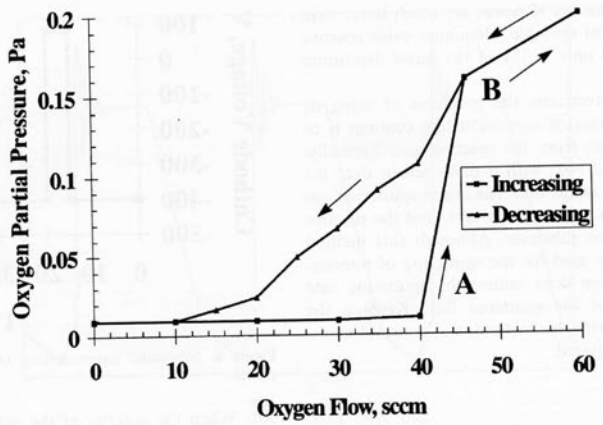

Figure 3. Hysteresis plot for the reactive sputtering of titanium in an argon/oxygen atmosphere with flow control of the reactive gas. The target power was 8 kW, and the total pressure during deposition was 1.1 Pa.

back signal for the partial pressure of the reactive gas, it is possible to control the partial pressure of the reactive gas at any desired set point as is shown in Figure 4 for the reactive sputtering of titanium in an argon/oxygen atmosphere. There are no forbidden compositions with partial pressure control, and it is possible to operate at any point between A and B in Figure 4. At point B, the target is fully poisoned, and the sputtering rate is very low. As the partial pressure is lowered toward point A, the deposition rate increases, and the challenge is to operate at as low a partial pressure that will produce the desired composition.

There are two main benefits of partial pressure control of the reactive gas. The first is that it is possible to reactively sputter hard compounds such as TiN at the same deposition rate as is found for the pure metal.[4] No higher rate can be achieved. Secondly, partial pressure control provides precise control of the composition of the compound, and it is possible to produce the same compound material in every run.

Reactive sputtering of oxides until just recently had been a difficult task. Oxygen reacts much more quickly with the target surface than does nitrogen, and it often forms an insulating compound on the target surface, which leads to difficulty in sputtering the desired material. When an insulating material forms on the surface of the sputtering target during deposition, those insulating surfaces build up a charge and then discharge during dc reactive sputtering, which results in arcing. This arcing is particularly violent for reactive dc sputtering of Al_2O_3, and it can result in damage to the power supply and liquid droplet ejection from the target surface.

Radio frequency (rf) power can be used for the reactive sputtering of oxides, but it has its own set of problems. Essentially half of the power is not used for sputtering, and

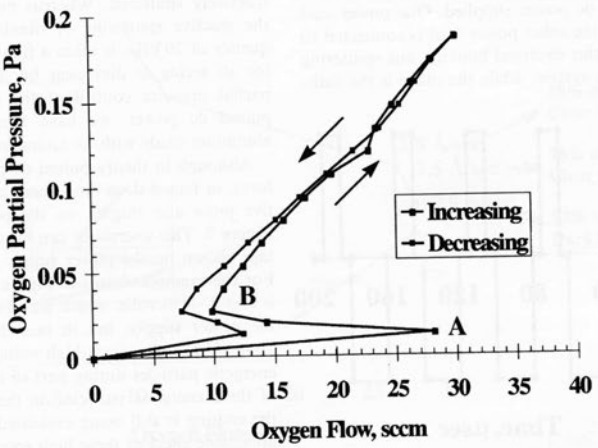

Figure 4. Hysteresis plot for the reactive sputtering of titanium in an argon/oxygen atmosphere with partial pressure control of the reactive gas. The target power was 5 kW, and the total pressure during deposition was 1.1 Pa.

the deposition rates for reactive rf power are much lower than that for the pure metal. For example, aluminum oxide reactive sputters with rf power at only 2–3% of the metal deposition rate.

One method used to overcome the problems of using dc power for reactive sputtering of nonconducting coatings is to shield the sputtering target from the reactive gas. Typically, the target is enclosed in a box, with a mesh screen over the target to let the sputtered atoms out. The argon sputtering gas is injected into the system next to the target, and the reactive gas is injected next to the substrate. Although this method does allow dc power to be used for the sputtering of nonconducting coatings, the screen does reduce the sputtering rate since it intercepts part of the sputtered flux. Keeping the screen open is a problem with this method, and constant maintenance of the screen is required.

Pulsed dc power

Within the past few years, it has been shown[7–11] that bipolar pulsed dc power can be used for the reactive sputter deposition of oxides. With bipolar pulsed power, the polarity of the target power is switched from negative to positive, and during the positive pulse any charging of the oxide layer is discharged when electrons are attracted to the positive surface. During the negative pulse, ions are attracted to the target surface, and sputtering takes place initially from all surfaces on the target even those that have formed a compound since the charge on that surface has been neutralized during the positive pulse.

Bipolar pulsed power is classified as either symmetric or asymmetric, which refers to the pulse height in the positive and negative directions.[12] Symmetric bipolar pulsed dc power has equal pulse heights in both the positive and negative directions, as is shown in Figure 5, and the width of both the positive and negative pulses can be varied independently as can the time off between pulses. Symmetric bipolar pulsed dc power is often used for the reactive deposition of an oxide coating from two magnetron cathodes. These two cathodes, which are located side by side, are both connected to the same symmetric bipolar pulsed dc power supplied. One power lead goes to one cathode, and the other power lead is connected to the second cathode. With this electrical hookup, one sputtering target is the anode for the system, while the other is the cathode. When the polarity of the voltage on the targets changes, the anode and cathode switch as well. Sputtering from the cathode surface during the negative pulse keeps the target surface clean, and when it switches to act as an anode, it is not covered by an oxide. This procedure avoids the disappearing anode problem, which can occur in pulsed dc sputtering of oxides when all surfaces in the chamber become covered with an insulating oxide.

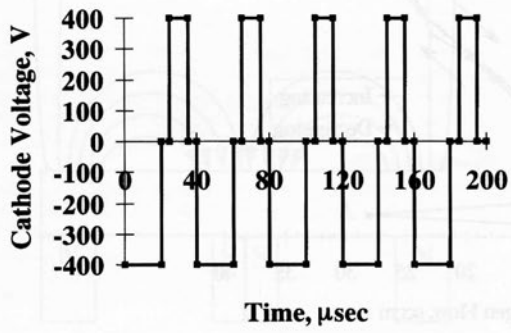

Figure 5. Schematic representation of symmetric bipolar pulsed dc power.

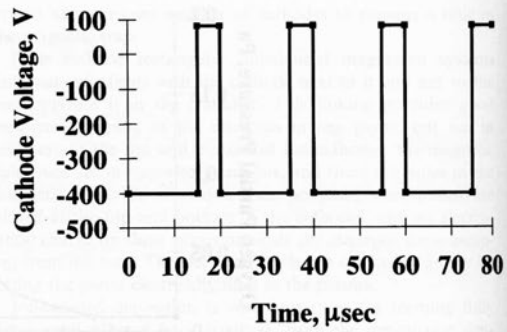

Figure 6. Schematic representation of asymmetric bipolar pulsed dc power.

Asymmetric bipolar pulsed dc power, on the other hand, has unequal pulse heights. The negative pulse height is greater than the positive one, and there is no off time between pulses as is shown in Figure 6. The width of the positive pulse is a fraction of the negative pulse width, and its width is usually 10–20% of the width of the negative one. A significant portion of the power cycle is spent in the sputtering mode, and the deposition rate from asymmetric power can be close to that of pure dc power. The frequency of pulsed dc power covers a wide range from 0 (normal dc) up to 250 kHz, and typical operating frequencies for the pulsed dc power during reactive sputtering of oxides are in the 20–100 kHz range.

The frequency selected is a function of the material being reactively sputtered. Whereas no arcing can be achieved for the reactive sputtering of titanium dioxide at a pulsing frequency of 30 kHz, it takes a frequency between 50 and 70 kHz for all arcing to disappear for aluminum oxide.[11] With both partial pressure control of the reactive gas and asymmetric pulsed dc power, we have been able to reactively sputter aluminum oxide with no arcing at a frequency of 70 kHz.

Although in theory pulsed dc power has a rectangular wave form, in fact it does not. There can be overshoot in the negative pulse and ringing on the positive pulse as is shown in Figure 7. This overshoot can be significant, and the target voltage shown on the power supply can be quite misleading.[13,14] For the example shown in Figure 7, the average target voltage is about −450 volts, which was displayed on the front panel of the power supply, but in fact the peak-to-peak voltage was about 1500 volts. Such high voltages will produce much more energetic particles during part of the pulse cycle, and the effect of these energetic particles on the structure and properties of the coating is still being evaluated. Initially there has been no noticeable effect of these high energetic neutrals on the properties of the coatings, but there may be applications where this high energy could be detrimental. In many ways, the voltages

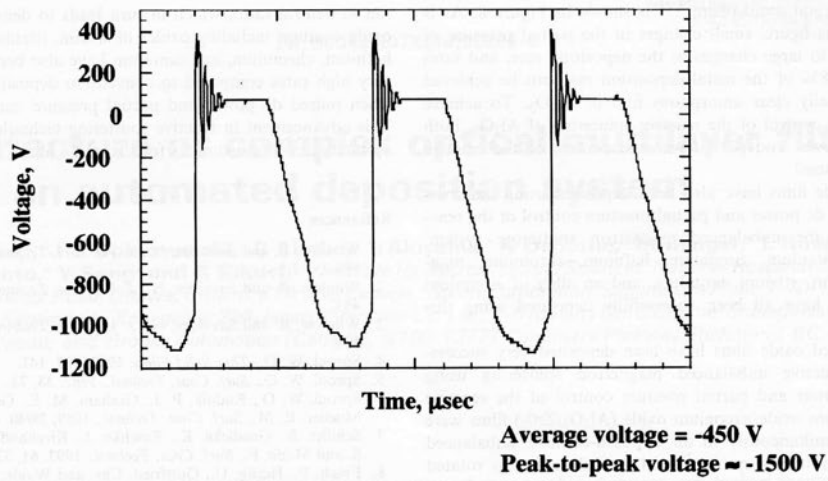

Figure 7. Trace of pulsed dc power during the reactive sputter of aluminum in an argon/oxygen atmosphere.

produced during asymmetric pulsed dc sputtering are similar to the voltages found in dc diode systems.

Reactive unbalanced magnetron sputtering of multilayered coatings

Reactive unbalanced magnetron sputtering in an opposed-cathode system has been used very successfully to deposit nanometer-scale multilayer nitride and oxide films that have enhanced physical properties.[15–19] The first work in this area was with titanium nitride/niobium nitride (TiN/NbN) and titanium nitride/vanadium nitride (TiN/VN) coatings. Partial pressure control of the reactive gas was crucial to achieve the cubic form of NbN, and the high degree of ion bombardment from the unbalanced magnetron sources led to fully dense well-adhered films. The hardness of the TiN/NbN and TiN/VN films was greater than 50 GPa, which is more than twice the hardness of either component in these two multilayered films, when the superlattice period, which is the bilayer thickness of the TiN and NbN or TiN and VN, was in the range of 50 to 80 Å. The individual layer thicknesses were approximately equal.

The importance of the combination of pulsed dc power and partial pressure control of the reactive gas really came into the spotlight with the reactive unbalanced magnetron sputtering of non-conducting oxides such as aluminum oxide (Al_2O_3). Without this combination of pulsed dc power and partial pressure control, it really was not possible to reactively sputter Al_2O_3 at high deposition rates in a practical way. A portion of the hysteresis loop for the reactive sputtering of aluminum in

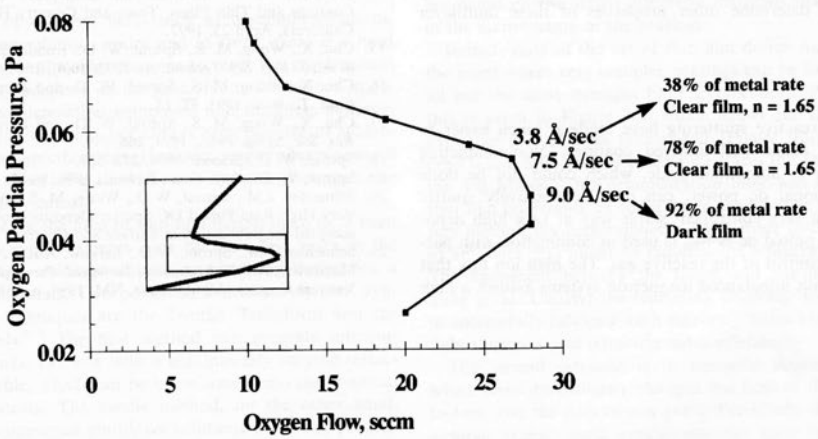

Figure 8. Nose region of the hysteresis curve for the reactive sputtering of aluminum in an argon/oxygen atmosphere. Full curve is shown in the inset in the lower left corner of the diagram.

an oxygen/argon atmosphere[20,21] is shown in Figure 8. As is shown in this figure, small changes in the partial pressure of oxygen lead to large changes in the deposition rate, and rates as high as 78% of the metal deposition rate can be achieved for an optically clear amorphous film of Al_2O_3. To achieve this sensitive control of the reactive sputtering of Al_2O_3, both pulsed dc power and partial pressure control of the reactive gas must be used.

Other oxide films have also been deposited using the combined pulsed dc power and partial pressure control of the reactive gas in the unbalanced magnetron sputtering system. Oxides of titanium, zirconium, hafnium, chromium, magnesium, silicon, yttrium, tantalum, and an alloy of zirconium and yttrium have all been successfully deposited using this technology.

Multilayered oxide films have been deposited very successfully via reactive unbalanced magnetron sputtering using pulsed dc power and partial pressure control of the reactive gas. Aluminum oxide/zirconium oxide ($Al_2O_3/Zr0_2$) films were deposited simultaneously in an opposed-cathode unbalanced magnetron sputtering system,[19] and the substrate was rotated between the two cathodes. The deposition rate was approximately 75% of each metal rate, and both individual layer thicknesses of the Al_2O_3 and ZrO_2 were about 45 Å each, which gave a bilayer thickness of 90 Å. The films were optically clear, and the structure of the multilayer film was amorphous as determined by X-ray diffraction.

Most recently, multilayer oxide films of yttrium oxide and zirconium oxide (Y_2O_3/ZrO_2) have been deposited in the opposed-cathode unbalanced magnetron sputtering system again using pulsed dc power and partial pressure control of the reactive gas.[14] The Y_2O_3/ZrO_2 films were similar to the Al_2O_3/ZrO_2 in that they were optically clear, but they were different because the Y_2O_3/ZrO_2 were crystalline with a cubic structure. The cubic structure of the Y_2O_3 forced the ZrO_2, which normally has a monoclinic structure, into a cubic structure. The overall film had a dense columnar structure, and within a column there was a true superlattice structure for the Y_2O_3/ZrO_2 film. Satellite peaks were clearly visible in the X-ray diffraction patterns from these films. Work is currently underway to determine other properties of these multilayer oxide films.

Summary

Advances in reactive sputtering have made it much easier to deposit fully dense well adhered coatings. Non-conducting coatings such as aluminum oxide, which could not be done with conventional dc power, can now be reactively sputter deposited in a very controlled, stable way at very high deposition rates if pulsed dc power is used in conjunction with partial pressure control of the reactive gas. The high ion flux that is available with unbalanced magnetron systems assures a high ion to neutral ratio, which in turn leads to dense films. Other oxide coatings including oxides of silicon, titanium, zirconium, hafnium, chromium, and tantalum have also been deposited at very high rates compared to convention deposition techniques when pulsed dc power and partial pressure control are used. This advancement in reactive sputtering technology is opening up many new opportunities for the oxide films.

References

1. Window, B. and Savvides, N., *J. Vac. Sci. Technol. A*, 1986, **4**(2), 196.
2. Window, B. and Savvides, N., *J. Vac. Sci. Technol. A*, 1986, **4**(3), 453.
3. Window, B. and Savvides, N., *J. Vac. Sci. Technol. A*, 1986, **4**(3), 504.
4. Sproul, W. D., *Thin Solid Films*, 1983, **107**, 141.
5. Sproul, W. D., *Surf. Coat. Technol.*, 1987, **33**, 73.
6. Sproul, W. D., Rudnik, P. J., Graham, M. E., Gogol, C. A. and Mueller, R. M., *Surf. Coat. Technol.*, 1989, **39/40**, 499.
7. Schiller, S., Goedicke, K., Reschke, J., Kirchhoff, V., Schneider, S. and Milde, F., *Surf. Coat. Technol.*, 1993, **61**, 331.
8. Frach, P., Heisig, U., Gottfried, Chr. and Walde, H., *Surf. Coat. Technol.*, 1993, **59**, 177.
9. Graham, M.E. and Sproul, W.D., 37th Annual Technical Conference Proceedings, Society of Vacuum Coaters, Albuquerque, New Mexico, 1994, p. 275.
10. Sproul, W. D., Graham, M. E., Wong, M. S., Lopez, S., Li, D. and Scholl, R. A., *J. Vac. Sci. Technol. A.*, 1995, **13**(3), 1188.
11. Schiller, S., Goedicke, K., Kirhhoff, V. and Kopte, T., 38th Annual Technical Proceedings, Society of Vacuum Coaters, Albuquerque, NM, 1995, p. 293.
12. Sellers, J., Asymmetric Bipolar Pulsed DC, ENI Tech Note, ENI, Division of Astec America, Inc., 100 Highpower Road, Rochester, NY 14623.
13. Schneider, J.M., Sproul, W.D. and Matthews, A., Phase Formation and Mechanical Properties of Alumina Coatings Prepared at Substrate Temperatures < 500°C by Ionized and Conventional Sputtering, paper presented at the International Conference on Metallurgical Coatings and Thin Films, Town and Country Hotel, San Diego, California, April 23, 1997 and accepted for publication in Surface and Coatings Technology.
14. Sproul, W.D., Wong, M.S., Yashar, P., Wang, Y.Y., Barnett, S.A. and Chung, Y.W., Stabilization of Metastable Phases in Polycrystalline Nanometer-Scale Multilayered Coatings, paper presented at the International Conference on Metallurgical Coatings and Thin Films, Town and Country Hotel, San Diego, California, April 23, 1997.
15. Chu, X., Wong, M. S., Sproul, W. D., Rohde, S. L. and Barnett, S. A., *J. Vac. Sci. Technol. A.*, 1992, **10**(4), 1604.
16. Chu, X., Wong, M. S., Sproul, W. D. and Barnett, S. A., *Surf. Coat. Technol.*, 1993, **57**, 13.
17. Chu, X., Wong, M. S., Sproul, W. D. and Barnett, S. A., *Mat. Res. Soc. Symp. Proc.*, 1993, **286**, 379.
18. Sproul, W. D., *Science*, 1996, **273**, 889.
19. Sproul, W. D., *Surf. Coat. Technol.*, 1996, **86-87**, 170.
20. Schneider, J.M., Sproul, W.D., Wong, M.-S. and Matthews, A., Very High Rate Pulsed DC Sputter Deposition of AlO_x Coatings, accepted for publication in Surface and Coatings Technology.
21. Schneider, J.M., Sproul, W.D., Lefkow, A.R.T., Rechner, J. and Matthews, A., *39th Annual Technical Proceedings*, Society of Vacuum Coaters, Albuquerque, NM, 1996, p. 168.

Appendix 1036-B

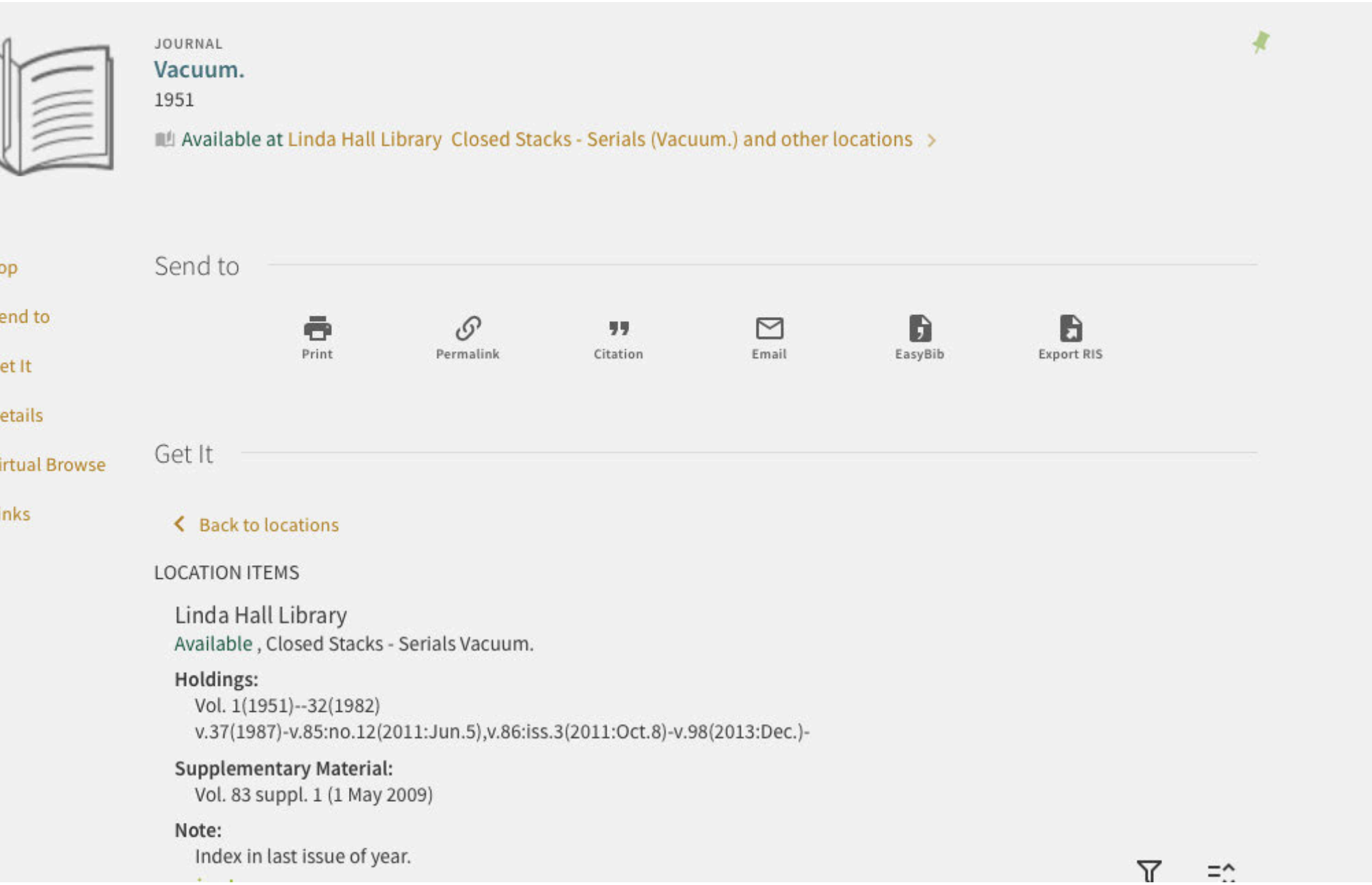
JOURNAL
Vacuum.
1951
Available at Linda Hall Library Closed Stacks - Serials (Vacuum.) and other locations
Send to
Print
Permalink
Citation
Email
EasyBib
Export RIS
Get It
Back to locations
LOCATION ITEMS
Linda Hall Library
Available , Closed Stacks - Serials Vacuum.
Holdings:
Vol. 1(1951)--32(1982)
v.37(1987)-v.85:no.12(2011:Jun.5),v.86:iss.3(2011:Oct.8)-v.98(2013:Dec.)-
Supplementary Material:
Vol. 83 suppl. 1 (1 May 2009)
Note:
Index in last issue of year.

Send to

Get It

Details

Virtual Browse

Links

Details

Title	Vacuum.
Subjects	Vacuum -- Periodicals Periodicals
Identifier	LC : 54017378 ISSN : 0042-207X OCLC : (OCoLC)1465970
Other title	Vacuum
Publisher	Orlando, FL etc. Elsevier etc. v. 1- Jan. 1951-
Creation date	1951
Format	v. ill.. 26 cm.
Frequency	Fourteen no. a year, 2005-
General notes	"The international journal & abstracting service for vacuum science & technology." Some issues have supplements.
Citation/References note	Chemical abstracts 0009-2258
Local notes	Selected volumes/issues gift of University of Vermont Libraries.

```
01765cas a2200505   4500
992818493405961
20191029185931.0
cr cn|||||||||
750722c19519999fluqr p   a   0   a0eng
##$a   54017378
##$a3 $b3 $en $j0 $k1 $m1
7#$a21440110R $2DNLM
7#$aV00120000 $2DNLM
7#$a011151106 $2Uk
##$a1768938 $a213527348
0#$a0042-207X $l0042-207X $z0506-3469 $2z
##$aVACUAV
##$a007608 $bUSPS
##$a(OCoLC)1465970 $z(OCoLC)1768938 $z(OCoLC)213527348
##$a(MoKL)281849-lhalldb
##$a(lhalldb)281849-lhalldb
##$z(OCoLC)1768938 $z(OCoLC)213527348
##$aDLC $beng $cFUL $dCOO $dNSD $dDLC $dNSD $dDLC $dOCL $dSER $dRCS $dAIP $dOCL $dNST $dNSD $dNST $dNSD $dCUS $dOCLCQ $dNLM $dIUL $dOCLCQ $dCLU $d
##$ansdp $apcc
##$aLHLA
00$aQC166 $b.V33
00$aW1 $bVA244
#4$a533.12*
0#$aVacuum
#0$aVacuum
00$aVacuum.
##$aOrlando, FL [etc.] $bElsevier [etc.]
##$av. $bill.. $c26 cm.
##$aFourteen no. a year, $b2005-
##$aFrequency varies, 1951-2004
0#$av. 1- Jan. 1951-
##$a"The international journal & abstracting service for vacuum science & technology."
##$aSome issues have supplements.
2#$aChemical abstracts $x0009-2258
##$aAlso available online.
##$aSelected volumes/issues gift of University of Vermont Libraries.
#0$aVacuum $vPeriodicals.
#7$aPeriodicals. $2fast $0(OCoLC)fst01411641
##$aDLC $aFU $aIaAS $aMsU $aNjMuA $aTxHR
20$9853 $81 $av. $u12 $vr $i(year) $j(month) $wm
41$9863 $81.1 $a20 $i1970 $j01
##$aVol. 77, issue 1 (17 Dec. 2004) $aVol. 80, no. 1/3 (14 Oct. 2005) (surrogate)
##$aLTI 04/26/2017
```

Appendix 1036-C

PERGAMON

Vacuum 56 (2000) 159–172

VACUUM
SURFACE ENGINEERING, SURFACE INSTRUMENTATION & VACUUM TECHNOLOGY

www.elsevier.nl/locate/vacuum

Magnetron sputtering: a review of recent developments and applications

P.J. Kelly*, R.D. Arnell

Centre for Advanced Materials and Surface Engineering, University of Salford, Salford M5 4WT, UK

Received 20 September 1999

Abstract

Magnetron sputtering has become the process of choice for the deposition of a wide range of industrially important coatings. Examples include hard, wear-resistant coatings, low friction coatings, corrosion resistant coatings, decorative coatings and coatings with specific optical, or electrical properties. Although the basic sputtering process has been known and used for many years, it is the development of the unbalanced magnetron and its incorporation into multi-source 'closed-field' systems that have been responsible for the rise in importance of this technique. Closed-field unbalanced magnetron sputtering (CFUBMS) is an exceptionally versatile technique for the deposition of high-quality, well-adhered films. The development, fundamental principles and applications of the CFUBMS process are, therefore, discussed in some detail in this review. Also discussed are other important recent developments in this area, including the pulsed magnetron sputtering process, variable field magnetrons, and the combining of sputtering techniques with other surface coating, or surface modification techniques in duplex production processes.

Keywords: Closed-field unbalanced magnetron sputtering; Pulsed sputtering; Variable magnetrons

1. Introduction

Magnetron sputtering has developed rapidly over the last decade to the point where it has become established as the process of choice for the deposition of a wide range of industrially important coatings. The driving force behind this development has been the increasing demand for high-quality functional films in many diverse market sectors. In many cases, magnetron sputtered films now outperform films deposited by other physical vapour deposition (PVD) processes, and can offer the same functionality as much thicker films produced by other surface coating techniques. Consequently, magnetron sputtering now makes a significant impact in application areas including hard, wear-resistant coatings, low friction coatings, corrosion-resistant coatings, decorative coatings and coatings with specific optical, or electrical properties [1].

The basic sputtering process has been known and, despite its limitations, used for many years. The introduction of what are now termed 'conventional', or 'balanced' magnetrons in the early 1970s [2,3] was an important step forward in overcoming these limitations. However, it was the development of the unbalanced magnetron in the late 1980s [4–6] and its incorporation into multi-source 'closed-field' systems in the early 1990s [7,8] that transformed the capabilities of this technique, and has subsequently been responsible for its rise in importance. Closed-field unbalanced magnetron sputtering (CFUBMS) is an exceptionally versatile technique, suitable for the deposition of high-quality, well-adhered films of a wide range of materials at commercially useful rates. The development and fundamental principles of this process are, therefore, discussed in some detail in this paper. Also discussed are examples and applications of advanced coatings produced using this technique, including the latest generation of carbon-based and molybdenum disulphide-based coatings.

The pulsed magnetron sputtering (PMS) process is another very important recent development in the sputtering field [9]. The DC reactive sputtering of fully dense,

* Corresponding author. Tel.: +44-161-295-4734; fax: +44-161-295-5108.

E-mail address: p.kelly@sa ford.ac.uk (P.J. Kelly).

0042-207X/00/$ - see front matter
PII: S0042-207X(99)00189-X

defect-free coatings of insulating materials, particularly oxides, is highly problematic. The process is hampered by low deposition rates and the occurrence of arc events at the target, which are detrimental to the structure, properties and composition of the coating. However, pulsing the magnetron discharge in the mid-frequency range (10–200 kHz) has been found to prevent arc events and stabilise the reactive sputtering process. High-quality oxide coatings can now be deposited using the PMS process at rates approaching those achieved for metallic coatings. The PMS process is discussed in Section 7 of this review.

Two other recent developments are also discussed; variable field magnetrons and duplex production processes. In all PVD processes, ion bombardment of the growing film is a critical parameter which strongly influences the structure and properties of the growing film [10,11]. In a magnetron sputtering system, for any given set of deposition conditions, the ion current delivered to the growing film depends on the strength and design of the magnetic array in the magnetron. Clearly, in most cases this is fixed. However, new magnetrons have now been developed in which the magnetic array can be varied in situ without the use of electromagnets [12]. This facility allows the ion current to the substrate to be controlled and optimised at all stages of the deposition process.

Finally, there is now a move towards combining magnetron sputtering with other deposition, or surface modification techniques, in so-called duplex surface engineering processes (this title can actually be applied to any process which combines two surface engineering techniques) [13]. The aims in such cases are to extend the performance of the component beyond that which either process can achieve on its own, and to allow the use of cheaper base materials in high-performance applications. A typical example would be the plasma nitriding of a low alloy steel component, followed by coating it with a wear-resistant material, such as titanium nitride (TiN). The hardened nitrided layer provides additional load support to the TiN coating, improving its adhesion. The resulting component combines high wear resistance with high load-bearing capacity and good fatigue strength [14]. This, and other examples of duplex processes, are discussed in Section 9.

2. Magnetron sputtering

In the basic sputtering process, a target (or cathode) plate is bombarded by energetic ions generated in a glow discharge plasma, situated in front of the target. The bombardment process causes the removal, i.e., 'sputtering', of target atoms, which may then condense on a substrate as a thin film [1]. Secondary electrons are also emitted from the target surface as a result of the ion bombardment, and these electrons play an important role in maintaining the plasma. The basic sputtering process has been known for many years and many materials have been successfully deposited using this technique [15,16]. However, the process is limited by low deposition rates, low ionisation efficiencies in the plasma, and high substrate heating effects. These limitations have been overcome by the development of magnetron sputtering and, more recently, unbalanced magnetron sputtering.

Magnetrons make use of the fact that a magnetic field configured parallel to the target surface can constrain secondary electron motion to the vicinity of the target. The magnets are arranged in such a way that one pole is positioned at the central axis of the target and the second pole is formed by a ring of magnets around the outer edge of the target. Trapping the electrons in this way substantially increases the probability of an ionising electron–atom collision occurring. The increased ionisation efficiency of a magnetron results in a dense plasma in the target region. This, in turn, leads to increased ion bombardment of the target, giving higher sputtering rates and, therefore, higher deposition rates at the substrate. In addition, the increased ionisation efficiency achieved in the magnetron mode allows the discharge to be maintained at lower operating pressures (typically, 10^{-3} mbar, compared to 10^{-2} mbar) and lower operating voltages (typically, -500V, compared to -2 to -3 kV) than is possible in the basic sputtering mode.

The differences in design between a conventional magnetron and an unbalanced magnetron are only slight. However, the difference in performance between the two types of magnetron is very significant. In a conventional magnetron the plasma is strongly confined to the target region. A region of dense plasma typically extends some 60 mm from the target surface. Films grown on substrates positioned within this region will be subjected to concurrent ion bombardment, which, as mentioned earlier, can strongly influence the structure and properties of the growing film. Substrates placed outside this region, however, will lie in an area of low plasma density. Consequently, the ion current drawn at the substrate (typically, < 1 mA/cm^2) is generally insufficient to modify the structure of the film. The energy of the bombarding ions can be increased by increasing the negative bias applied to the substrate. However, this can lead to defects in the film and increased film stress, and therefore, be detrimental to the overall film properties. Thus, it is difficult to deposit fully dense films on large, or complex components using conventional magnetrons [17].

To deposit dense films without introducing excessive intrinsic stresses, a high flux (> 2 mA/cm^2) of relatively low energy (< 100 eV) ions is generally preferred [18]. These conditions are readily provided by unbalanced magnetrons.

3. Unbalanced magnetron sputtering

In an unbalanced magnetron the outer ring of magnets is strengthened relative to the central pole. In this case, not all the field lines are closed between the central and outer poles in the magnetron, but some are directed towards the substrate, and some secondary electrons are able to follow these field lines. Consequently, the plasma is no longer strongly confined to the target region, but is also allowed to flow out towards the substrate. Thus, high ion currents can be extracted from the plasma without the need to externally bias the substrate. Earlier studies had shown that in some magnetron designs not all the field lines closed in on themselves [19] (indeed, very few, if any, magnetrons are truly fully balanced). However, it was Windows and Savvides who first appreciated the significance of this effect when they systematically varied the magnetic configuration of an otherwise conventional magnetron [4–6]. They, and other researchers, have subsequently shown that substrate ion current densities of 5 mA/cm^2 and greater, i.e., approximately an order of magnitude higher than for a conventional magnetron, can be routinely generated when using an unbalanced magnetron [6,20,21]. A comparison between the plasma confinement obtained in different magnetron modes is shown schematically in Fig. 1.

Thus, in addition to providing a high flux of coating atoms (compared to a basic sputtering source), an unbalanced magnetron also acts as a very effective ion source. Furthermore, the ion current drawn at the substrate is directly proportional to the target current. Deposition rate is also directly proportional to target current. As a result, and unlike other ion-plating processes [22,23], the ion-to-atom arrival ratio at the substrate remains constant with increasing deposition rate [24].

The design of unbalanced magnetron discussed above was termed 'type-2' by Window and Savvides. However, they also considered the opposite case ('type-1'), where the central pole was strengthened relative to the outer pole. In this case the field lines which do not close in on themselves are directed towards the chamber walls and the plasma density in the substrate region is low (see Fig. 1). This design is not commonly used, because of the resulting low ion currents at the substrate. However, a recent project at Salford utilised this characteristic for the production of novel, high surface area, chemically reactive metallic films [25]. Through a systematic study of the deposition process, conditions were determined under which coatings with a controlled and reproducible porosity were obtained. Indeed, coatings with porosities of the order of 1000 times greater than a fully dense material were produced [26]. Further, as shown in Fig. 2, the temperature at which these coatings spontaneously reacted in air was shown to be dependent on the effective surface area of the films, as determined by AC impedance testing. Films of this type have a number of diverse potential applications, such as catalysts, pyrophoric devices, or non-reflective coatings.

4. Closed-field unbalanced magnetron sputtering

Despite the benefits offered by unbalanced magnetrons, it is still difficult to uniformly coat complex components at acceptable rates from a single source. Therefore, in order to commercially exploit this technology, multiple magnetron systems have been introduced.

In a multiple magnetron system, the magnetic arrays in adjacent magnetrons can be configured with either identical, or opposite magnetic polarities. In the former case the configuration is described as 'mirrored' and in the latter case 'closed field', and both configurations are shown in Fig. 3. In the mirrored case, the field lines are directed towards the chamber walls. Secondary electrons following these lines are lost, resulting in a low plasma density in the substrate region. Conversely, in the closed

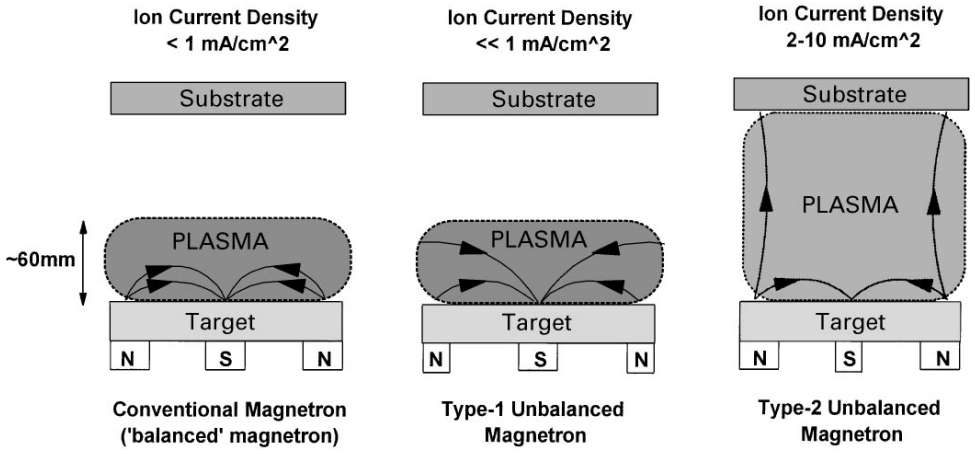

Fig. 1. Schematic representation of the plasma confinement observed in conventional and unbalanced magnetrons.

field configuration, the field lines are linked between the magnetrons. Losses to the chamber walls are low and the substrate lies in a high density plasma region. The effectiveness of the closed field configuration is shown in Fig. 4, which is taken from a study at Salford University [27]. As can be seen, operating in the closed field mode results in an ion-to-atom ratio incident at the substrate some 2–3 times greater than that obtained under the same conditions in the mirrored, or single unbalanced magnetron configurations. Also, the influence of the closed magnetic field on the ion-to-atom ratio becomes more marked as the distance from the target increases.

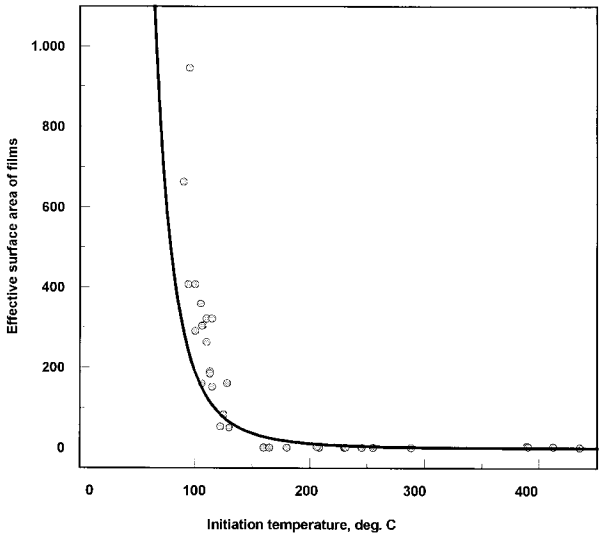

Fig. 2. The relationship between effective surface area (relative to fully dense material) and ignition temperature for chemically reactive metallic films.

In the UK, Teer Coatings Ltd. were quick to recognise the potential of multiple magnetron systems, and, in the early 1990s, developed a patented design of commercial and research scale CFUBMS systems [28]. In these, and other similar systems developed elsewhere [8,29], an even number of vertically opposed magnetrons surround the rotating substrate holder. Adjacent magnetrons have opposite magnetic polarities and the field lines are closed. As stated above, such systems are capable of transporting high ion currents to the substrate. However, recent developments in magnetron design and the use of high strength rare earth magnets in the magnetic arrays have led to significant further increases in the magnitude of the ion currents drawn at the substrate. Early magnetrons generally made use of ferrite magnets which gave a maximum field strength of the order of 300–500 G at the target surface [27,30]. With improved magnetron design and the introduction of rare earth magnets, field strengths in excess of 1 kG are now obtainable at the target surface. The increased field strength increases the ionisation efficiency in the plasma, which in turn, results in much higher ion currents at the substrate. This effect is illustrated in Fig. 5, which consists of data supplied by Teer Coatings [31], and compares the ion current measured at the substrate for single balanced and unbalanced magnetrons; an early (pre-1995) CFUBMS system using ferrite magnets; and a more recent, modified CFUBMS system using rare earth magnets.

5. Advanced coatings by CFUBMS

In general, the most commercially useful coatings tend to be ceramic materials, including oxides, nitrides and carbides. These materials can be deposited by sputtering

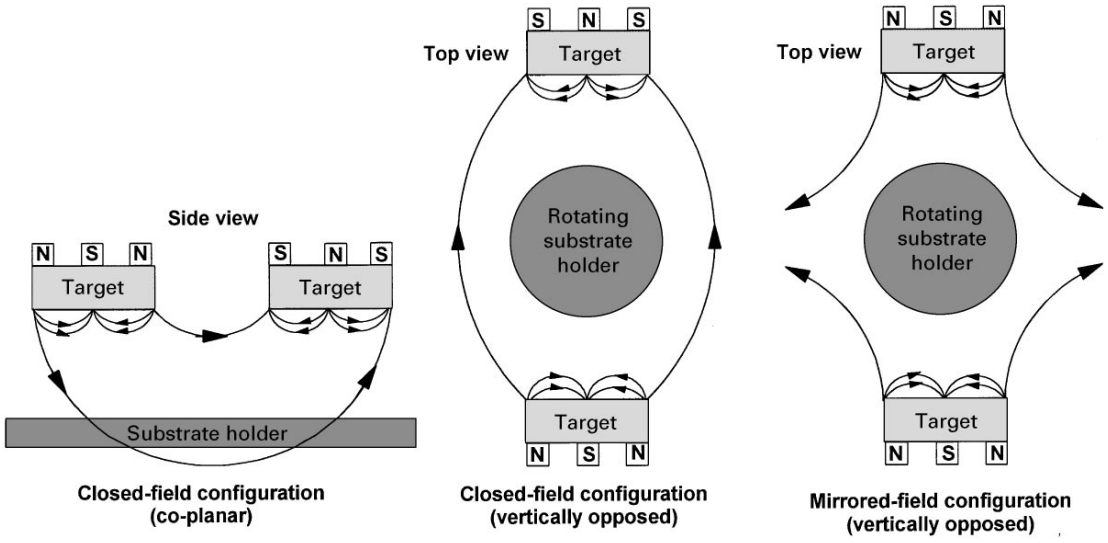

Fig. 3. Dual unbalanced magnetron configurations.

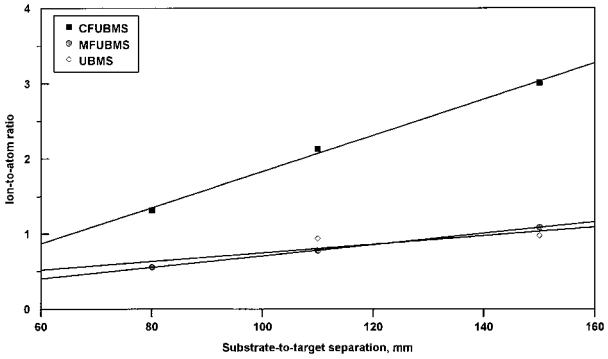

Fig. 4. The variation with substrate–to-target separation in the ion-to-atom ratio incident at the substrate for closed field (CFUBMS), mirrored field (MFUBMS) and single magnetron (UBMS) configurations.

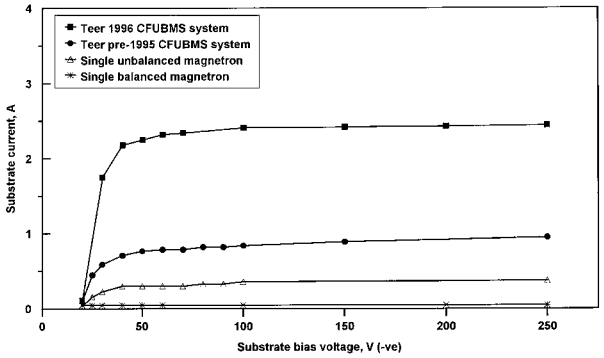

Fig. 5. A comparison of the current–voltage characteristics for various Teer Coatings Ltd. magnetron sputtering systems (after Ref. [30]).

a metallic target in the presence of the appropriate reactive gas. Single element nitrides, most commonly titanium nitride, are now routinely produced by magnetron sputtering. However, the multiple magnetron CFUBMS systems are ideally suited to the deposition of multi-component, or alloy nitrides, as each of the magnetron targets can, in principle, be of a different material. In this manner, materials such as (TiAl)N, (TiZr)N and (CrZr)N have all been deposited. In each case, these coatings can exceed the performance of TiN in specific applications [32]. By sputtering the targets at different rates, any desired alloy composition can be attained. Further, by varying either the sputtering rates, or the flow of reactive gas during deposition, composition, and, therefore, properties can be graded through the thickness of the coating. In this manner, properties can be optimised, both at the coating/substrate interface for adhesion, and at the coating surface for the desired functionality.

The production of diamond-like carbon (DLC) coatings by CFUBMS combines many of the features described above and offers a good example of how the versatility of this process has recently led to significant improvements in the performance of the coating [33]. This process is discussed in more detail in Section 9. Other examples, again highlighting the versatility of the CFUBMS process, are the production of novel multilayer pyrotechnic coatings [34] and corrosion resistant supersaturated Al/Mg alloy coatings [35]. In these two examples an alternative closed field arrangement was used, with two magnetrons in co-planar positions, rather than vertically opposed (see Fig. 3).

Two other recently developed, commercially available coating materials which also make use of the attributes of the CFUBMS system are the molybdenum disulphide (MoS_2)-based MoST coatings [36] and the carbon-based Graphit-iC[1] coatings [37].

MoST coatings are MoS_2/metal composite coatings which are much harder, more wear resistant and less sensitive to atmospheric moisture than traditional MoS_2 coatings, yet they still retain the low friction characteristics of MoS_2. These coatings are deposited by CFUBMS in four-magnetron systems incorporating three MoS_2 targets and one titanium target. An initial titanium interlayer ($\sim$ 100 nm thick) is deposited to optimise adhesion. The MoST coating is then deposited by simultaneously sputtering from the three MoS_2 targets and the Ti target, whilst the substrate holder is rotated. Analysis has determined that the coating structure is an amorphous, homogeneous solid solution of Ti in MoS_2, the titanium content of which can be readily varied by controlling the relative MoS_2 and Ti target powers.

The MoST coating combines a number of remarkable properties. Indentation tests show a hardness of greater than 15 GPa, whilst scratch adhesion tests indicate a critical load greater than 120 N, and friction coefficients as low as 0.005 have been recorded in dry nitrogen. One of the major advantages of MoST coatings over traditional MoS_2 coatings is the ability of the coating to perform in humid conditions. MoS_2 coatings are generally only suitable for use in dry or vacuum conditions. However, many tests have confirmed MoST coatings can perform successfully in atmospheres of 40–50% humidity, under which conditions the coefficient of friction can be as low as 0.02 [36].

MoST coatings have many industrial applications. They are particularly suitable for the dry machining of steels, cast irons, and aluminium, titanium and nickel alloys. By way of example, Fig. 6 shows the improvement in tool life offered by MoST coatings over traditional MoS_2 coatings in a dry punching operation. Also, Fig. 7 shows the improvement in feed rate obtained using a MoST coated tool, compared to other tools, for end mill operations on a wrought aluminium alloy [38].

Graphit-iC coatings are a new type of hard carbon coating that can outperform established DLC coatings in

[1] MoST and Graphit-iC are trademarks of Teer Coatings Ltd.

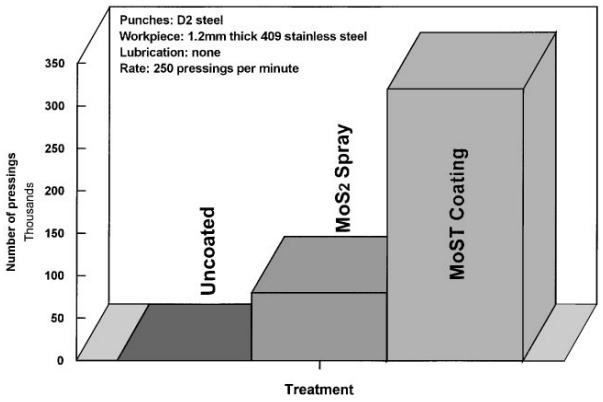

Fig. 6. An example of the improvement in life offered by MoST coatings over conventional MoS_2 and uncoated tools in a dry punching operation (after Ref. [37]).

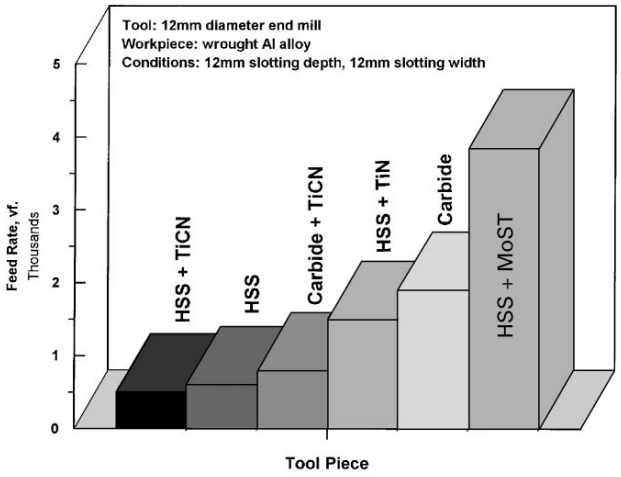

Fig. 7. A comparison of feed rates achieved for uncoated and coated end mill tools (after Ref. [37]).

certain applications [37,39]. The coatings are again deposited in a four magnetron system. In this case, though, there are three carbon targets and one chromium target. A thin chromium bond layer is deposited, followed by a pure carbon coating. Alternatively, by controlling target powers and substrate rotation speed, a metal/carbon multi-layer coating can be deposited. Analysis by Raman spectroscopy has shown that Graphit-iC coatings exhibit predominantly sp^2-type bonding, unlike DLC coatings, where the bonding is mainly sp^3-type. Despite this, coating hardness values of between 15 and 40 GPa have been recorded, depending on deposition conditions. In addition, Graphit-iC coatings exhibit lower coefficients of friction, lower wear rates and higher load bearing capacity than DLC coatings. Typical applications for these coatings include automobile engine parts, cutting and forming tools and moving parts, such as taps and valves, operating in an aqueous environment.

6. The development of a structure zone model for the CFUBMS system

Much has been made in the preceding sections of the ability of the CFUBMS system to deliver high ion currents to the substrate. The impact of this factor on the properties of coatings deposited using this technique has been assessed in extensive studies at Salford University [40]. One aim of this study was to develop a new structure zone model relating to this technique.

Structure zone models (SZMs) have long been used as a convenient means of displaying the relationships between process parameters and the structures and, therefore, the properties of PVD coatings. Several such models have been developed to describe the structure of coatings deposited by various sputtering processes [41–44], the best known being the one developed by Thornton [41]. In this, and all similar models, the homologous temperature, T/T_m, (where T is the substrate temperature, and T_m is the melting temperature of the coating material) of the coating is used to describe the thermally induced mobility of the coating atoms. A second variable attempts to describe the influence of the simultaneous bombardment of the growing film by energetic particles. Parameters chosen for this second axis include coating pressure [41,44], substrate bias voltage [42], and a combined energy parameter described as the average energy per depositing atom [43]. In these models, the coatings are categorised as having one of three main structural types. At low homologous temperatures ('zone 1') atomic shadowing is the dominant growth mechanism, and the coating structure consists of tapered columnar grains separated by pores, or voids. The term 'porous columnar' is, therefore, used to describe this type of structure. At higher homologous temperatures ('zone 2') atomic mobility is increased, allowing surface diffusion processes to dominate. In this zone the structure still has a distinct columnar appearance, but there are no voids between the columns, and the structure is described as 'dense columnar'. At still higher homologous temperatures ('zone 3') the bulk diffusion processes of recrystallisation and grain growth can occur, and the coatings have 'fully dense' equiaxed grain structures.

In the Salford study [40], aluminium, zirconium and tungsten coatings were deposited by CFUBMS under systematically varied conditions, and characterised in terms of their structures and properties. Also, for each set of conditions, the ratios of the fluxes of ions and condensing atoms at the substrate were estimated from ion current density and deposition rate measurements. The system chosen for characterisation was a Teer Coatings Ltd. UDP 450 CFUBMS rig.

Aluminium coatings were deposited at homologous temperatures over the range 0.43 to 0.68. All had fully dense, highly ductile structures, which 'necked-down' completely on fracture. SEM and TEM investigations confirmed that all had zone 3-type structures, using the classification system described above. The zirconium and tungsten coatings were deposited at homologous temperatures over the ranges 0.22–0.28 and 0.13–0.17, respectively, and all had dense columnar, zone 2-type structures. By way of an example, Fig. 8 shows a through thickness TEM micrograph of a tungsten coating deposited at $T/T_m = 0.13$. Large (100–200 nm) polygonal grain-like regions are clearly visible, separated by regions of high dislocation density. No pores are visible between the columns, confirming the zone 2 classification.

The formation of zone 2 structures at T/T_m as low as 0.13, and zone 3 structures at T/T_m as low as 0.43 are major departures from the Thornton structure zone model. This is illustrated in Fig. 9, which compares, in terms of homologous temperature, the positions of the zonal boundaries given in other published SZMs for sputtered coatings [41,42], with the boundaries observed in the Salford study. It is clear that operating in the closed field mode has suppressed the formation of porous structures and promoted the formation of fully dense structures at relatively low substrate temperatures. Consequently, since none of the existing SZMs models are adequate to describe the CFUBMS process, Kelly and Arnell developed a new SZM relating to this system [40].

As mentioned earlier, several attempts have been made to describe, in terms of a single parameter, the role played by energetic particle bombardment in determining the structure of sputtered films. One approach is to use an energy parameter which combines both ion energy and ion flux [43,45]. However, it is widely recognised that this approach is of limited applicability and that ion energy and ion flux must be considered separately when modelling the effects of concurrent ion bombardment on coating microstructure [46–49]. Thus, in order to incorporate both of these factors, and the homologous temperature of the coating, a novel three-dimensional SZM has been developed. In the model, which is shown as Fig. 10, the coating structure is described in terms of homologous temperature, ion-to-atom ratio and bias voltage (to represent ion energy). The conventional schematic representation of structure is dispensed with, as it is assumed to be well known. Being a three-dimensional model, the zone 2/zone 3 boundary shown on the model approximates to the surface of a quadrant of a hemisphere. A second boundary is also shown on the model, inside the zone 2 region. This boundary marks the lowest levels of each parameter used in the study, and effectively represents the lower limits of normal operating. This boundary should not be taken as the zone 1/zone 2 boundary, as only coatings with zones 2 and 3 structures were actually produced in this study. It was found that the CFUBMS system inherently produces operating conditions which effectively suppress the formation of porous columnar zone 1-type structures.

By allowing coatings to be described in terms of three critical parameters, the Kelly-Arnell model is a significant advance on existing models. However, it is clear that a number of assumptions were made in the development of this model. There are sources of error in the estimation of ion-to-atom ratio, and, in using bias voltage to represent ion energy, it is assumed that the plasma potential is constant. However, the development of this model is on-going, and it is felt that it will, ultimately, accurately

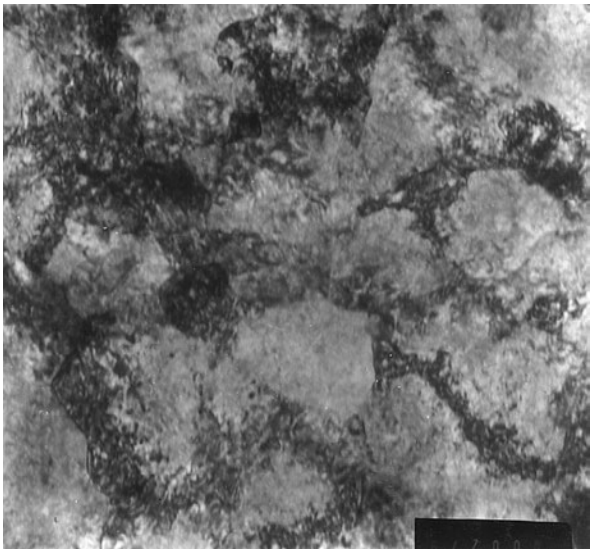

Fig. 8. Through thickness TEM micrograph of a tungsten coating deposited at $T/T_m = 0.13$. The lighter regions in the micrograph are polygonal grain-like regions, which are surrounded by darker regions of high-dislocation density.

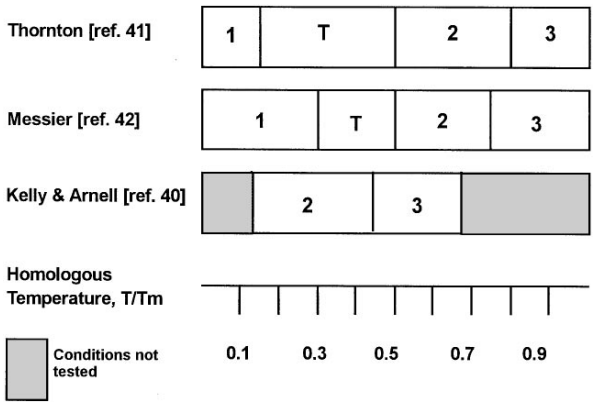

Fig. 9. A comparison, in terms of homologous temperature, of the positions of the zonal boundaries given in published structure zone models relating to other sputtering systems with the boundaries observed for the CFUBMS system.

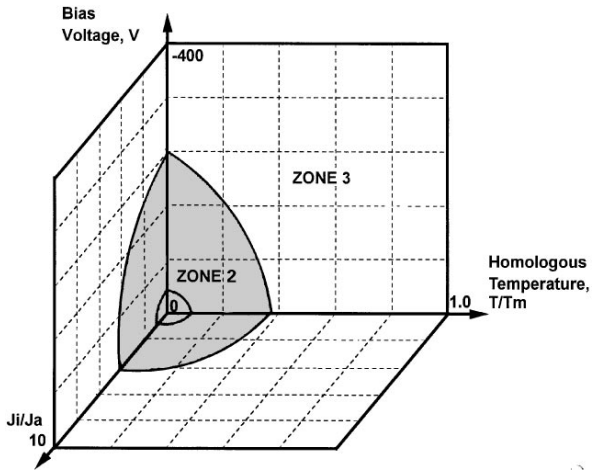

Fig. 10. Structure zone model relating to the CFUBMS system, in which structures are described in terms of homologous temperature, ion-to-atom ratio and bias voltage.

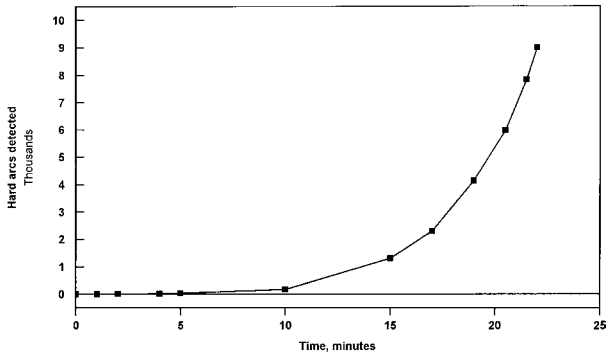

Fig. 11. Variation with time of the cummulative number of hard arcs detected during the deposition of an aluminium oxide film by reactive DC magnetron sputtering.

reflect the parameters which determine coating structure in the CFUBMS system.

7. Pulsed magnetron sputtering

The pulsed magnetron sputtering (PMS) process has transformed the production of highly insulating films, particularly oxides such as alumina. Oxide coatings can be produced by the reactive magnetron sputtering of a metallic target in a controlled oxygen atmosphere. They can also be produced by the direct RF (radio frequency; usually 13.56 MHz) sputtering of an oxide target. However, both of these processes are problematic. RF sputtering can produce high-quality films, but deposition rates are very low (typically in the μm/h range). Also, RF sputtering systems are complex and difficult to scale up for commercial applications.

The problems associated with the reactive magnetron sputtering of highly insulating materials are widely reported [9,50–54]. As the deposition process proceeds, areas on the target away from the main racetrack become covered with an insulating layer, as do the target earth shields. This coverage of the target with the reaction product is referred to as 'target poisoning'. The poisoned layers charges up, until breakdown occurs in the form of an arc. Arc events at the target can result in the ejection of droplets of material from the target surface. The ejected material can cause defects in the growing film, which are particularly detrimental to the performance of optical, or corrosion-resistant films. Also, the damaged area on the target may become a source of further arc discharges, leading to an increasing frequency of arcing, an effect which is clearly illustrated in Fig. 11 [55]. The reactive sputtering process is controlled by a feedback loop. Arc events prevent stable operation of the process by causing rapid fluctuations in the deposition parameters. This, in turn, can affect the stoichiometry of the growing film. In summary therefore, arc events during reactive sputtering are a serious problem, because they can affect the structure, composition and properties of the growing film, and can also lead to damage of the magnetron power supply.

The recently developed pulsed magnetron sputtering process (PMS) overcomes many of the problems encountered when operating in the reactive sputtering mode. It has been found that pulsing the magnetron discharge in the medium frequency range (10–200 kHz) when depositing insulating films can significantly reduce the formation of arcs and, consequently reduce the number of defects in the resulting film [9,50–54]. Furthermore, deposition rates during pulsed reactive sputtering approach those obtained for the deposition of pure metal films [53,54,56], i.e., of the order of tens of microns per hour. The PMS process, therefore, now enables the high rate deposition of defect-free ceramic films. As such, this process has attracted considerable commercial interest, and has led to the development of a new generation of magnetron power supplies and pulse units.

Although AC power supplies are becoming available, the PMS process generally utilises pulsed DC power. In this case, the target is sputtered at the normal operating voltage (typically, -400 to -500 V) for a fixed 'pulse-on' time. The pulse-on time is limited, such that charging of the poisoned regions does not reach the point where breakdown and arcing occurs. The charge is then dissipated through the plasma during the 'pulse-off' period by switching the target voltage to a more positive value. There are two modes of operation: unipolar pulsed sputtering, where the target voltage is pulsed between the normal operating voltage and ground; and bipolar pulsed sputtering, where the target voltage is actually reversed and becomes positive during the pulse-off period.

Due to the much higher mobility of electrons in the plasma than ions, it is usually only necessary to reverse the target voltage to between 10 and 20% of the negative operating voltage to fully dissipate the charged regions and prevent arcing (if the target voltage is not fully reversed, this mode should most accurately be described as 'asymmetric bipolar pulsed DC').

Fig. 12 shows a schematic representation of the target voltage waveform for a pulsed DC power supply operating in the asymmetric bipolar pulse mode. In this example the pulse frequency is 20 kHz, the pulse-off time is 5 μs (i.e., 10% of the full pulse cycle), and the reverse voltage is set to 10% of the normal operating voltage. The effectiveness of operating in this mode is amply illustrated by the micrographs shown as Figs. 13a and b (taken from Ref. [54]). Fig. 13a is a SEM micrograph of the fracture section of an aluminium oxide coating deposited by DC reactive sputtering. In this case, the deposition process was completely unstable, with arcing occurring at the target throughout. The coating has a granular, porous structure and a sub-stoichiometric composition. By contrast, Fig. 13b is a SEM micrograph of the fracture section of an aluminium oxide coating deposited by pulsed DC reactive sputtering, using the operating conditions described above. Arc events were suppressed during deposition, and the process was highly stable. Consequently, the coating has a stoichiometric Al_2O_3 composition, and is extremely dense with no discernible structural features or defects.

The coating shown in Fig. 13b was deposited using an Advanced Energy MDX DC magnetron driver in conjunction with an Advanced Energy SPARC-LE 20 pulse unit. In the SPARC-LE 20 unit, the pulse parameters are fixed. However, the more sophisticated SPARC-LE V unit allows control over pulse frequency, reverse time (i.e., pulse-off time) and reverse voltage. Recent work at Salford, investigating the deposition of alumina films, has shown that each of these parameters play an important role in the overall deposition process [55]. For example, pulsing the magnetron discharge at frequencies below

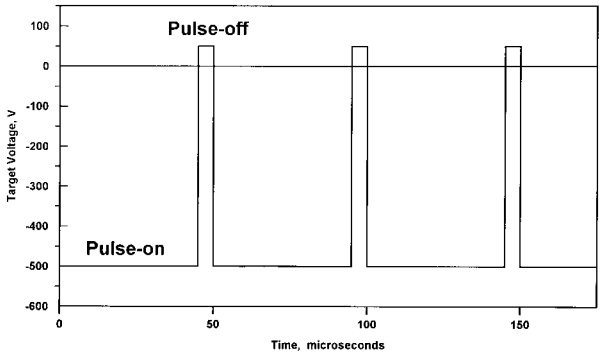

Fig. 12. Schematic representation of the target voltage waveform for a pulsed DC power supply operating in asymmetric bipolar pulse mode.

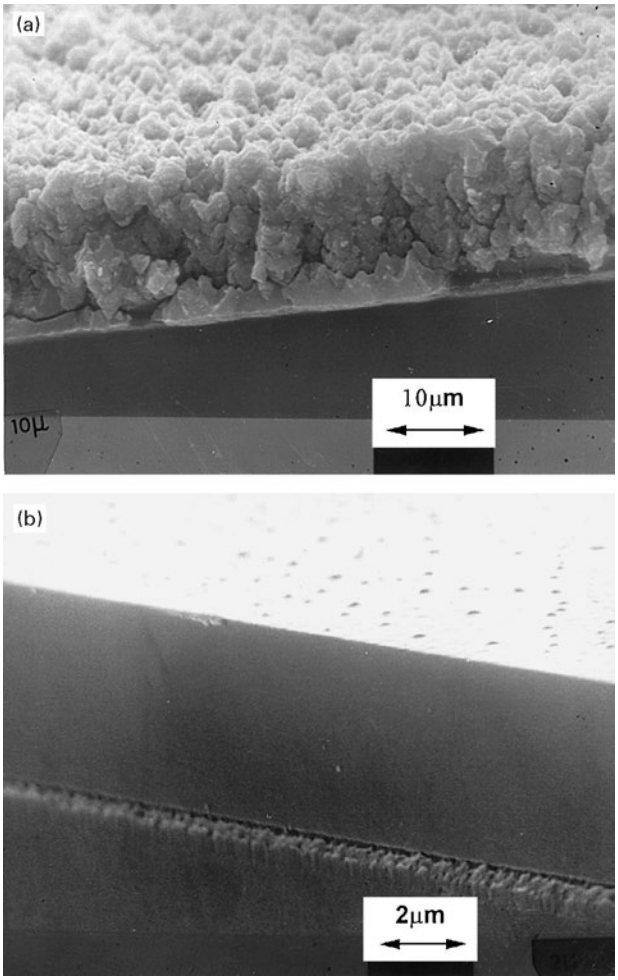

Fig. 13. SEM micrographs of the fracture sections of aluminium oxide deposited by (a) DC reactive sputtering, and (b) pulsed DC reactive sputtering.

20 kHz was found to be ineffective at suppressing arcing. Whereas, at frequencies of 20 kHz and above, arc events can be completely suppressed, but reverse time becomes the critical parameter. At these frequencies, the most effective arc suppression was observed when the reverse time was increased to the point at which the pulse-off time approached, or was equal to the pulse-on time (i.e., 50% of the full pulse cycle). Reverse voltage did not appear to influence the number of arc events detected. However, it did have a significant effect on the deposition rate of the coating. Indeed, increasing the reverse voltage from 10 to 20% of the normal operating voltage, whilst maintaining all other parameters constant, resulted in an increase in the deposition rate of almost 50%. This effect has been attributed to enhanced target cleaning during the voltage reversal at the end of the pulse-off periods [57]. Optimum conditions for the deposition of alumina films, therefore, appear to be pulse frequencies of 20 kHz

and above, with equal pulse-on and pulse-off times, and the reverse voltage set to 20% of the normal operating voltage.

In addition to the dramatic improvements obtained in structure seen in Fig. 13, significant improvements are also obtained in the physical properties of alumina coatings deposited using the conditions described above. For example, Fig. 14 shows the transmission spectra for aluminium oxide coatings deposited by DC reactive sputtering and pulsed DC reactive sputtering, using the SPARC-LE 20 pulse unit. At a wavelength of 550 nm, the transmission of the PMS coating is $> 97\%$. In contrast, the DC sputtered coating has a transmission of only 45% at this wavelength [58].

The PMS process has also been extended to dual magnetron systems [59]. In this case, both magnetrons are attached to the same pulse unit, and the process is described as dual bipolar pulsed sputtering. Each magnetron acts alternately as an anode and a cathode. By operating in this manner, the anode and cathode surfaces are prevented from poisoning, and very long-term process stability is achieved (> 300 h). Industrial applications of this process include the deposition of high-quality optical coatings on materials such as architectural, or automotive glass and polymer web [60,61].

One final recent development in this field is the use of pulsed DC power at the substrate. Pulsing the substrate bias voltage has been found to significantly increase the ion current drawn at the substrate. In magnetron systems, the current drawn at the substrate normally saturates at bias voltages of the order of -100 V [4]. Further increases in bias voltage do not lead to a further increase in current (see Fig. 5 for examples of magnetron current–voltage characteristics). It is generally assumed that the saturation current is an ion current, as any electrons approaching the substrate will be repelled at this voltage. Recent work by Teer Coatings [62], though, has shown that if the bias voltage is pulsed, not only is the magnitude of the saturation current greater than for the DC bias case, but the current drawn at the substrate continues to increase as the bias voltage is increased. In addition, as can be seen in Fig. 15, both of these effects become more marked as the pulse frequency is increased. The exact mechanism causing these effects is not yet clear. However, it is known that plasmas generated by oscillating fields are more energetic (i.e., have higher plasma densities and electron temperatures) than DC plasmas [63]. Pulsing the substrate bias voltage, therefore, offers a novel means of controlling the ion current density drawn at the substrate. This could be utilised, both during deposition to optimise the coating structure and adhesion, and also during sputter cleaning and substrate heating, where enhanced ion currents could allow shorter process times.

8. Variable field strength magnetrons

For any given set of deposition parameters, the performance of a magnetron, i.e., the fluxes of ions and coating atoms that it can deliver to the substrate, is determined by the design of the magnetic array and the strength of the magnets in that array. As discussed in Section 6, the ion-to-atom ratio incident at the substrate is one of the fundamental parameters which determine coating properties. However, both ion current and deposition rate are directly proportional to target current. Thus, when using magnetrons of fixed magnetic configuration, the ion-to-atom ratio can be varied only over a very limited range [40]. To overcome this limitation, new magnetrons have been designed in which the degree of unbalancing can be varied in situ, without the use of costly and cumbersome electromagnets [12]. In order to achieve this, both the inner and outer sets of magnets in the magnetic array can be moved relative to each other. This system allows the magnetron to operate in all modes from virtually balanced, to strongly unbalanced. Further, the degree of unbalancing, and, therefore, the ion-to-atom ratio at the substrate, can be varied at any stage of the deposition

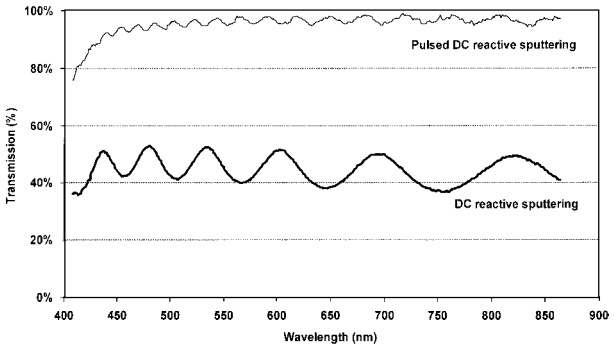

Fig. 14. Transmission spectra for aluminium oxide coatings deposited by DC reactive sputtering and pulsed DC reactive sputtering (after ref. [57]).

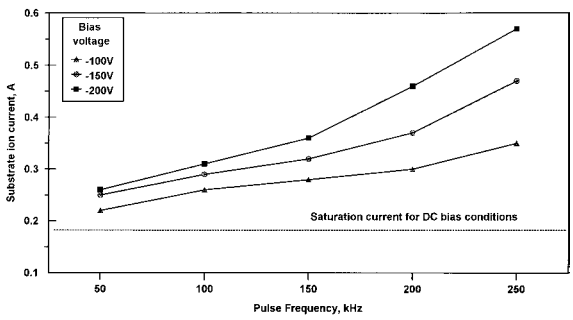

Fig. 15. The variation with pulse frequency and bias voltage of the substrate ion current for pulsed DC bias conditions (after ref. [61]).

process, or even continuously throughout the deposition process.

The effect of varying the magnetron configuration on the magnetic field is shown in Fig. 16 [12]. This figure shows the magnetic field strength at the target for a Gencoa VT130450 VTech variable magnetron operating in balanced, intermediate (i.e., weakly unbalanced) and strongly unbalanced configurations. The measurements were made with a 6 mm thick copper backing plate installed on the magnetron in place of a target. In the balanced mode the outer pole is fully retracted from the target and the inner pole fully advanced, in the intermediate mode both poles are fully advanced, and in the strongly unbalanced mode the outer pole is fully advanced and the inner pole fully retracted. In this design, the range of movement from fully advanced to fully retracted is of the order of 15 mm. The variation in the relative strengths of the inner and outer poles as the magnets are moved can be clearly seen in Fig. 16. It should be noted that, although, in principle, variable magnetrons could be designed to operate from 'type-1' unbalanced, right through to 'type-2' unbalanced (see Fig. 1), there is little commercial demand for 'type-1' systems. Thus, the range of movement of the magnets has been limited in these magnetron designs.

Variable magnetrons add an extra dimension to the sputtering process. They allow the operator to fine tune the fluxes of atoms and ions incident at the substrate during the deposition process. For example, high levels of ion bombardment during the initial stages of deposition may be beneficial to coating adhesion. However, continued excessive bombardment may be detrimental, because it can result in the formation of high stresses and defects in the coating. Variable magnetrons allow the operator to reduce the ion-to-atom ratio at any stage during deposition to counteract these problems. Furthermore, during the deposition of graded, or multi-layer coatings, variable magnetrons allow conditions to be selected to optimise the properties of each component in the coating. Also, the characteristics of a target change as it erodes. This can lead to variations in deposition rate over the life of a target. In processes where this is critical, variable magnetrons offer the potential of maintaining constant target characteristics and, therefore, constant erosion rates.

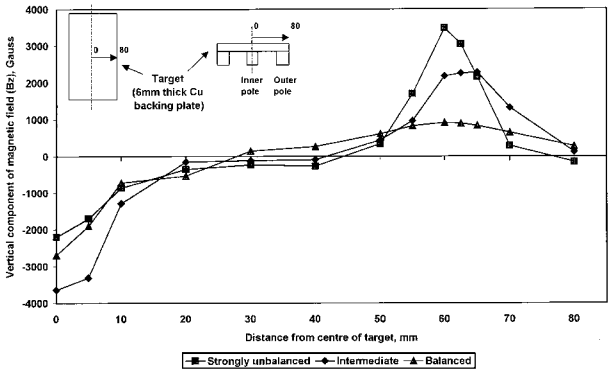

Fig. 16. The variation in magnetic field strength across the target, from the central pole to the outer pole, for a variable magnetron operating in balanced, weakly unbalanced (intermediate), and strongly unbalanced modes. Sign convention: + ve values are north poles, − ve values are south poles.

9. Duplex surface engineering

The recent developments in magnetron sputtering, described in this paper, now allow very high-performance coatings to be produced. Indeed, in many applications, magnetron sputtered coatings now outperform coatings produced by other techniques. However, their market penetration is currently limited to certain 'niche' sectors. Traditional surface engineering techniques still dominate the market place, and are likely to do so for several years to come [13]. Part of the reason for this is the perceived high cost of sputter (and other PVD) coated components [64]. However, this is deceptive, as the cost of a component is more than compensated for when the subsequent increase in performance is considered. For example, data from Balzers Ltd. suggests that coating a forming punch by PVD can add 35% to the cost of the tool, compared to only 8% for a gas-nitrocarburising treatment. However, the PVD coated tool can offer an increase in life over an uncoated tool of up to 32 times, compared to the 1.5–4.5 times increase in life offered by the other technique [65]. The economics are further enhanced if reduced downtime to change tools and the reduced number of rejected components are also considered. In another example from Balzers [66], it was found that using PVD-coated high-speed steel taps to machine steel tubes, in place of uncoated tools, reduced the total manufacturing costs per 100 parts from SFr 108.35 to only SFr 42.85.

Another factor which has limited the exploitation of advanced PVD processes is their unsuitability for use with many substrate materials such as low alloy steel and titanium alloys. In the case of hard coatings, this is due to the lack of load-bearing support provided by the substrate; whereas, in the case of corrosion resistant coatings, pin-hole defects have compromised the performance of the coating. To address these problems, and to extend the commercial viability of advanced PVD processes, duplex surface engineering processes have been developed.

Bell describes duplex surface engineering as 'the sequential application of two (or more) established surface technologies to produce a surface composite with combined properties which are unobtainable through any individual surface technology' [14]. Two general groups are identified; those in which the individual processes complement each other and the combined effects result

from both processes (group 1), and those where one process supplements, or reinforces the other, acting as a pre-, or post-treatment, and the resultant properties are mainly related to one process (group 2). Examples from both groups of process are given in Refs. [13,14].

PVD treatment of a pre-nitrided steel is a good example of a group 1 process. Plasma nitriding produces a relatively thick (~ 500 μm), hardened (~ 10 GPa) sub-surface. A 3–5 μm thick titanium nitride (TiN) layer can then be deposited onto the nitrided surface using various PVD techniques, including magnetron sputtering. Components treated in this way exhibit the low wear characteristics of the ceramic coating, combined with the high load-bearing capacity and high fatigue strength characteristics of the nitrided layer. The effectiveness of this technique is shown in Fig. 17, which compares the wear volume for various untreated, individually treated and duplex treated En40B steel specimens in a ball-on-wheel test. Bell illustrates how the substrate, plasma nitriding treatment and the PVD coating all contribute to the overall composite component with the required properties in a convenient manner [14], which is reproduced here as Fig. 18.

A similar example of duplex surface engineering is the DLC coating-oxygen diffusion process for titanium alloys [14]. Titanium alloys combine high strength-to-weight ratios and exceptional corrosion resistance, but are also characterised by poor tribological properties and poor load bearing capacity. Again, the tribological properties of the titanium alloy could be significantly improved through the use of a PVD coating. However, premature failure of the coating will occur in high load situations. A duplex solution to this problem has been developed, combining an oxygen diffusion pre-treatment with a CFUBMS deposited graded DLC coating (as referred to in Section 5). The oxygen diffusion process provides a hardened sub-surface for improved load bearing, and the DLC coating provides excellent low friction and wear characteristics at the surface. However, DLC coatings are usually associated with high levels of residual stress and poor adhesion when deposited directly onto a component. The versatility of the CFUBMS process has provided a solution to this problem. An intermediate layer is deposited in which the composition is graded from titanium, through titanium nitride, to titanium carbo-nitride and finally to titanium carbide. The DLC coating is then deposited onto this layer. Control of the CFUBMS process allows the whole procedure to be carried out without interruption and there are no sharp interfaces. The intermediate layer is only some 1–2 μm thick, yet by grading the composition in this way high interfacial stresses are avoided and the coating adhesion is significantly improved.

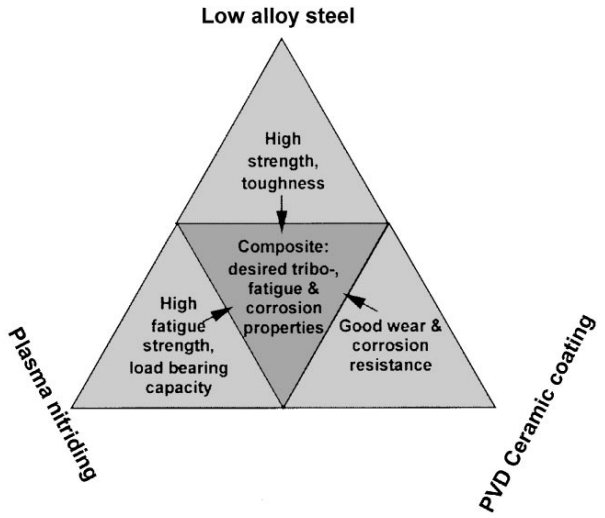

Fig. 18. The design philosophy behind obtaining improved properties through duplex surface engineering processes (after Ref. [14]).

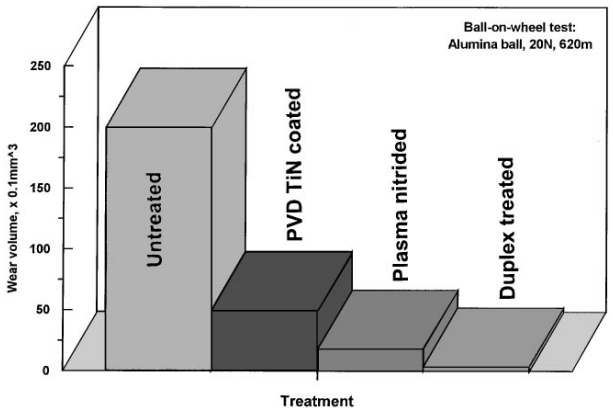

Fig. 17. Ball-on-wheel wear test results for untreated, PVD TiN coated, plasma nitrided and duplex treated En40B steel (after Ref. [14]).

10. Conclusions

Several recent developments made in the magnetron sputtering field have been discussed in this paper. These include closed field unbalanced magnetron sputtering, pulsed magnetron sputtering, variable field strength magnetrons and duplex surface engineering techniques. Together, these developments have transformed the capabilities of magnetron sputtering, and helped to establish it as the process of choice for the production of many industrially important coating/substrate systems. The results of a number of recent fundamental studies in this field have also been included and several industrial applications are discussed. Overall, therefore, this paper provides a review of the current status of the magnetron

sputtering process and considers future areas of exploitation for this technique.

Acknowledgements

A number of people have contributed material for inclusion in this paper. The authors would particularly like to thank Vanessa Fox of Teer Coatings, Dermot Monaghan of Gencoa, Janet O'Brien of Salford University, and Greg Roche and Dan Carter of Advanced Energy Industries for their help. We would also like to thank BNFL and DERA Fort Halstead for funding some of the work described here.

References

[1] Rossnagel SM. Sputter Deposition. In: Sproul WD, Legg KO, editors. Opportunities for Innovation: Advanced Surface Engineering. Switzerland: Technomic Publishing Co., 1995.
[2] McLeod PS, Hartsough LD. J Vac Sci Technol 1977;14(1):263–5.
[3] Waits RK. J Vac Sci Technol 1978;15(2):179–87.
[4] Window B, Savvides N. J Vac Sci Technol A 1986;4(2):196–202.
[5] Window B, Savvides N. J Vac Sci Technol A 1986;4(2):453–6.
[6] Savvides N, Window B. J Vac Sci Technol A 1986;4(2):504–8.
[7] Teer DG. Surf Coat Technol 1989;39/40:565.
[8] Sproul WD, Rudnick PJ, Graham ME, Rohde SL. Surf Coat Technol 1990;43/44:270–8.
[9] Schiller S, Goedicke K, Reschke J, Kirchoff V, Schneider S, Milde F. Surf Coat Technol 1993;61:331–7.
[10] Rossnagel SM, Cuomo JJ. Vacuum 1988;38(2):73–81.
[11] Colligon JS. J Vac Sci Technol A 1995;13(3):1649–57.
[12] Gencoa Product Information: V-Tech Magnetrons. Gencoa, 4 Wavertree Boulevard South, Liverpool L7 9PF, UK. Web address: www.Gencoa.com.
[13] Matthews A, Leyland A. Surf Coat Technol 1995;71:88–92.
[14] Bell T, Dong H, Sun Y. Tribology Int 1998;31(1–3):127–37.
[15] Behrisch R, editor. Sputtering by particle bombardment. In: Applied Physics, vol. 47, Berlin: Springer, 1981.
[16] Townsend PD, Kelly JC, Hartley NEW. Ion Implantation, Sputtering and their Applications. London: Academic Press, 1976.
[17] Musil J, Kadlec S. Vacuum 1990;40(5):435–44.
[18] Adibi F, Petrov I, Greene JE, Hultman L, Sundgren JE. J Appl Phys 1993;73(12):8580–9.
[19] Nyaiesh AR. Thin Solid Films 1981;86:267–77.
[20] Howson RP, Ja'afer HA, Spencer AG. Thin Solid Films 1990;193194:127–37.
[21] Sproul WD. Vacuum 1998;51(4):641–6.
[22] Bunshah RF, Juntz RS. J Vac Sci Technol 1972;9:1404.
[23] Hecht RJ, Mullaly JR. J Vac Sci Technol 1975;12:836.
[24] Kelly PJ, Arnell RD. Surf Coat Technol 1997;97:595–602.
[25] O'Brien J, Arnell RD. Surf Coat Technol 1996;8687:200–6.
[26] O'Brien J. 'The production of porous and chemically reactive coatings by magnetron sputtering.' PhD Thesis, University of Salford, 1998.
[27] Kelly PJ, Arnell RD. Surf Coat Technol 1998;108–109:317–22.
[28] Teer DG, UK patent No. 2 258 343, USA patent No. 5 554 519, European patent No. 0 521 045.
[29] Munz WD, Hauzer FJM, Schulze D, Buil B. Surf Coat Technol 1991;49:161–7.
[30] Rohde SL, Hultman L, Wong MS, Sproul WD. Surf Coat Technol 1992;50:255–62.
[31] Teer Coatings Ltd. Technical Data Sheet, CFUBMSIP. Teer Coatings Ltd., 290 Hartlebury Trading Estate, Hartlebury, Kidderminster, Worcestershire DY10 4JB, UK.
[32] Monaghan DP, Teer DG, Laing KC, Efeoglu I, Arnell RD. Surf Coat Technol 1993;59:21–5.
[33] Monaghan DP, Teer DG, Logan PA, Efeoglu I, Arnell RD. Surf Coat Technol 1993;60:525–30.
[34] Kelly PJ. Proceedings of the 19th International Pyrotechnics Seminar, Christchurch, New Zealand, February 1994, pp. 319–38.
[35] Baldwin KR, Bates RI, Arnell RD, Smith CJE. Corrosion Sci 1996;38(1):155–70.
[36] Fox V, Hampshire J, Teer DG. Surf Coat Technol 1999;112: 118–22.
[37] Yang S, Camino D, Jones AHS, Teer DG, The deposition and tribological behaviour of sputtered carbon hard coatings. Presented at the International Conference on Metallic Coatings and Thin Films, ICMCTF'99, San Diego, 12–15 April 1999; Surf Coat Technol, in press.
[38] Teer Coatings Ltd. Technical Data Sheet, MoST – Performance Improvements. Teer Coatings Ltd., 290 Hartlebury Trading Estate, Hartlebury, Kidderminster, Worcestershire DY10 4JB, UK (1998).
[39] Teer Coatings Ltd. Technical Data Sheet, Graphit-iC. Teer Coatings Ltd., 290 Hartlebury Trading Estate, Hartlebury, Kidderminster, Worcestershire DY10 4JB, UK.
[40] Kelly PJ, Arnell RD. J Vac Sci Technol A 1998;16(5):2858–69.
[41] Thornton JA. J Vac Sci Technol 1974;11(4):666–70.
[42] Messier R, Giri AP, Roy RA. J Vac Sci Technol A2 1984(2):500–3.
[43] Musil J, Kadlec S, Valvoda V, Kuzel R, Cerny R. Surf Coat Technol 1990;43/44:259–69.
[44] Craig S, Harding GL. J Vac Sci Technol 1981;19(2):205–15.
[45] Kay E, Parmigiani F, Parrish W. J Vac Sci Technol A 1988; 6(6):3074–81.
[46] Hultman L, Munz W-D, Musil J, Kadlec S, Petrov I, Greene JE. J Vac Sci Technol A 1991;9(1):434.
[47] Ino K, Shinohara T, Ushiki T, Ohmi T. J Vac Sci Technol A 1997;15:2627.
[48] Adibi F, Petrov I, Greene JE, Hultman L, Sundgren JE. J Appl Phys 1993;73:8580.
[49] Sproul WD. J Vac Sci Technol A 1994;12:1595.
[50] Scherer M, Schmitt J, Latz R, Schanz M. J Vac Sci Technol A 1992;10:1772.
[51] Frach P, Heisig U, Gottfried Chr, Walde H. Surf Coat Technol 1993;59:277.
[52] Glocker DA. J Vac Sci Technol A 1993;11:2989.
[53] Sproul WD, Graham ME, Wong MS, Lopez S, Li D, Scholl RA. J Vac Sci Technol A 1995;13:1188.
[54] Kelly PJ, Abu-Zeid OA, Arnell RD, Tong J. Surf Coat Technol 1996;86–87:28–32.
[55] Henderson PS, Kelly PJ, Arnell RD. Optimising the deposition conditions for reactively pulsed magnetron sputtered oxide films. Paper presented at the International Conference on Metallic Coatings and Thin Films, ICMCTF99, San Diego, April 12–15, 1999.
[56] Sproul WD. Vacuum 1998;51(4):641–6.
[57] Sellers JC. Surf Coat Technol 1998;98:1245–50.
[58] Personal communication to the authors by D Carter, Advanced Energy Industries Inc., Fort Collins, CO, USA, June 1999.
[59] Brauer G, Ruske M, Szczyrbowski J, Teschner G, Zmelty A. Vacuum 1998;51(4):655–9.
[60] Szczyrbowski J, Brauer G, Ruske M, Zmelty A, Conventional and temperable low-E coatings based on Twin Mag sputtered TiO_2 and Si_3N_4 layers. Paper presented at second International Pulsed Plasma Surface Technologies Workshop, PPST'99, San Diego, April 8–10.
[61] Kirchoff V, Winkler T, Fahland M. Pulsed magnetron sputtering on plastic webs. Paper presented at second International Pulsed

Plasma Surface Technologies Workshop, PPST'99, San Diego, April 8–10.

[62] Fox V, Personal communication to Kelly PJ, Arnell RD. Teer Coatings Ltd., 290 Hartlebury Trading Estate, Hartlebury, Kidderminster, Worcestershire DY10 4JB, UK, August 1999.

[63] Rossnagel SM, Cuomo JJ, Westwood WD, editors. Handbook of plasma processing technology fundamentals, etching, deposition and surface interactions. Park Ridge, NJ: Noyes Publications, 1990.

[64] Matthews A, Leyland A, Dorn B, Stevenson PR, Bin-Sudin M, Rebholz C, Voevodin A, Schneider J. J Vac Sci Technol A 1995;13(3):1202–7.

[65] Balzers Ltd. Technical Data Sheet, BALINIT hard coating of forming tools. Balzers Limited, Tool Coating Division, Bradbourne Drive, Tilbrook, Milton Keynes MK7 8AZ, UK.

[66] Balzers Ltd. Technical Data Sheet, Recoating of reground cutting tools. Balzers Limited, Tool Coating Division, Bradbourne Drive, Tilbrook, Milton Keynes MK7 8AZ, UK.

Appendix 1039

ELSEVIER

Surface and Coatings Technology 135 (2000) 48–59

SURFACE & COATINGS TECHNOLOGY

www.elsevier.nl/locate/surfcoat

A novel reactive magnetron sputtering technique for producing insulating oxides of metal alloys and other compound thin films

I. Safi*

Department of Physics, Loughborough University, Loughborough, LE11 3TU, UK

Received 20 March 2000; accepted in revised form 16 August 2000

Abstract

Problems associated with reactive magnetron sputtering from elemental (i.e. non-compound) targets have been successfully solved in this work. The elements of this achievement are: (i) the use of mid-frequency (i.e. 40 kHz) AC power in the floating mode, between two magnetrons, allowed the reactive sputtering process to be arc-free and hence eliminating the undesired effects of arcing in reactive sputtering such as driving the process to become unstable, creating defects in the films and reducing the target lifetime. (ii) The combination of DC and mid-frequency AC power in a novel way using a filter to protect the DC power supply from the AC one (or the independently DC powered magnetrons method) permitted the composition of the produced films to be easily and independently manipulated by varying the magnitude of power applied to each magnetron. (iii) The use of very fast feedback methods to automatically control the admission rate of oxygen into the sputtering chamber (i.e. plasma emission monitoring or voltage control) allowed the stoichiometry of the deposited films to be independently controlled. This also allowed the deposition rate of the sputtered films to be high. (iv) Sputtering from two magnetrons made the production of alloys or multi-element compounds, which are either difficult or impossible to be formed from single targets, an easy task. (v) Substrate rotation enhanced atomic level mixing of the film constituents. The stoichiometry of the film was controlled by plasma emission monitoring or voltage control on one magnetron, and dopants were added by sputtering from the other magnetron. This means that the former magnetron served two purposes; the first was to sputter metal and oxidise it, and the second purpose was to oxidise the metal sputtered from the other magnetron. This novel technique opens the door wide for investigating virtually all potentially promising thin oxide films. Using this technique, a large range of alloy-oxide films was deposited at high rates. In fact, the independent control of both the metallic composition and stoichiometry was very valuable in identifying the optimum properties of these films. That is, giving transparent films of different refractive indices for optical applications. Furthermore, such a technique may also be capable of investigating other types of thin films (e.g. hard coatings, semiconducting films, superconducting films, etc.).

Keywords: Thin film; Oxide; Reactive sputtering; Two magnetrons; AC and DC technique; PEM; Voltage control; Composition; Stoichiometry; Arcing

*Corresponding address. P.O. Box 4470, Damascus, Syria. Tel.: +963-11-5117808.

0257-8972/00/$ - see front matter
PII: S0257-8972(00)00985-3

1. Introduction

Reactive sputtering, where a metal target is sputtered by an inert gas (e.g. argon) in the presence of a reactive gas (e.g. oxygen), to produce a film of electrically insulating material has proved to be difficult to introduce as an industrial process. The simple concept is that metal is sputtered from the target and is incident on the substrate/growing-film-surface, together with reactive gas from the residual atmosphere, to form a compound. The reaction occurs when these species meet on the surface. Energy is provided from the substrate temperature, the high energy of sputtered material or by ions used to bombard the surface. Magnetron sputtering has allowed the sputtering to be undertaken at sufficiently low pressures such that the mean free path for sputtered material is greater than the target-to-substrate distance and the energy of this material and the efficiency of its transfer from the target can be maintained. The magnetron can also be arranged, through unbalancing the magnetic field, and/or operating it in a system to create a closed field, to direct a dense plasma to the surface of the growing film. This plasma can cause an insulating or isolated surface to acquire a floating bias, which leads to it being bombarded with low energy argon ions, to provide energy for excitation energies for chemical and structural reactions. The growth of the film can be controlled in this manner and it does not require the film or substrate to be electrically conducting. If additional bias is required, RF can be used. The problems, which have to be solved, occur at the cathode surface.

The presence of reactive gas in a region of high energy and freshly exposed metal surfaces, which is the sputtering race-track of the magnetron, leads to rapid reaction. If the surface reacts faster than it sputters, a surface compound film is formed, which in general sputters at a much lower rate than the metal, a process which has become to be called 'poisoning'. The transition between metal sputtering and 'poisoning' is dependent upon the power used to sputter and the partial pressure of the reactive gas and occurs at a different level when approached from the metal or 'poisoned' condition. This process leads to a hysteresis being seen between the sputtering parameters and the flow of reactive gas into the chamber and there is a region of this flow where the process is unstable. It becomes one of the rapid deposition of a partially reacted metal or the slow deposition from a poisoned target of a fully reacted film. This problem can be solved by controlling the state of the sputtering surface, and hence the partial pressure of the reactive gas, through the light emitted by the sputtering metal or other gases in the discharge, or in some cases, from the voltage of the sputtering cathode. These techniques provide a fast feedback to the control of the flow of the gas. However, great care has to be taken with the time constants associated with the changes of gas pressure in a vacuum chamber.

A further solution lies in separating the deposition and reactive process in a cyclic process where a thin metal film is deposited and then converted. In our versions of this process, the substrate is moved (successive plasma anodisation, or SPA) or the magnetron is made to change function from a provider of sputtered metal to one of oxygen and energetic argon ions (successive pulsed plasma anodisation, or SPPA). In both cases, the unbalanced magnetron, the provider of argon-ion energy, is required to operate in the presence of a partial pressure of oxygen.

When the reaction product is insulating and the power is DC, other problems appear. A region of the target-cathode remains covered with reaction product, the racetrack region only can be balanced to be sputtering metal faster than it is reacting with the proportion of reactive gas in the system. This insulating region is subject to bombardment of ions and becomes highly charged, due to charge accumulation or through secondary-electron emission. This leads to rapid localised discharges, arcs, which disrupt the sputtering discharge and causes arc-evaporation from regions of the target, with particle 'spitting' and consequent contamination of the film. If the process is not properly designed, and carefully balanced, an insulating film may be formed on the anode of the discharge and on the chamber walls to give a discharge which changes character with time. These problems can be overcome by using RF in reactive sputtering and target biasing. RF introduces its own problems and is not suitable for the high-rate, large-area processes that are required.

More recently, a solution to these problems has appeared. The insulating surface has to be discharged before the charge accumulates to an extent where an arc is formed. This has been done by providing a reverse potential pulse to the surface within the charge accumulation time. This can be a short pulse applied to a DC supply or AC power applied between two cathodes. The frequency required turns out to be approximately 40 kHz, which can be provided, without the tuning systems necessary with RF, and at low cost. The latter process has the further advantage of creating a continuously cleaned anode, because for the other half of the cycle it is the sputtering cathode. This emerging technique has been utilised recently by a few workers [1–10]. The results were very promising. For example, Szczyrbowski and Braatz [7] have reactively deposited films of SiO_2 at high rates using 40 kHz-AC power applied between two Si magnetrons. In addition to the excellent optical and mechanical properties of the deposited films, no arcing was observed during the entire lifetime of the target, which was more than a week. Schiller et al. [11] have reactively deposited films of

Al_2O_3 from two Al magnetrons using an AC power at different frequencies ranged from 50 Hz to 164 kHz. They reported a significant decrease in the defect density of the deposited films with increasing frequency. The curve, for non-absorbing films, saturated at frequencies greater than 50 kHz, which was an indication of an arc-free process beyond this frequency. They also reported a deposition rate of approximately 60% of that of metallic Al. The rate was almost independent of the frequency in the range they investigated. Scherer et al. [9] have also adopted the two cathodes technique to reactively deposit films of Al_2O_3, SiO_2 and Si_3N_4 using 40 kHz-AC power. They reported deposition rates comparable to those obtained with the DC power.

A further problem is encountered if it is desired to reactively sputter two metals at the same time to produce mixed metal oxides of controlled composition. The metals operate in different ranges of partial pressure of the reactive gas for their optimum deposition, which also changes with the power that is used, and it is difficult to operate a system with both sources operating in the desired metal sputtering mode.

This paper reports on the deposition of mixed metal oxides using a simultaneous oxidisation stage, controlled by spectral radiation from the discharge (plasma emission monitoring, or PEM), or the cathode voltage in constant-power sputtering. This is used in conjunction with movement of the sample between that source and one sputtering the other metal. The process was optimised with witness pieces admitted through an air lock into a continuously operating system. The second metal was oxidised in the unbalanced magnetron discharge of the first, i.e. a SPA process, whose sputtered metal was simultaneously converted. Power (40 kHz) was applied between the two cathodes and a DC bias used to adjust the ratio of metals in the mixed oxide. The stoichiometry was determined by the partial pressure, i.e. the PEM signal, in that chamber, the power applied and the rate of rotation.

2. The techniques

2.1. Mid-frequency AC powered magnetrons in floating mode with a DC bias

For the coating composition to be easily controlled, the amount of power (or current) received by one/both of the floating magnetrons has to be independently varied. This was achieved by DC-biasing one of these magnetrons. In most cases, the two floating magnetrons were operated at a constant AC power, using the 40-kHz supply, whereas the DC power, applied to one of the magnetrons, was varied. Such a method of combined AC and DC power application enjoys the following major advantages:

1. It paves the way to produce coatings of virtually any desired composition by simply varying the ratio of the applied DC and AC powers.
2. It retains the advantages of applying mid-frequency AC power, between two floating magnetrons.
3. It also retains the advantages of applying DC power, such as high deposition rates onto large area substrates.

The AC power supply was isolated from the DC with a capacitor and the DC from the AC with a LCL filter. Fig. 1 shows a schematic diagram of this filter. It should be emphasised, that the plasma was earthed through the chamber wall to provide the DC return path for the current. Initial experiments were carried out with two Al targets, sputtered in an Ar atmosphere. An oscilloscope was used to measure the DC potential developed on the magnetrons, relative to earth, in the following cases:

1. On one of the magnetrons when the applied power

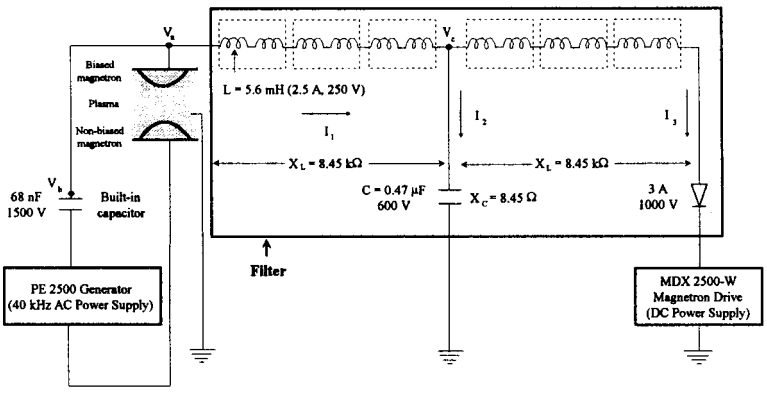

Fig. 1. The filter used to protect the DC power supply from AC currents.

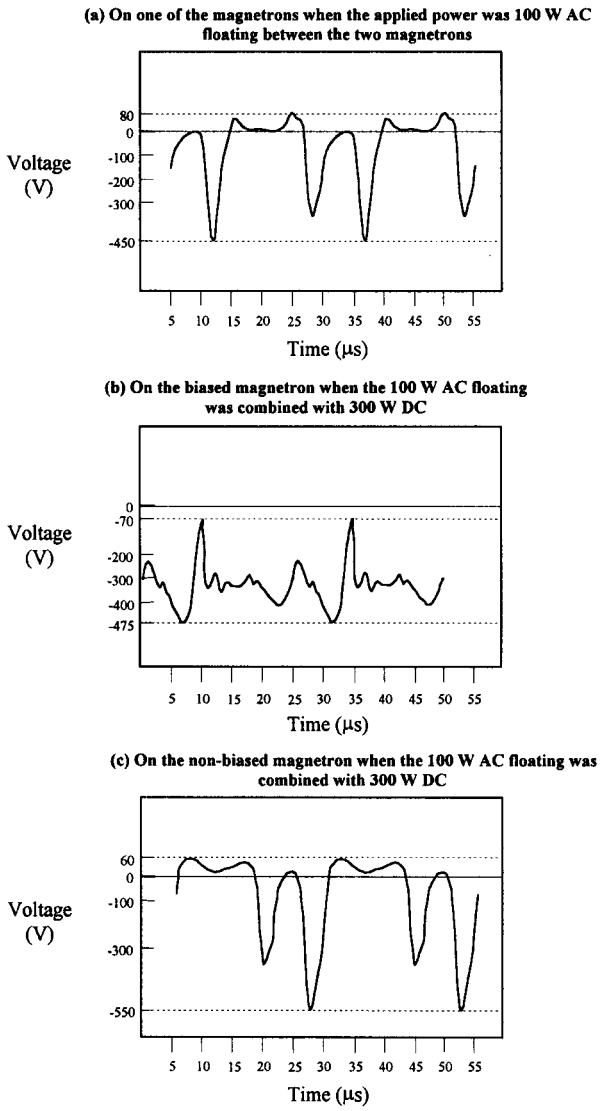

Fig. 2. A reproduction of the photographs taken from the oscilloscope for the DC potentials, relative to earth, developed on a floating, biased and non-biased Al magnetron.

was 100 W AC floating between the two magnetrons (Fig. 2a).

2. On both the biased (Fig. 2b) and the non-biased (Fig. 2c) magnetrons, when the 100-W AC floating was combined with a 300-W DC power to bias one of the magnetrons (a common case).

A similarity can be noticed between Fig. 2a,c. To understand the reason behind that, the reader is referred to Fig. 1. The capacitor shown in the AC part of the circuitry is an internal component of the output stage of the AC power supply. Its purpose is to block any DC component of current should there be any, emanating from the AC power supply, and has twofold ramifications. The first is that the current, in the AC part of the circuit, is to be the same in both directions when a DC bias is applied. Secondly, without a DC bias, the capacitor is charged/discharged following the voltage waveform of the AC power supply. Alternatively, when a DC bias is applied to one of the magnetrons, the capacitor is charged/discharged (via the biased magnetron) following the voltage difference $V_a - V_b$, where V_a is the fixed DC voltage and V_b is the alternating AC one. This leads to a slight change in the AC current in the AC part of the circuit from that when only the AC power was applied. As a result, a slight change in the voltage of the non-biased magnetron should also occur to maintain AC current magnitude in both directions. In other words, for periods when the AC current flow is in the same direction to the DC current, the capacitor will charge due to the latter. This accumulated charge is discharged onto the biased magnetron. In order to maintain AC current magnitude in both directions, the non-biased magnetron must develop an appropriate bias, as can be noticed by comparing the positive voltage regions of Fig. 2a,c. Consequently, Fig. 2a can be regarded as a representative voltage waveform for such a circuit. Comparing Fig. 2a,c, it is suggested that the AC current (in the AC part of the circuit) is indeed approximately equal in both cases. The magnitudes in both directions are approximately equal, within the biased magnetron arrangement.

On the other hand, whenever the DC potential of the magnetron is negative with respect to the plasma potential (earth potential in this case), sputtering will occur. It is easy to see, then, from Fig. 2b, that the biased magnetron is sputtering continuously, albeit to various degrees. Fig. 2c shows that the non-biased cathode is not sputtering continuously; although it attains a potential of approximately -550 V, these periods are short compared to the 'off times', when its potential goes positive with respect to plasma potential. In summary, we have:

1. The biased magnetron is tied to DC potential. The current to it is the sum of the DC current driven from the DC power supply and the current that is driven from the AC power supply. The existence of a DC bias means that the plasma has to be earthed, by contact with the chamber walls, to allow the DC current to flow.
2. The non-biased magnetron will adjust its internal DC voltage so as the AC current flowing around the AC part of the arrangement is equal in magnitude for both current directions (i.e. to both magnetrons). This results in a constant AC power applied to each cathode, provided the target materials are identical.

2.2. Plasma emission monitoring (PEM)

This method of control has been described in detail in a previous paper [6]. In the course of this work, the plasma contained mainly the emission lines corresponding to argon, oxygen and the target material. Therefore, to control the emission line/s of one of these elements, the optical filter had to be chosen so as either the wavelength/s of light it transmitted was unique to this element, or the emission intensity at the selected wavelength/s was sufficiently higher than the corresponding ones of the other two elements.

For example, for the reactive sputter-deposition of In oxide, a band pass filter had been used for controlling on In emission line at 451.1 nm. Sufficient signals up to approximately 150 mV were obtained at applied powers of the order of 300 W. At this wavelength, there is neither an argon nor an oxygen line, sufficiently intense, to interfere with the In one. A more universal technique was required for the large number of materials investigated in this work. A high-pass filter, with a cut-off wavelength at approximately 620 nm, was successfully used to control the reactive sputter-deposition of W, V, Mo and Ti oxide. At wavelengths greater than approximately 620 nm, the intensities of the emission lines of these metals are very weak. Thus, the transmitted signal by this filter is either due to argon or oxygen-lines. The signal fell as oxygen was admitted and it is concluded that the strong signal was due to argon, and the control was carried out on the argon lines, the fall in intensity being attributed to changes in the discharge current and coupling to the components of the atmosphere as the oxygen was added. Signals up to approximately 1.5–2 V were obtained at applied powers of the order of 300 W.

2.3. Voltage control

Voltage control has been described in detail in a previous paper [6]. This method of control has been used in this work in the cases of Al, Zn, Cu and Pb when they were sputtered in an Ar/O_2 atmosphere.

Fig. 3 shows a schematic of the voltage control loop. A user connector, located on the rear panel of the Advanced Energy™ power supplies which was used in this work, provides a 0–5-V DC analogue signal representing the cathode voltage (i.e. the output voltage of the power supply). The DC signal was 0 V when the output voltage of the supply was also 0 V and it was 5 V at the full-scale output voltage of the supply. This 0–5-V DC signal was used as an input to a voltage controller. The signal was taken through two controls; one of which backs it off against another potential to provide a zero reference. The difference from this zero signal was then amplified by a variable gain amplifier to give an output ranged from 0 to 1 V. The output signal

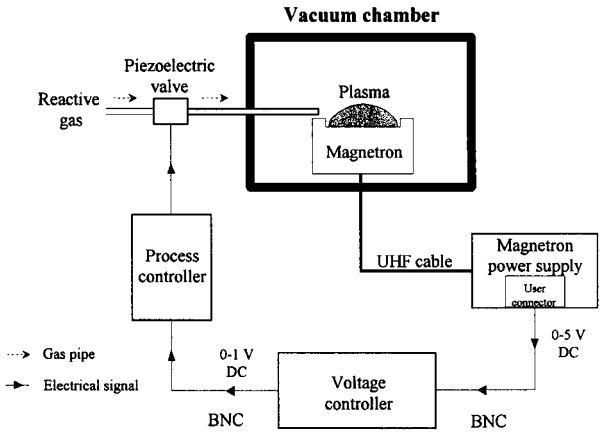

Fig. 3. Voltage control (VC) system used in controlling the reactive magnetron sputtering processes.

from the voltage controller was then applied to a standard pressure controller (process controller) which was connected to a piezoelectric control valve of a very fast response. The 'zero reference' was the signal corresponding to the voltage seen when the target was fully poisoned, the '1' was that for metal sputtering. Any intermediate degree of target poisoning (i.e. an intermediate value of cathode voltage) can be represented, in this technique, by a value of input voltage to the controller in the range 0–5 V, and a value of output voltage in the range 0–1 V. The input to the voltage controller was taken from the DC power supply, when it was used, as it represented the dominating power applied to the main magnetron relative to the floating power applied by the AC power supply. This arrangement provided better control.

2.4. Substrate condition probe

The information that was required was the ion current density to the substrate and its floating potential. In other words, the number and energy of ions that bombarded the growing films relative to the number of atoms deposited. To obtain this information, we used what we termed a 'substrate condition probe'. Fig. 4 shows a cross-sectional and a bottom view (i.e. the surface with a direct contact with the plasma) of this probe. It essentially consisted of a central cylindrical head, whose diameter was 6 mm, surrounded by a 25×37 mm guard. The guard, which was entirely isolated from the head, was utilised to minimise the plasma edge-effect from the probe head. The probe was placed in the plane of the substrate following the same procedure of placing a substrate; it was mounted in the jig, which was in turn inserted into the platen.

The I–V characteristics were then obtained by biasing the probe head. The current to the guard was excluded. Probe measurements were performed using

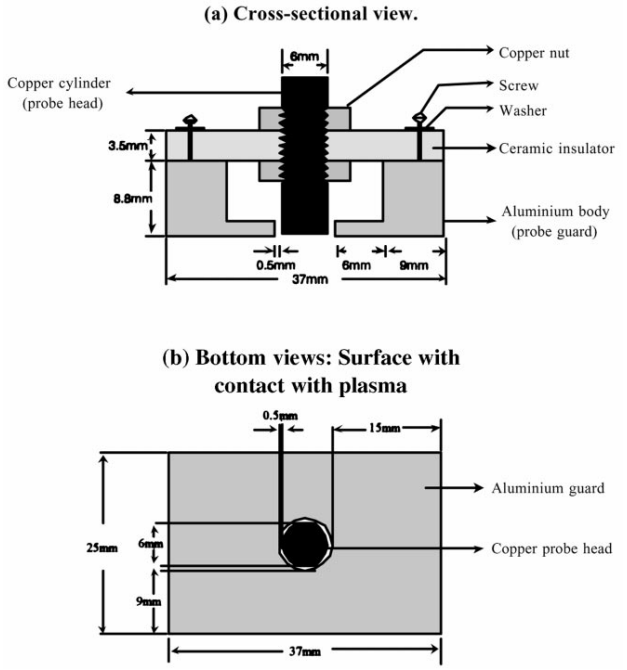

Fig. 4. A cross-sectional and a bottom view of the probe.

In and Sn targets attached to the main and secondary magnetrons, respectively. Keeping the working pressure at 2×10^{-3} torr, two sets of experiments were carried out. The first was when the probe was held opposite to the centre of the In magnetron using different DC powers (i.e. at 100, 200 and 300 W). In addition, the characteristics of the probe when it was facing the erosion zone of the In magnetron, when the applied power was 300 W, was also plotted for comparison. The results are shown in Figs. 5 and 6. In the second set of experiments, the probe was held opposite to the centre of the In magnetron throughout. The applied powers were 50 W and 100 W AC floating between the two magnetrons, and 300 W DC combined with 100 W AC. The results are shown in Fig. 7. The following remarks can be deduced from these figures:

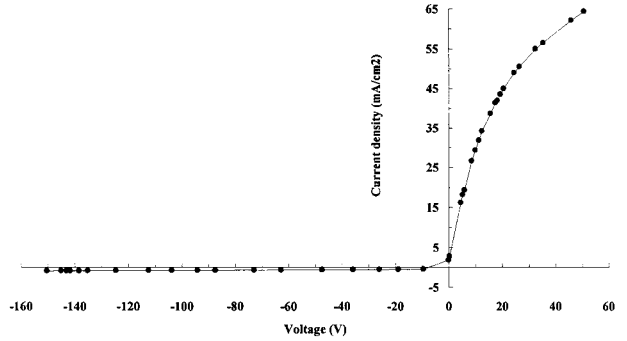

Fig. 5. The I–V characteristics of the probe when an In magnetron was held at 300 W DC and the probe was held opposite to the centre of the magnetron.

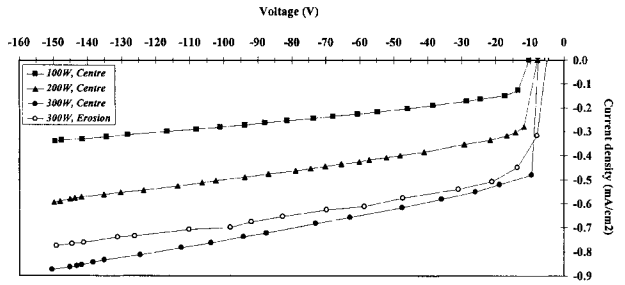

Fig. 6. The negative part of the I–V characteristics of the probe, at different DC powers to an In magnetron, when it was held opposite the centre of the magnetron. The curve when the probe was held opposite the erosion zone is also plotted.

1. The ion-current to the probe increased with the applied DC power to the magnetron. On the other hand, at a fixed DC power (e.g. 300 W), such a current was higher when the probe was held opposite the centre of the magnetron than when it was opposite the erosion zone. Similarly, the ion-current to the probe also increased with the applied floating AC power.
2. At a fixed magnitude of power (e.g. 100 W), the ion-current to the probe was lower in the DC case than in the floating AC one. Furthermore, the ion-current to the probe in the case of the 100-W AC combined with 300-W DC was the highest (Fig. 7).
3. The floating potential of the probe was almost independent of the applied AC power and slightly dependent on the DC power. However, the order of magnitude of these floating potentials was slightly lower when DC powers were applied.

The above conclusions are in very good agreement with the results obtained by Window and Savvides [12] and the results of Glocker [8]. In addition, the ion-current and floating potential, when the probe was opposite to the erosion zone, are less than the corresponding values when the probe was opposite to the centre of

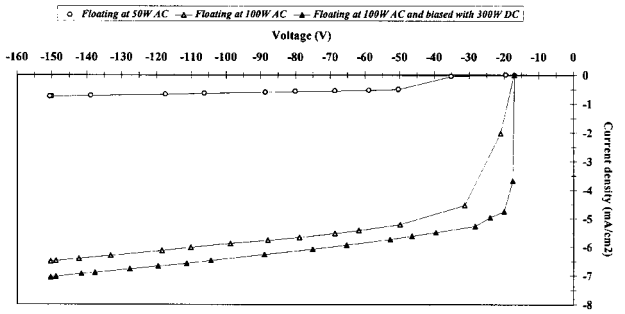

Fig. 7. The negative part of the I–V characteristics of the probe at different AC powers to a non-biased and biased floating In magnetron when the probe was held opposite the centre of the magnetron.

the magnetron under the same conditions (i.e. applied power). This result is also in good agreement with those of Howson et al. [13] and Spencer et al. [14].

It is informative to compute the arrival ratio of Ar ions to metal atoms at the substrate. It was found that this was 0.7 and the energy delivered to the substrate by ions per In atom was approximately 21 eV [1–6].

On the other hand, in the case when the applied power to the magnetron was 300 W DC combined with 100 W AC, $J_i^s = 7.1$ mA/cm^2, $V_f = -17$ V and $V_p = 0$ V (Fig. 7), where J_i^s, V_f and V_p are the ion current density to the substrate, the floating potential of the substrate and the plasma potential, respectively. Considering the case of indium oxide, which had a thickness of 152 nm, it was found that $N_i^s/N_m^s = 5.7$, where N_i^s and N_m^s are the number of ions bombarding 1 cm^2 of the substrate per second and the number of deposited metal atoms on 1 cm^2 of the substrate per second, respectively. Consequently, the energy delivered to the substrate by ions per In atom was approximately 100 eV.

Although the two magnetrons were unbalanced in the system used in this work, the measured floating potentials of the substrate were relatively low, whereas, the measured ion current densities were moderate. This could be due to the fact that target-to-substrate distance is less than the null-point of the magnetrons, which means that, at such low distance, ions cannot acquire high kinetic energies when they impinge on the substrate, with the lower floating potential that the substrates have. The small target-to-substrate distance also affects, but less severely, the ion current density, as the substrate can not collect all ions available because it is not in the way of the focused beam leaking from the cathode, rather it is in the base of that beam. The average ion densities in the AC plasma are approximately four times that of the DC plasma. This last difference, between the AC and the DC plasmas is significant. According to optical emission measurements, the plasma extinguishes on each half-cycle and has to be reignited. The increase in ion densities in the AC plasma was attributed to target voltage spikes during the reignition of the plasma on each half-cycle, as it is evident on the negative-going part of each cycle. Such spikes cause rapid electron acceleration in the pre-sheath region leading to significantly more efficient ionisation of gas and hence much higher plasma bombardment.

3. Experimental details

3.1. The sputtering system

The chamber comprised a 42-cm diameter stainless steel chamber, 12-cm deep internally, giving a short pump down time with the turbomolecular pump, backed by a two-stage rotary pump, compared with conventional bell-jar systems [3]. The chamber base accommodated two identical magnetrons. The magnetron, which had both the oxygen inlet to the chamber and the optical fibre input tip of PEM control loop attached to its pod will be, henceforth, called the 'main magnetron'. The other magnetron was connected to the argon inlet to the chamber.

An axially mounted aluminium platen was located above the magnetron cathode surfaces, and it was onto this platen, which was electrically isolated, the substrates were loaded from the airlock allowing a target-to-substrate distance of approximately 40 mm. The centrally oriented metal shaft was attached to the platen so that it could be rotated around this axis with a DC motor at a rotation speed of up to 60 rev./min.

The partial pressure of the sputtering gas, argon, was produced through a mass flow controller balanced by the vacuum pumping and measured with the system pirani.

For the admission of reactive gas a solenoid valve was replaced by a piezoelectric valve, having a faster response in order to cope with much faster changes in the desired supply of reactive gas required to maintain a certain cathode status, compared with that of inert gas. This was controlled to produce a pre-determined optical emission signal or cathode potential in much the same way as is used to control pressure. In addition, the total distance between the reactive gas pipe exit in the chamber and the piezoelectric valve was minimised to help reducing the time constant of the pipe. These modifications, allied with the pipe outlet being very close to the target in the very confined volume provided by the gettering enabled very efficient control of the reactive deposition processes to be obtained.

3.2. The airlock system

The system was designed so that the magnetrons could be operated continuously during the changing of substrates. We have found this to be of prime importance for iterative reactive processing, in which the partial pressure of the reactive gas is varied gradually until the desired film properties are attained. In order that this could be done the system was airlocked, that is, the main deposition chamber always remained in operation whilst the samples could be loaded/unloaded via a separately pumped airlock. The airlock was 10 cm in diameter and 4.6 cm deep, had a 0.361 l volume, and could typically be evacuated from atmosphere to approximately 40 mtorr in approximately 2 min, via two-stage rotary pump.

Samples were mounted singly in a jig, which was then attached to the end of a loading arm, which was moved

linearly through double Wilson-type vacuum seals, mounted off axis (2.2 cm from the centre) in the perspex window plate, which allow visual location of the substrate.

4. Optical measurements

4.1. Calculations of refractive indices from reflectance spectra

In this section, the case of transparent non-absorbing films deposited on transparent substrates will be considered. It should be mentioned first that the wavelength λ of the incident light is chosen so that it is comparable to the film thickness d_{film} to allow interference effects to occur [15].

The maximum and minimum reflectance of a thin film on an infinitely thick substrate are given by:

$$R_{max} = \left(\frac{n_{film}^2 - n_{amb} n_{subs}}{n_{film}^2 + n_{amb} n_{subs}} \right)^2 \quad (1)$$

$$R_{min} = \left(\frac{n_{subs} - n_{amb}}{n_{subs} + n_{amb}} \right)^2 \quad (2)$$

where R_{max}, R_{min}, n_{film}, n_{subs} and n_{amb} are a reflectance maximum, reflectance minimum, the refractive index of the thin film, the refractive index of the substrate and the refractive index of the ambient medium, respectively. By solving Eq. (1) for n_{film}, we get:

$$n_{film} = \left(n_{amb} n_{subs} \frac{1 + \sqrt{R_{max}}}{1 - \sqrt{R_{max}}} \right)^{1/2} \quad (3)$$

The relative precision of n_{film} is given by

$$\frac{\Delta n_{film}}{n_{film}} = \frac{\sqrt{R_{max}}}{2(1 - R_{max})} \frac{\Delta R_{max}}{R_{max}} \quad (4)$$

For example, if $R_{max} = 36\%$, it is then sufficient to measure R_{max} to an accuracy of approximately 2% (i.e. $\Delta R_{max} = 0.7\%$) so that the relative error for n_{film} is not larger than 1%.

In this work, films were deposited on glass substrates with $n_{subs} = 1.525$ and the spectrophotometric measurements were carried out in air (i.e. $n_{amb} = 1$).

Transmittance and reflectance spectra of transparent films, produced in this work, were measured using a Hitachi U-2000 double-beam spectrophotometer with a simple reflection attachment, which allowed comparison of the sample with freshly prepared aluminium coating. In spectrophotometric measurements carried out in this work, both transmittance and reflectance spectra were measured in the spectral range 350–750 nm with a scanning speed of 400 nm/min.

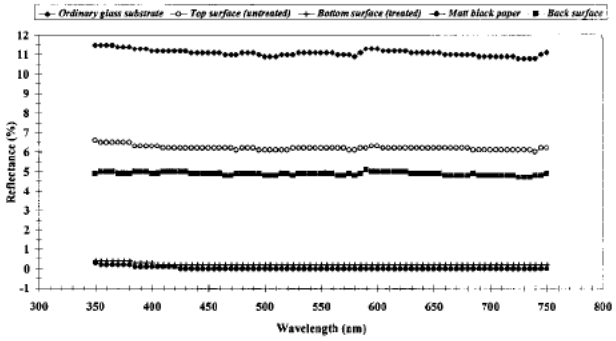

Fig. 8. Reference spectra of uncoated glass substrates in different cases. The reflectance spectrum of matt black paper is included for comparison.

In order to obtain values for the absolute reflection coefficients that were required, it was necessary to make corrections of the measured reflectance spectra of the deposited films. The corrections involved:

1. Measuring the reflectance spectrum of the bottom surface of an uncoated glass substrate in order to subtract it from the measured values of reflectance. This was achieved by treating the bottom surface of an uncoated glass substrate with emery paper so virtually eliminating reflection from it (Fig. 8). The reflectance spectra of the untreated (or top) surface and that of an ordinary glass substrate were then measured. The reflectance spectrum of the back surface was obtained by subtracting the reflectance values of the top surface from those of the ordinary substrate, and was averaged to be 5%.
2. Measuring the reflectance spectrum of a single crystal silicon wafer and comparing it with a calculated one [16] to derive a correction curve of the measured reflectance in order to obtain the absolute reflectance of the coatings (Fig. 9). The correction ratio was, on average, 0.76.

Thus, the relation between the measured reflectance, R^{measur}, and the actual one, R, is

$$R \approx 0.76(R^{measur} - 5\%) \quad (5)$$

or

$$R \approx 0.76 R^{measur} - 4\% \quad (6)$$

As a result, if R_{max}^{measur} is the measured value of a reflectance maximum, the corresponding actual value, R_{max}, is given by

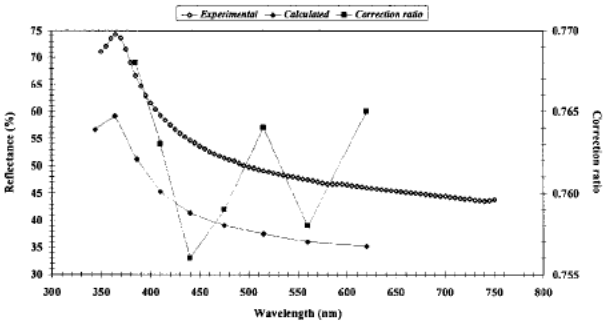

Fig. 9. Calculated and experimental reflectance spectra of a single crystal silicon wafer. Also shown is the correction ratio as a function of wavelength. Data of the calculated curve are from [16].

$$R_{\max} \approx 0.76 R_{\max}^{\text{measur}} - 4\% \tag{7}$$

Thus, by substituting the value of $R_{\max}$:

$$n_{\text{film}} = \left(1.525 \frac{1 + \sqrt{0.76 R_{\max}^{\text{measur}} - 0.04}}{1 - \sqrt{0.76 R_{\max}^{\text{measur}} - 0.04}}\right)^{1/2} \tag{8}$$

Instead of ellipsometry, Eq. (8) was used to calculate refractive indices of films produced in the course of this work, for the following reasons:

1. It is independent of optical thickness of coatings and consequently gives consistent results for variable optical thickness.
2. The possibility of obtaining refractive indices over many wavelengths rather than at 632.8 nm using the ellipsometer that was available.
3. The ratio of the area of light beam of the spectrophotometer (~ 10.8 mm^2) and that of the laser beam of the ellipsometer (~ 0.8 mm^2) is approximately 14. This gives better integration over the coated area of the substrate.

4.2. Calculations of thickness from reflectance spectra using interference methods

After calculating n_{film}, using Eq. (8) the film thickness could be calculated using equations $n_{\text{film}} d_{\text{film}} = (2k+1)\frac{\lambda_{\max}}{4}$ and $n_{\text{film}} d_{\text{film}} = k\frac{\lambda_{\min}}{2}$, where $\lambda_{\max}$ is a wavelength at which a reflectance maximum occurs and $\lambda_{\min}$ is a wavelength at which a reflectance minimum occurs. The calculation procedure depended on the shape of the reflectance spectrum of interest.

If there were two consecutive maxima in the scanned spectral range, then for the first maximum $4 n_{\text{film}} d_{\text{film}} = (2k+1)\lambda_{\max_1}$ and that for the second maximum is $4 n_{\text{film}} d_{\text{film}} = [2(k-1)+1]\lambda_{\max_2}$. By solving these two equations, it is found that

$$d_{\text{film}} = \left| \frac{\lambda_{\max_1} \lambda_{\max_2}}{2 n_{\text{film}} (\lambda_{\max_2} - \lambda_{\max_1})} \right| \tag{9}$$

Eq. (9) is also valid in the case of two consecutive minima. The problem of this equation is that it ignores changes of n_{film} with wavelength. However, it was considered to be sufficiently accurate for the estimation of d_{film} for the purpose of this work, especially in the relatively narrow range of wavelength studied where variations in n_{film} were not expected to be so significant.

Finally, it should be indicated that the results of the thickness measurements were satisfactorily consistent in the course of this work.

5. Results

5.1. Aluminium oxides

The system was established using aluminium cathodes in both magnetrons. Aluminium oxide is a very insulating oxide with a high secondary electron emission coefficient, which leads to extreme arcing if DC reactive sputtering is attempted.

In this work, Al_2O_3 films were prepared using the mid-frequency AC powered magnetrons technique. The main and secondary targets were both Al and the two magnetrons were operated in the floating mode at $P^{\text{AC}}_{\text{Al} \leftrightarrow \text{Al}} = 1$ kW. Substrates were held static over the main magnetron. In this case, no incorporation of an alloying material was required. Voltage control on the main Al magnetron was used. The percentage of aluminium magnetron voltage set point, $\text{Al}^{\%}_{\text{vc}}$, was gradually decreased and a film was deposited and characterised at each value of $\text{Al}^{\%}_{\text{vc}}$. The deposition time was 3 min. Fig. 10 shows the dependence of transmittance at 550 nm, T_{550}, of the visibly transparent Al_2O_3 films, and the corresponding deposition rate, on $\text{Al}^{\%}_{\text{vc}}$. Obviously, films of higher T_{550} are deposited at lower rates. The percentage of Al magnetron voltage set point, and the corresponding O_2 flow rate, at which the best Al_2O_3 film occurred (i.e. the one of the highest transmittance and deposition rate) were 73.7% and 3.6 sccm, respectively. The transmittance at 550 nm, refractive index and deposition rate of this film were 89.5%, 1.67 and 2.02 nm/s, respectively. Clearly, such a result is comparable with the best reported results [9,17,18], taking into account that the applied power in this work was only 1 kW. Fig. 11 shows the transmittance and reflectance spectra of the best Al_2O_3 film. Finally, it is worth mentioning that, in addition to glass, aluminium oxide films have also been deposited, using this technique, on stainless steel and single crystal silicon substrates for extended periods of time (up to 45 min) and at high rates without any sign of arcing.

5.2. Mixed insulating oxides

Finally, a large number of oxide films of Mo, W, V, Pb, Ti, Sn and Cu doped with dopants such as Zn, Sn, Ti, Nb, Ta, Mo or Bi have been deposited, at different combinations of powers and at different stoichiometries, and characterised. They were initially investigated for conductivity. Although the transparent films were insulating under the deposition conditions and procedures followed (i.e. unintentional heating or biasing of substrates and no post-deposition heat treatment), their optical properties (e.g. a very wide range of refractive indices) are of great interest in optical applications.

Table 1 summarises the preparation conditions and the optical properties of some of the transparent insulating oxide films prepared in this work, where P_{Cu}^{DC}, P_{W}^{DC}, P_{V}^{DC}, P_{Mo}^{DC} and P_{Pb}^{DC} are the DC biasing powers applied to the floating Cu, W, V, Mo and Pb magnetrons, respectively, and $Cu_{vc}^{\%}$ and $Pb_{vc}^{\%}$ are the percentages of metallic Cu and Pb magnetrons voltages set-points (i.e. the occurrence), respectively. The floating AC power and deposition time were 100 W and 6 min, respectively, throughout.

6. Conclusion

According to the above discussion, the deposition technique, employed in the course of this work, enjoys the following major advantages

1. Substrate rotation enhances atomic level mixing of the film constituents. The stoichiometry of the film is controlled by PEM or voltage control, on one magnetron, and dopants are added by sputtering from the other magnetron. This means that the former magnetron serves two purposes; the first is to sputter metal and oxidise it, and the second purpose is to oxidise the metal sputtered from the other magnetron.
2. The combination of DC and mid-frequency AC power in a novel way, using a filter to protect the DC power supply from the AC one (or the independently DC powered magnetrons method), permits the composition of the produced films to be easily and independently manipulated by varying the magnitude of power applied to each magnetron. As a result, this system is able to obtain a sputter-deposited coating of an alloy or multi-element compound which is either difficult or impossible to be formed from a single target.
3. Depending on the materials involved, the use of very fast feedback methods, to automatically control the admission rate of the reactive gas (e.g. oxygen) into the sputtering chamber (i.e. PEM and voltage control), allows the stoichiometry of the deposited films to be independently controlled. The very efficient control of the admission rate of oxygen also allows the deposition rate of reactively sputtered films to be high.
4. The use of an airlocked system allows the implementation of an iterative deposition process to vary coating stoichiometry and composition. Hence, information regarding different composition and stoichiometry can be attained rapidly without cathode acquisition or preparation.
5. The system, described in this work, is superior to the dual magnetron technique described by Lewin and Howson [19] where two concentric cathode annuli of different materials (with separate magnetic fields) comprise one magnetron device in that the two sources sputter independently of each other. This permits variable compositions to be selected only to a limited extent in a reactive environment, the limit being reached when differential poisoning of the two cathode materials dominates. Clearly, precise stoichiometry control also suffers from this problem as a direct result of the close proximity of the cathode.
6. The use of mid-frequency (i.e. 40 kHz) AC power in the floating mode secures periodical effective

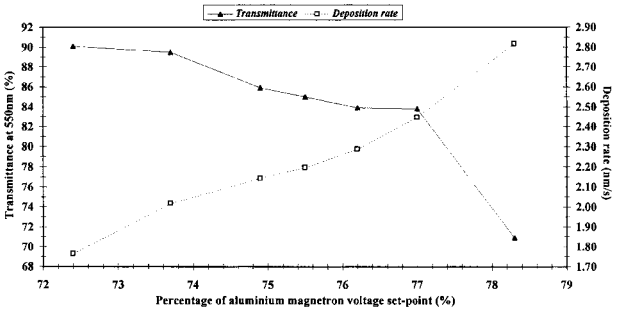

Fig. 10. Transmittance at 550 nm and the corresponding deposition rate vs. the percentage of aluminium magnetron voltage set-point of visibly transparent films of aluminium oxide. The floating AC power between the two Al magnetrons was 1 kW.

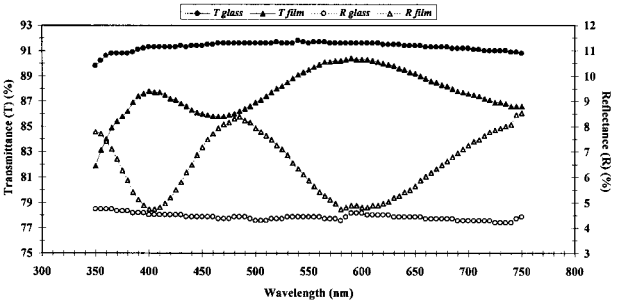

Fig. 11. Transmittance and reflectance spectra of the best transparent Al oxide film which occurred at 73.7% of Al magnetron voltage set-point. The floating AC power was 1 kW. The relevant spectra of an uncoated glass substrate are also plotted.

Table 1
A summary of the preparation conditions and optical properties of some of the transparent insulating oxide films prepared in this work[a]

Oxide	DC bias (W)	Occurrence (%)	n_{film}	T_{550} (%)	Deposition rate (nm/s)
Cu–Sn	$P^{DC}_{Cu} = 300$	$Cu^{\%}_{vc} = 30.8$	1.92	67.7	0.80
Mo–Nb	$P^{DC}_{Mo} = 150$	$Ar^{\%}_{pcm} = 53.9$	2.24	72.3	0.36
Mo–Nb	$P^{DC}_{Mo} = 300$	$Ar^{\%}_{pcm} = 49.3$	1.96	91.9	0.41
Mo–Nb	$P^{DC}_{Mo} = 450$	$Ar^{\%}_{pcm} = 46.3$	1.93	91.9	0.44
Mo–Sn	$P^{DC}_{Mo} = 100$	$Ar^{\%}_{pcm} = 54.0$	2.00	81.4	0.30
Mo–Sn	$P^{DC}_{Mo} = 300$	$Ar^{\%}_{pcm} = 51.4$	2.17	90.8	0.37
Mo–Ta	$P^{DC}_{Mo} = 450$	$Ar^{\%}_{pcm} = 45.9$	2.09	90.9	0.42
Pb	$P^{DC}_{Pb} = 400$	$Pb^{\%}_{vc} = 54.0$	2.46	74.2	1.25
Pb–Bi	$P^{DC}_{Pb} = 100$	$Pb^{\%}_{vc} = 52.0$	2.44	80.9	0.84
Pb–Bi	$P^{DC}_{Pb} = 300$	$Pb^{\%}_{vc} = 42.8$	2.40	88.4	1.28
Pb–Bi	$P^{DC}_{Pb} = 400$	$Pb^{\%}_{vc} = 41.4$	2.39	84.0	1.55
Ti	$P^{DC}_{Ti} = 400$	$Ar^{\%}_{pcm} = 65.1$	2.63	80.1	0.05
Ti–Nb	$P^{DC}_{Ti} = 400$	$Ar^{\%}_{pcm} = 69.1$	2.60	67.1	0.09
Ti–Ta	$P^{DC}_{Ti} = 400$	$Ar^{\%}_{pcm} = 67.7$	2.28	69.9	0.17
V–Mo	$P^{DC}_{V} = 200$	$Ar^{\%}_{pcm} = 68.9$	1.80	77.9	0.52
V–Mo	$P^{DC}_{V} = 300$	$Ar^{\%}_{pcm} = 65.6$	1.79	81.4	0.48
W	$P^{DC}_{W} = 400$	$Ar^{\%}_{pcm} = 51.6$	2.23	76.4	0.76
W–Mo	$P^{DC}_{W} = 150$	$Ar^{\%}_{pcm} = 53.8$	2.29	91.2	0.34
W–Mo	$P^{DC}_{W} = 450$	$Ar^{\%}_{pcm} = 50.0$	2.20	87.0	0.71
W–Nb	$P^{DC}_{W} = 200$	$Ar^{\%}_{pcm} = 62.1$	2.29	90.8	0.38
W–Nb	$P^{DC}_{W} = 350$	$Ar^{\%}_{pcm} = 51.9$	2.21	84.8	0.70
W–Nb	$P^{DC}_{W} = 400$	$Ar^{\%}_{pcm} = 55.1$	2.14	74.0	1.37
W–Sn	$P^{DC}_{W} = 100$	$Ar^{\%}_{pcm} = 51.9$	2.14	91.5	0.36
W–Ta	$P^{DC}_{W} = 200$	$Ar^{\%}_{pcm} = 60.6$	2.29	78.1	0.59
W–Ta	$P^{DC}_{W} = 400$	$Ar^{\%}_{pcm} = 56.8$	2.21	70.7	0.83
W–Ta	$P^{DC}_{W} = 600$	$Ar^{\%}_{pcm} = 56.3$	2.12	86.3	1.05
W–Ti	$P^{DC}_{W} = 150$	$Ar^{\%}_{pcm} = 55.6$	2.31	91.1	0.35
W–Ti	$P^{DC}_{W} = 450$	$Ar^{\%}_{pcm} = 52.0$	2.24	87.9	0.64

[a]The floating AC power was 100 W throughout.

discharging of the insulating layer, due to the symmetrical operation of the electrodes. This allows the reactive sputtering process to be arc-free [9], and hence, eliminating the undesired effects of arcing in reactive sputtering such as driving the process to become unstable, creating defects in the films and reducing the target lifetime. Consequently, the defect density in insulating films is reduced by orders of magnitude [11] in comparison with the DC technique.

7. The well-defined DC conducting anode allows the sputtering process to have long-term stability, at a given set point. In addition, the high deposition rates obtained are comparable with those of the DC technique [7,9].
8. Unlike the additional complexity of the RF technique, the coupling of the AC power to the cathodes, in the frequency range used, is simple. Consequently, the AC technique can be easily adopted for sputtering from larger area cathodes [9]. On the other hand, the AC plasma used with an unbalanced magnetron leads to higher density plasma and increased bombardment of the growing insulating films with ions.
9. This technique opens the door wide for investigating virtually all potentially promising thin films (e.g. hard coatings, semiconducting films, superconducting films, etc.).

References

[1] N. Danson, I. Safi, G.W. Hall, R.P. Howson, Surf. Coat. Technol. 99 (1998) 147–160.
[2] R.P. Howson, N. Danson, I. Safi, Thin Solid Films 351 (1999) 32–36.

[3] R.P. Howson, I. Safi, G.W. Hall, N. Danson, Nucl. Instrum. Methods Phys. Res. B 121 (1997) 96–101.
[4] I. Safi, N. Danson, R.P. Howson, Surf. Coat. Technol. 99 (1998) 33–41.
[5] I. Safi, R.P. Howson, Thin Solid Films 343-44 (1999) 115–118.
[6] I. Safi, Surf. Coat. Technol. 127 (2-3) (2000) 203–219.
[7] J. Szczyrbowski, C. Braatz, SPIE 1727 (1992) 122–136.
[8] D.A. Glocker, J. Vac. Sci. Technol. A 11 (6) (1993) 2989–2993.
[9] M. Scherer, J. Schmitt, R. Latz, M. Schanz, J. Vac. Sci. Technol. A 10 (4) (1992) 1772–1776.
[10] G. Este, W.D. Westwood, J. Vac. Sci. Technol. A 6 (3) (1988) 1845–1848.
[11] S. Schiller, K. Goedicke, J. Reschke, V. Kirchhoff, S. Schneider, F. Milde, Surf. Coat. Technol. 61 (1993) 331–337.
[12] B. Window, N. Savvides, J. Vac. Sci. Technol. A 4 (3) (1986) 453–456.
[13] R.P. Howson, H.A. Ja'Fer, A.G. Spencer, Thin Solid Films 193-94 (1990) 127–137.
[14] A.G. Spencer, K. Oka, R.P. Howson, R.W. Lewin, Vacuum 38 (1988) 857–859.
[15] F. Abeles, in: E. Wolf (Ed.), Progress in Optics, II, North-Holland Publishing Company, Amsterdam, 1963, pp. 249–288.
[16] D.E. Gray, American Institute of Physics Handbook, McGraw-Hill Book Company, New York, 1972.
[17] M. Scherer, P. Wirz, Thin Solid Films 119 (1984) 203–209.
[18] P.J. Clarke, J. Vac. Sci. Technol. A 12 (2) (1994) 594–597.
[19] R.W. Lewin, R.P. Howson, Proc. 6th Int. Conf. on Ion and Plasma Assisted Techniques, Brighton, UK, (1987) pp. 464–469.

Appendix 1039-A

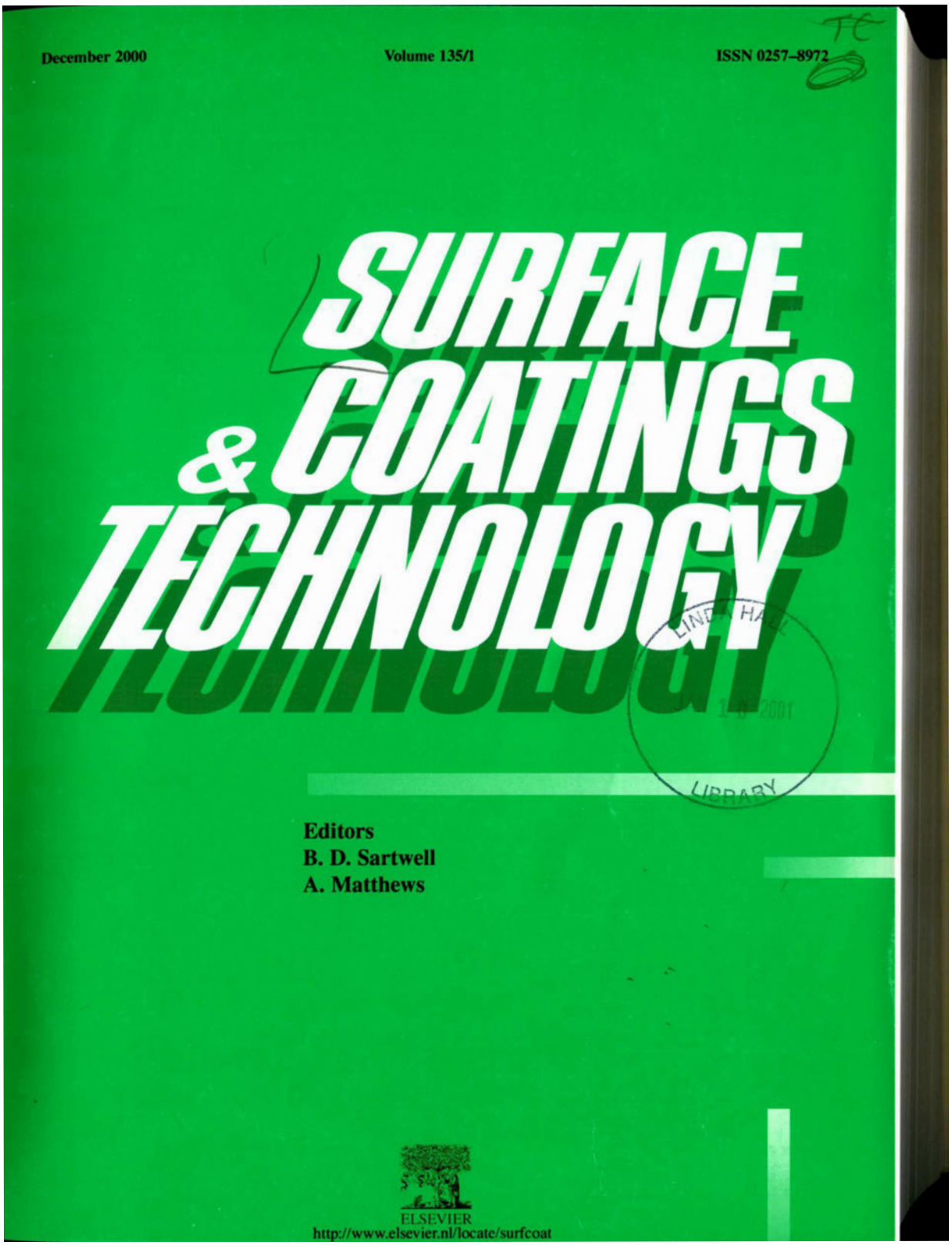
December 2000
Volume 135/1
ISSN 0257-8972
SURFACE & COATINGS TECHNOLOGY
LIBRARY
Editors
B. D. Sartwell
A. Matthews
ELSEVIER
http://www.elsevier.nl/locate/surfcoat

SURFACE AND COATINGS TECHNOLOGY

Scope

The increasing requirement for high technology materials with specific performance characteristics in various types of environments has dictated that these materials possess near-surface properties different from their bulk properties. This journal is a principal forum for the interchange of information on the science, technology and applications of thin and thick coatings and modified surfaces which alter the properties of materials. The scope includes all types of coatings and surface modification techniques (including physical vapour deposition, chemical vapour deposition, electroplating and surface modification by directed energy techniques). Of particular emphasis are the emerging advanced processes such as thermal spraying, sputter deposition, activated reactive evaporation, ion plating, molecular beam epitaxy, ion implantation and pulsed laser surface deposition. Contributions range from original scientific articles concerned with applied research or direct applications of coatings to reviews of current technology in specific areas. Papers are solicited on topics which include one or more of the following areas: (1) characterization of coatings and modified surfaces, which includes the determination of composition, structure, adhesion, and internal stresses; (2) the application of coatings and modified surfaces to alter the mechanical, chemical or optical properties of materials. Mechanical properties include friction, wear, erosion, hardness and load bearing capacity. Chemical properties include corrosion and oxidation. Optical and electro-optical properties include reflectivity, selective absorption and electroluminescence. Particular emphasis is also placed on the emerging surface engineering technologies and coatings with a diversity of applications such as diamond, diamond-like carbon, and cubic boron nitride. Other interdisciplinary areas include thermal barrier coatings and coatings for biomedical applications and materials conservation.

Abstracting/Indexing Services

This journal is cited by the following services:
Engineering Index, FIZ Karlsruhe, Metal Finishing Abstracts, Current Contents — Engineering, Technology and Applied Sciences, Physikalische Berichte, Cambridge Scientific Abstracts, Chemical Abstracts, Fluid Abstracts, Metals Abstracts, Physics Abstracts, PASCAL/Centre National de Recherche Scientifique, Solid State Abstracts.

Pre-publication abstracts of articles in *Surface and Coatings Technology* and other related journals are now available weekly in electronic form via CoDAS, a new direct alerting service in condensed matter and materials science run jointly by Elsevier Science and Institute of Physics Publishing. For details on a free one-month subscription contact Paul Bancroft on fax +441179294318 or e-mail bancroft@ioppublishing.co.uk

Publication Information: *Surface and Coatings Technology* (ISSN 0257-8972). For 2000 volumes 122–134 are scheduled for publication. Subscription prices are available upon request from the Publisher or from the Regional Sales Office nearest you or from this journal's website (http://www.elsevier.nl/locate/surfcoat). Further information is available on this journal and other Elsevier Science products through Elsevier's website: (http://www.elsevier.nl). Subscriptions are accepted on a prepaid basis only and are entered on a calendar year basis. Issues are sent by surface standard mail (surface within Europe, air delivery outside Europe). Priority rates are available upon request. Claims for missing issues should be made within six months of the date of dispatch.

Orders, claims and product enquiries: please contact the Customer Support Department at the Regional Sales Office nearest you:

New York: Elsevier Science, PO Box 945, New York, NY 10159-0945, USA;
phone: (+1) (212) 633 3730 [toll free number for North American customers: 1-888-4ES-INFO (437-4636)];
fax: (+1) (212) 633 3680; e-mail: usinfo-f@elsevier.com

Amsterdam: Elsevier Science, PO Box 211, 1000 AE Amsterdam, The Netherlands;
phone: (+31) 20 4853757; fax: (+31) 20 4853432;
e-mail: nlinfo-f@elsevier.nl

Tokyo: Elsevier Science, 9-15 Higashi-Azabu 1-chome, Minato-ku, Tokyo 106-0044, Japan;
phone: (+81) (3) 5561 5033; fax: (+81) (3) 5561 5047;
e-mail: info@elsevier.co.jp

Singapore: Elsevier Science, No. 1 Temasek Avenue, no.17-01 Millenia Tower, Singapore 039192;
phone: (+65) 434 3727; fax: (+65) 337 2230;
e-mail: asiainfo@elsevier.com.sg

Rio de Janeiro: Elsevier Science, Rua Sete de Setembro 111/16 Andar, 20050-002 Centro, Rio de Janeiro - RJ, Brazil;
phone: (+55) (21) 509 5340; fax: (+55) (21) 507 1991;
e-mail: elsevier@campus.com.br [Note (Latin America): for orders, claims and help desk information, please contact the Regional Sales Office in New York as listed above]

US mailing notice: *Surface and Coatings Technology* (ISSN 0257-8972) is published semimonthly by Elsevier Science S.A. (PO Box 211, 1000 AE Amsterdam, The Netherlands). Annual subscription price in the USA US$4969.00 (valid in North, Central and South America), including air speed delivery. Periodical postage rate paid at Jamaica, NY 11431.
USA POSTMASTER: Send address changes to *Surface and Coatings Technology,* Publications Expediting, Inc., 200 Meacham Avenue, Elmont, NY 11003.
AIRFREIGHT AND MAILING in the USA by Publications Expediting Inc., 200 Meacham Avenue, Elmont, NY 11003.

Abstracting Services
This journal is cited by the following Abstracting/Indexing Services: Automatic Subject Citation Alert, Cambridge Scientific Abstracts, Chemical Abstracts, Current Contents–Physical, Chemical & Earth Sciences, Engineering Index, FIZ Karlsruhe, Metals Abstracts, PASCAL/Centre National de la Recherche Scientifique, Physics Abstracts, Physikalische Berichte, Science Citation Index.

International Standard Serial Number 0257-8972

Advertising information. Advertising orders and enquiries may be sent to: **USA, Canada and South America:** Mr Tino de Carlo, The Advertising Department, Elsevier Science Inc., 655 Avenue of the Americas, New York, NY 10010-5107, USA; phone: (+1) (212) 633 3815; fax: (+1) (212) 633 3820; e-mail: t.decarlo@elsevier.com. **Japan:** The Advertising Department, Elsevier Science K.K., 9-15 Higashi-Azabu 1-chome, Minato-ku, Tokyo 106-0044, Japan; phone (+81) (3) 5561 5033; fax: (+81) (3) 5561 5047. **Europe and ROW:** Rachel Leveson-Gower, The Advertising Department, Elseiver Science Ltd, The Boulevard, Langford Lane, Kidlington, Oxford OX5 1GB, UK; phone: (+44) (1865) 843565; fax: (+44) (1865) 843976; e-mail: r.leveson-gower@elsevier.co.uk

Printed in The Netherlands

♾ The paper used in this publication meets the requirements of ANSI/NISO Z39.48-1992 (Permanence of Paper).

ELSEVIER

Volume 135 Number 1, December 2000

SURFACE & COATINGS TECHNOLOGY

www.elsevier.nl/locate/surfcoat

Contents

ELSEVIER

Surface and Coatings Technology 135 (2000) 48–59

SURFACE & COATINGS TECHNOLOGY

www.elsevier.nl/locate/surfcoat

A novel reactive magnetron sputtering technique for producing insulating oxides of metal alloys and other compound thin films

I. Safi*

Department of Physics, Loughborough University, Loughborough, LE11 3TU, UK

Received 20 March 2000; accepted in revised form 16 August 2000

Abstract

Problems associated with reactive magnetron sputtering from elemental (i.e. non-compound) targets have been successfully solved in this work. The elements of this achievement are: (i) the use of mid-frequency (i.e. 40 kHz) AC power in the floating mode, between two magnetrons, allowed the reactive sputtering process to be arc-free and hence eliminating the undesired effects of arcing in reactive sputtering such as driving the process to become unstable, creating defects in the films and reducing the target lifetime. (ii) The combination of DC and mid-frequency AC power in a novel way using a filter to protect the DC power supply from the AC one (or the independently DC powered magnetrons method) permitted the composition of the produced films to be easily and independently manipulated by varying the magnitude of power applied to each magnetron. (iii) The use of very fast feedback methods to automatically control the admission rate of oxygen into the sputtering chamber (i.e. plasma emission monitoring or voltage control) allowed the stoichiometry of the deposited films to be independently controlled. This also allowed the deposition rate of the sputtered films to be high. (iv) Sputtering from two magnetrons made the production of alloys or multi-element compounds, which are either difficult or impossible to be formed from single targets, an easy task. (v) Substrate rotation enhanced atomic level mixing of the film constituents. The stoichiometry of the film was controlled by plasma emission monitoring or voltage control on one magnetron, and dopants were added by sputtering from the other magnetron. This means that the former magnetron served two purposes; the first was to sputter metal and oxidise it, and the second purpose was to oxidise the metal sputtered from the other magnetron. This novel technique opens the door wide for investigating virtually all potentially promising thin oxide films. Using this technique, a large range of alloy-oxide films was deposited at high rates. In fact, the independent control of both the metallic composition and stoichiometry was very valuable in identifying the optimum properties of these films. That is, giving transparent films of different refractive indices for optical applications. Furthermore, such a technique may also be capable of investigating other types of thin films (e.g. hard coatings, semiconducting films, superconducting films, etc.).

Keywords: Thin film; Oxide; Reactive sputtering; Two magnetrons; AC and DC technique; PEM; Voltage control; Composition; Stoichiometry; Arcing

* Corresponding address. P.O. Box 4470, Damascus, Syria. Tel.: +963-11-5117808.

0257-8972/00/$ - see front matter
PII: S0257-8972(00)00985-3

1. Introduction

Reactive sputtering, where a metal target is sputtered by an inert gas (e.g. argon) in the presence of a reactive gas (e.g. oxygen), to produce a film of electrically insulating material has proved to be difficult to introduce as an industrial process. The simple concept is that metal is sputtered from the target and is incident on the substrate/growing-film-surface, together with reactive gas from the residual atmosphere, to form a compound. The reaction occurs when these species meet on the surface. Energy is provided from the substrate temperature, the high energy of sputtered material or by ions used to bombard the surface. Magnetron sputtering has allowed the sputtering to be undertaken at sufficiently low pressures such that the mean free path for sputtered material is greater than the target-to-substrate distance and the energy of this material and the efficiency of its transfer from the target can be maintained. The magnetron can also be arranged, through unbalancing the magnetic field, and/or operating it in a system to create a closed field, to direct a dense plasma to the surface of the growing film. This plasma can cause an insulating or isolated surface to acquire a floating bias, which leads to it being bombarded with low energy argon ions, to provide energy for excitation energies for chemical and structural reactions. The growth of the film can be controlled in this manner and it does not require the film or substrate to be electrically conducting. If additional bias is required, RF can be used. The problems, which have to be solved, occur at the cathode surface.

The presence of reactive gas in a region of high energy and freshly exposed metal surfaces, which is the sputtering race-track of the magnetron, leads to rapid reaction. If the surface reacts faster than it sputters, a surface compound film is formed, which in general sputters at a much lower rate than the metal, a process which has become to be called 'poisoning'. The transition between metal sputtering and 'poisoning' is dependent upon the power used to sputter and the partial pressure of the reactive gas and occurs at a different level when approached from the metal or 'poisoned' condition. This process leads to a hysteresis being seen between the sputtering parameters and the flow of reactive gas into the chamber and there is a region of this flow where the process is unstable. It becomes one of the rapid deposition of a partially reacted metal or the slow deposition from a poisoned target of a fully reacted film. This problem can be solved by controlling the state of the sputtering surface, and hence the partial pressure of the reactive gas, through the light emitted by the sputtering metal or other gases in the discharge, or in some cases, from the voltage of the sputtering cathode. These techniques provide a fast feedback to the control of the flow of the gas. However, great care has to be taken with the time constants associated with the changes of gas pressure in a vacuum chamber.

A further solution lies in separating the deposition and reactive process in a cyclic process where a thin metal film is deposited and then converted. In our versions of this process, the substrate is moved (successive plasma anodisation, or SPA) or the magnetron is made to change function from a provider of sputtered metal to one of oxygen and energetic argon ions (successive pulsed plasma anodisation, or SPPA). In both cases, the unbalanced magnetron, the provider of argon-ion energy, is required to operate in the presence of a partial pressure of oxygen.

When the reaction product is insulating and the power is DC, other problems appear. A region of the target-cathode remains covered with reaction product, the racetrack region only can be balanced to be sputtering metal faster than it is reacting with the proportion of reactive gas in the system. This insulating region is subject to bombardment of ions and becomes highly charged, due to charge accumulation or through secondary-electron emission. This leads to rapid localised discharges, arcs, which disrupt the sputtering discharge and causes arc-evaporation from regions of the target, with particle 'spitting' and consequent contamination of the film. If the process is not properly designed, and carefully balanced, an insulating film may be formed on the anode of the discharge and on the chamber walls to give a discharge which changes character with time. These problems can be overcome by using RF in reactive sputtering and target biasing. RF introduces its own problems and is not suitable for the high-rate, large-area processes that are required.

More recently, a solution to these problems has appeared. The insulating surface has to be discharged before the charge accumulates to an extent where an arc is formed. This has been done by providing a reverse potential pulse to the surface within the charge accumulation time. This can be a short pulse applied to a DC supply or AC power applied between two cathodes. The frequency required turns out to be approximately 40 kHz, which can be provided, without the tuning systems necessary with RF, and at low cost. The latter process has the further advantage of creating a continuously cleaned anode, because for the other half of the cycle it is the sputtering cathode. This emerging technique has been utilised recently by a few workers [1–10]. The results were very promising. For example, Szczyrbowski and Braatz [7] have reactively deposited films of SiO_2 at high rates using 40 kHz-AC power applied between two Si magnetrons. In addition to the excellent optical and mechanical properties of the deposited films, no arcing was observed during the entire lifetime of the target, which was more than a week. Schiller et al. [11] have reactively deposited films of